Max Planck Graduate Center
mit der Johannes Gutenberg-Universität Mainz

JG|U UNIVERSITÄTSmedizin. Department of Dermatology MAINZ

Max Planck Institute for Polymer Research

MAX-PLANCK-GESELLSCHAFT

Nanocapsule-based vaccination for inhibition of tumor escape mechanisms

Dissertation

zur Erlangung des Grades

„Doktor der Naturwissenschaften“

der Fachbereiche

Physik, Mathematik und Informatik,
Chemie, Pharmazie und Geowissenschaften,
Biologie und der Universitätsmedizin

vorgelegt von

Matthias Philipp Domogalla

geb. am 12.12.1987

Mainz im November 2017

Tag der mündlichen Prüfung:

Dekan:

1. Berichterstatter:
2. Berichterstatter:

Für meine Familie

Table of Contents

Abstract

Tumor-associated tolerance mechanisms promote tumor growth and greatly inhibit the success of anti-cancer therapies. Regulatory T cells (Tregs) critically contribute to tumor-associated tolerance and are involved in IL-10- and signal transducer and activator of transcription (STAT) 3-mediated cancer-induced immunosuppression. In this study, $CD25^+$ T cells with focus on Tregs were cell-specifically addressed by using human IL-2 functionalized hydroxyethyl starch (HES-D-IL-2) nanocapsules (NC). After coupling to the NC surface, the targeting vector human IL-2 was still fully biological functional and only a negligible amount of non-attached IL-2 was present in the NC supernatant. Flow cytometry and laser scanning microscopy experiments revealed an enhanced uptake/binding and intracellular localization of HES-D-IL-2 by human $CD4^+CD25^+$ activated T cells compared to control NC. Additionally, HES NC with a twofold (HES-D-IL-$2_{/2}$) and tenfold (HES-D-IL-$2_{/10}$) reduced amount of surface IL-2 were generated. In all tested NC-coupled IL-2 concentrations, flow cytometric experiments highlighted a reduced uptake/binding of HES-D-IL-2 by human naïve $CD4^+CD25^-$ T cells in comparison to human activated T cells. Furthermore, the uptake by naïve and activated T cells was dose- dependent on the amount of IL-2 that was present on the NC surface. In contrast, human $CD4^+CD25^{high}$ Tregs demonstrated the highest uptake. Intriguingly, the uptake of HES-D-IL-2 by Tregs was IL-2 dose-independent, revealing a high IL-2 receptor affinity and preferably targeting of Tregs by low amounts of IL-2. Furthermore, CD25 staining and blockade by the monoclonal chimeric antibody basiliximab (anti-CD25-mAb) indicated a CD25-dependent uptake/binding of HES-D-IL-2. This was confirmed by competitive studies using naïve $CD4^+CD25^-$ and activated $CD4^+CD25^+$ human T cells. Furthermore *in vivo* experiments using wild-type C57BL/6 mice, and immunodeficient $RAG2^{-/-}\gamma^{-/-}$ mice reconstituted with human $CD4^+$ T cell or human peripheral blood mononuclear cells, revealed a successful CD25-specific targeting of murine and human $CD4^+$ and $CD8^+$ T cells *in vivo*.

In order to inhibit STAT3-mediated immune tolerance in Tregs, ovalbumin protein NC with known high intracellular release capacities were generated and applied to HeLa cells to perform proof-of-principle experiments. After encapsulation of the specific STAT3 inhibitor S3I-201, an inhibition of STAT3 phosphorylation was observed *in vitro*.

Targeting of Tregs and cytotoxic T cells by HES-D-IL-2 in combination with inhibition of STAT3-mediated tolerance by the ovalbumin protein NC may inhibit tumor-associated immunosuppression thus leading to enhanced tumor rejection.

Zusammenfassung

Tumor-assozierte Toleranzmechanismen fördern das Tumorwachstum und führen zu einer abgeschwächten therapeutischen Effektivität. Regulatorische T-Zellen (Tregs) tragen entscheidend zur Tumor-induzierten Toleranz bei und sind an der IL-10- und STAT3-mediierter Tumor-assoziierter Toleranzinduktion beteiligt. In der vorliegenden Studie wurden humane T-Zellen mit Fokus auf Tregs spezifisch mit IL-2 funktionalisierten Nanokapseln (HES-D-IL-2) addressiert. Funktionale Analysen zeigten, dass das IL-2 nach Anbindung an die Kapseloberfläche noch komplett biologisch funktional war und sich nur noch ein geringer Anteil an freiem IL-2 im Überstand der Kapseln befand. Mit Hilfe durchflusszytometrischer und konfokaler lasermikroskopischer Analysen wurde eine Aufnahme/Bindung und intrazelluläre Lokalisation von HES-D-IL-2 im Vergleich zu Kontrollkapseln in humanen aktivierten $CD4^+CD25^+$ T-Zellen festgestellt. Anschließend wurden Nanokapseln mit der zweifach (HES-D-IL-$2_{/2}$) und zehnfach (HES-D-IL-$2_{/10}$) reduizerter Menge an IL-2 auf der Oberfläche synthetisiert. In allen getesteten IL-2-Konzentrationen wiesen Vergleichsstudien eine geringere Aufnahme/Bindung von HES-D-IL-2 in naiven $CD4^+CD25^-$ T-Zellen im Vergleich aktivierten T-Zellen auf. Außerdem zeigte sich die Aufnahme in naive und aktivierte T-Zellen abhängig von der Menge an IL-2 auf der Kapseloberfläche. Im Gegensatz dazu war die Aufnahme/Bindung an regulatorische $CD4^+CD25^{high}$ T-Zellen am höchsten und interessanterweise unabhängig von der IL-2-Konzentration auf den Kapseln gleichbleibend hoch. Diese Ergebnisse deuten auf eine erhöhte IL-2-Rezeptoraffinität und ein bevorzugtes Targeting regulatorischer T-Zellen bei niedrigen IL-2-Konzentrationen hin. Zusätzlich demonstrierten die Färbung und das Blockieren von CD25, durch den monoklonalen Antikörper Basiliximab (anti-CD25 mAB), eine CD25-abhängige Aufnahme/Bindung der IL-2 funktionalisierten Nanokapseln. Diese CD25 Abhängigkeit konnte in Kompetitionsstudien mit naiven und aktivierten T-Zellen bestätigt werden. Außerdem konnte in Experimenten mit Wildtyp C57BL/6 und immundefiziente $RAG2^{-/-}\gamma^{-/-}$ Mäusen, die mit humanen $CD4^+$ T-Zellen oder mononukleären Zellen aus dem peripheren Blut rekonstituiert wurden, nachgewiesen werden, dass murine und humane $CD4^+$ und $CD8^+$ T-Zellen CD25-abhängig mit HES-D-IL-2 spezifisch *in vivo* adressiert werden können.

Um Treg-spezifisch, STAT3-mediierte,Tumor-assoziierte Immuntoleranz zu inhibieren, wurden Proteinkapseln aus Ovalbumin hergestellt die eine hohe intrazelluläre Freisetzungsrate aufweisen und an HeLa Zellen getestet, um Proof-of Principle Experimente durchzuführen. Nach Verkapselung des spezifischen Inhibitors S3I-201 wurde eine Inhibition der STAT3 Phosphorylierung *in vitro* beobachtet.

Das Zell-spezifische Addressieren von Tregs und Effektor T-Zellen in Kombination mit der Inhibition STAT3-vermittelten tumor-assoziierten Toleranzmechanismen könnte die Tumor-induzierte Immunsuppression verringern und zu einer verstärkten Tumorantwort führen.

I Introduction

Cancer is the one of the leading causes of death worldwide, especially in developed countries. For instance, in the United States of America more than 600 000 dying patients are projected to occur in 2017 [1]. Even though a lot of research is going on in that field for many patients there are often no satisfying options for cure or disease alleviation in particular in later cancer stages. This is probably due to a high heterogeneity between different cancer entities and cell heterogeneity within the individual cancer itself [2,3]. Douglas Hanahan and Robert A. Weinberg tried to cut down the complexity of all cancer types into six different hallmarks that determine the transformation of a normal cell into a solid malignant tumor [4]. These attributes include self-sufficiency in growth signals, insensitivity to anti-growth signals, tissue invasion & metastasis, limitless replicative potential, sustained angiogenesis, and evasion of apoptosis [4]. Just short time later it became apparent that the underlying enabling characteristics of these hallmarks are genomic instability and mutation, plus a tumor promoting inflammation. Additionally, two emerging principles were added to these general assumptions which are reprogramming of energy metabolism and evading immune destruction [5].

From the latter two respectively, the opposing role of the immune system in either facilitating cancer formation or its appearance in recognition and subsequent eradiation of emerging malignant cells becomes illusive and is controversically discussed [6]. The capability of tumor cells to avoid immune detection and destruction is called “cancer immunoediting” and occurs in a three step process which includes both, host-protective and tumor-promoting immune effects. Cancer immunoediting proceeds after healthy cells have become carcinogenic [7,8]. In the “elimination phase” those transformed cells are recognized and eradiated by the innate and adaptive immune system. Usually this complex process is finished long before the cancer cells become clinically apparent. However, if a short fraction of cells survive they enter the equilibrium phase which is characterized by a functional dormancy of cancer cells induced by cytokines as for example interferon (IFN) -γ and interleukin (IL) -12 [8,9]. As a consequence of the constant selective pressure that is present in the equilibrium phase some tumor cells might elude immune surveillance for example by antigen and MHC loss or induction of immunosuppressive mechanisms and subsequently enter the “escape phase” which is characterized by an fractious proliferation of tumor cells and the development of a clinical relevant disease [8].

Since the first attempt in 1893 when William Coley tried a vaccination of tumor patients with inoperable Sarcoma by using the Coley’s Toxin [10], there have been multiple attempts to target the immune system for cancer therapy [11-13]. Although cancer immunotherapy has become a very powerful tool in the clinics those therapies are inclined to induce serious side

effects ranging from systemic inflammation to autoimmunity [14]. Therefore, it is beneficial to develop drug delivery systems and targeting vectors that directly address desired organs or cell types and reduce toxicity plus off-target effects [15-17].

1.1. The human immune system – a general overview

During its lifetime the human body is constantly exposed to a variety of potentially harmful toxins or organisms for example bacteria, viruses, fungi, and parasites. Some of these organisms live as commensals while others are pathogenic. The task of the immune system is first to prevent pathogens from entering and second to limit the populating with commensals to areas on which they are useful or at least harmless. On the other hand, another indispensable aspect is the ability to keep immune responses in check and prevent systemic reactions and autoimmunity [18]. To compete with that challenge, a complex network of defense mechanisms has evolved which can fundamentally be divided into two different parts, the innate and the adaptive immunity [19]. After crossing the physical and chemical boundaries the first line of defense that a pathogen will encounter is the antigen-unspecific, yet quickly reacting innate immune system consisting of humoral and cellular barriers. The humoral part is constituted of for example natural antibodies, antimicrobial peptides or the complement system, whereas the cellular part consists of phagocytic cells like macrophages and neutrophils plus natural killer (NK) cells [19]. The innate immune system is unable to establish an immunological memory and its receptors are germline-coded pattern recognition receptors (PRRs) that discriminate between “self” and “non self” by recognition of pathogen-associated molecular patterns (PAMPs) or danger-associated molecular patterns (DAMPs). PRRs include for example toll like receptors (TLRs), NOD-like receptors (NLRs) or RIG-I like receptors (RLRs), whereas PAMPs and DAMPs are highly conserved molecular patterns that are present on the pathogens surface, needed for pathogenic reproduction or become detectable after tissue damage [20,21].

In contrast, the adaptive immune system that can fight pathogens in a highly specific way yet is activated at later time points. However, unlike the innate immune system it is capable to build up a memory, meaning that after a secondary exposure to the same antigen adaptive immune cells can react immediately and specifically [22]. Members of the adaptive immunity are first B cells that contribute to pathogen control by secreting antibodies. In addition to antigens, that are bound to molecules of the Major Histocompatibility Complex (MHC) antidbodies also recognize free antigens MHC-independently. They are secreted after T cell dependent priming of the B lymphocytes. In contrast, T cells need the antigen be presented in the context of MHC molecules and thus T cell priming depends on cell to cell contact [19].

As connective bridge between the innate and the adaptive immune system serve dendritic cells (DCs) which were first described by Banchereau and Steinman in 1973 [23,24]. DCs are

among B cells and macrophages so called antigen presenting cells (APCs) that can present antigens in the context of MHC class I and MHC class II molecules. However, DCs are considered the most potent APCs as they can prime and activate naïve T cells [25]. They are distributed all over the body's surface but also found in lymphatics and may be present in an immature or mature state. In most tissues DCs are present in an immature state constantly taking up antigens from their surroundings [25]. In that state, they are characterized by low expression of co-stimulatory and MHC molecules contrary to high expression of antigen uptake receptors like for example the different Fc receptors [26]. After antigen uptake in combination with a danger signal that is received by stimulation of their PRRs or antigen encounter in a pro-inflammatory milieu, DCs upregulate co-stimulatory molecules (like the B7 protein family members cluster of differentiation (CD) 80/CD86, CD40 or CD54), the lymph node homing receptor C-C chemokine receptor type 7 (CCR7) (which responds to C-C chemokine ligand (CCL) 19 and CCL21), and MHC molecules and migrate to the lymph nodes to activate $CD4^+$ and $CD8^+$ T cells [25,27,28]. According to the stimulus DCs receive during maturation they stimulate naïve T cells to become different types of effector T cell populations (Figure 1) [24,29]. However, DCs also constantly take up antigens in steady state non-inflammatory conditions or anti-inflammatory conditions for example in the presence of transforming growth factor-ß (TGF-ß), IL-10, glucocorticosteroids, or 1,25(OH)2 vitamin D3. That causes the development of DCs with rather tolerogenic properties [30,31].

1.2. T lymphocytes

In general, T lymphocytes can be separated into two different types based on the MHC molecule they recognize: $CD8^+$ cytotoxic T cells that detect peptides presented by MHC class I and $CD4^+$ T helper cells identifying antigens in the context of MHC class II, respectively [32]. MHC molecules are polymorphic, polygenic and co-dominantly expressed leading to a high diversity of MHC molecules within the human population [33]. MHC class I molecules present endogenous antigens that derive from cytosolic proteins and are expressed by all nucleated cells thus allowing surveillance of the protein expression profile of a distinct cell. This enables the recognition of virus infected or carcinogenic cells [34,35]. In contrast, MHC class II molecules are predominantly present on APCs and display exogenous peptides, enabling monitoring of surrounding tissues [35,36]. However, in a process called cross presentation DCs may also present exogenous peptides on MHC class I and endogenous peptide on MHC class II molecules to be able to activate both T cell subsets against intracellular and extracellular antigens [26]. After maturation, T cells leave the thymus as naïve T cells and migrate to lymphoid tissues in quest for DCs presenting their cognate peptide. T cells recognize antigens with their unique, dimeric T cell receptor (TCR) that consists of a α-chain plus a ß-chain and is generated through random gene rearrangement of different DNA

segments during T cell development. This process is called somatic variable-(diverse-)joining- (V-(D-)J-) recombination and leads to a high TCR diversity against almost every conceivable antigen [37]. Furthermore, combination of various α chains with a single ß-chain and exclusion of different nucleotides at the edges of the DNA segments (somatic hypermutation) lead to an even greater TCR diversity [37]. In addition, also T cell subtypes exist that express a γδ-chain yet those γδ T cells rather seem to be involved in innate immune processes or recognition of lipids [38,39].

After antigen recognition on a DC, T cells are activated to become proliferating differentiated T cells by three different signals that they receive from the APC. First, the recognition of a cognate peptide by their antigen-specific TCRs which is presented on MHC molecules (signal 1), second engagement of co-stimulatory molecules that are expressed by the APC with CD28 expressed on the T cell site (signal 2) and third a differentiation signal which is induced by cytokines (signal 3) [40]. In addition, activation of cytotoxic $CD8^+$ T cells requires additional stimulation by cytokines that are secreted by $CD4^+$ T helper cells or by the APC [41]. After activation and recognition of their antigen on another cell, they are capable of lysing the cell by e.g. a perforine/granzyme B-dependent mechanism (Figure 1) [42].

In contrast, $CD4^+$ T cells differentiate into different T helper subtypes like for example T_H1, T_H2 or T_H17 T helper cells, based on the cytokine expression profile of the T cell-stimulating APC (Figure 1) [29]. IL-12 facilitates generation of T_H1 cells which predominantly produce IFN-γ and tumor necrosis factor-α (TNF-α) and are important mediators of anti-viral, anti-bacterial (intracellular) or anti-tumor immunity yet may also induce autoimmune diseases [43], whereas IL-4 induces IL-4, IL-5 and IL-13 producing T_H2 cells that contribute to clearance of parasite infections but are also implicated in the pathogenesis allergies [44]. T_H17 cells arise by the synergic effect of IL-6, IL-23 and TGF-ß and secrete large amounts of IL-17A, IL-17F, IL-21 and IL-22. They are involved in anti-microbial and anti-fungal immunity but may also induce autoimmunity if not properly regulated [45]. Apart from effector T helper cells, $CD4^+$ T cells can also differentiate into regulatory T cells (Tregs). Their differentiation occurs either in the thymus (nTregs) or in the periphery (pTregs). Tregs contribute to preservation of immune homeostasis by limiting immune responses towards self-antigens, commensal bacteria or ingested food antigens (Figure 1) [46].

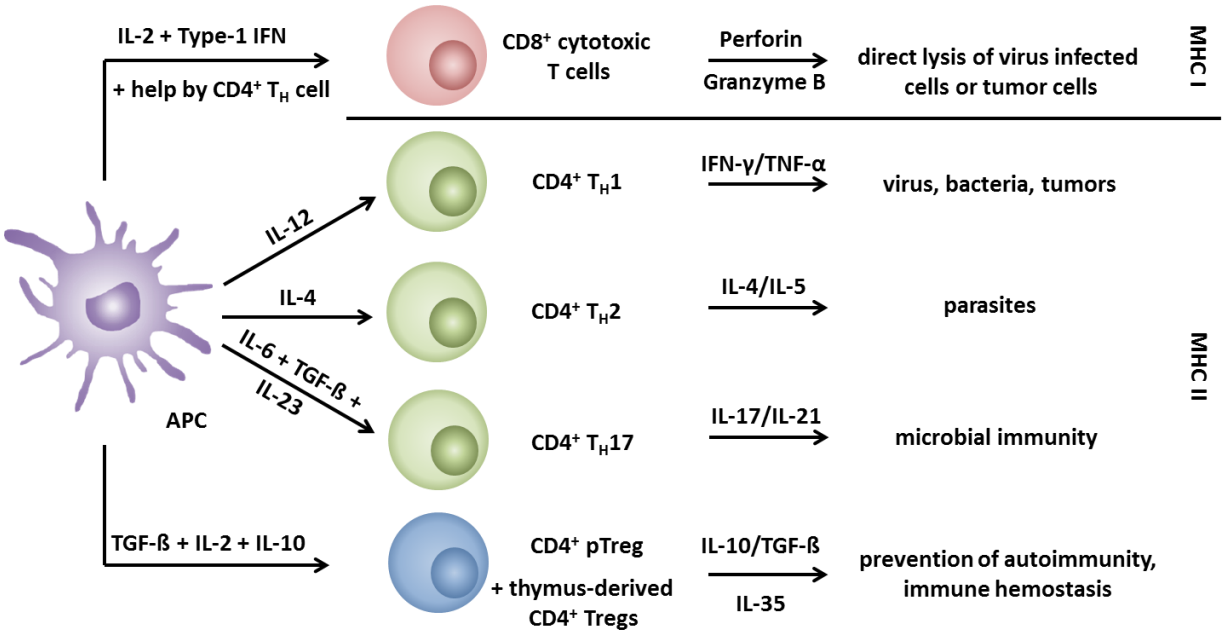

Figure 1: T cell differentiation.
APC stimulation results in T cell differentiation of naïve T cells into different effector T cell populations according to the cytokine stimulus (signal 3) of the APC in the context of of peptide/MHC molecule presentation. Effector T cells are then characterized by distinct functions and secretion of different cytokines. In contrast to $CD4^+$ T cells, $CD8^+$ T cells need additonal help from $CD4^+$ T cells for activation.

1.3. Mechanisms of immune tolerance

The induction of tolerance is an indispensable feature of the immune system to prevent excessive immune responses towards self-antigens, commensal bacteria or ingested antigens, thus preventing autoimmunity and undesired immune responses. Focusing on anti-tumor immune responses, tolerance induction may also foster tumor progression [47]. Immune tolerance is either established in the thymus, which is called central tolerance or in the periphery, termed peripheral tolerance [48].

1.3.1. Mechanisms of central tolerance

After generation in the bone marrow, double-negative ($CD4^-/CD8^-$) lymphoid progenitors migrate into the thymus for maturation. After passing through four distinct double-negative stages in which they begin expressing the newly arranged TCR, they become double-positive ($CD4^+/CD8^+$) and are positively selected for the ability to recognize antigens which are presented on body's own MHC peptides on cortical epithelial cells (positive selection) [49]. Subsequently, T cells are either $CD4^+$ or $CD8^+$ and enter a negative selection process which occurs in the thymic medulla and is conducted by presentation of self antigens on DCs and medullary epithelial cells through the autoimmune regulator AIRE. During the processes of positive and negative selection, T cells that do not recognize self-MHC molecules or exhibit strong activation towards self-peptides enter apoptosis and are eliminated [49,50]. Even though

only 5% of the T cell progenitors that enter the thymus escape those rough intrathymic clonal selection processes, this is not sufficient to prevent autoimmunity and excessive immune responses in the periphery. Since, other tolerance mechanisms have evolved and are summarized under the term peripheral tolerance.

1.3.2. Mechanisms of peripheral tolerance

Mechanisms of peripheral tolerance include ignorance of an antigen, induction of anergy, suppression by Tregs, and clonal deletion, respectively [51]. Ignorance describes the neglect of certain peptides and occurs towards low immunogenic antigens meaning that they are expressed at low levels, exhibit a low binding affinity or are located at immune privileged sites which are characterized by reduced expression of MHC molecules, expression of immunomodulatory receptors or secretion of tolerance-associated cytokines [51]. Anergy can result if a T cell engages its cognate antigen without any co-stimulatory signals and depicts a state of low IL-2 secretion plus antigen-unresponsiveness even after receiving strong activation signals [52]. In addition, $CD4^+$ Tregs, that are generated in the thymus (nTregs) by high TCR affinity towards MHC class II-self-antigen complexes in the presence of IL-2 contribute to control and limit undesired immune responses in the periphery [53,54]. Tregs as such were first described by Shimon Sakaguchi in 1995 as a subset of $CD4^+$ T cells that constitutively express the IL-2 receptor α-chain (CD25) at high levels and exhibit greatly enriched suppressive activity [55]. Adoptive transfer of Tregs alleviates autoimmune diseases or delays transplant rejection by various different mechanisms that include cell contact-dependent suppression and secretion of immunomodulatory cytokines. [46,56,57]. Forkhead-Box-Protein P3 (Foxp3) is the master transcription factor of Treg development and function and is sufficient to distinguish Tregs from other T cell types in mice. In humans additional markers are required for Treg discrimination thus nTregs are defined as $CD4^+CD25^+CD127^-Foxp3^+$ [56]. Other nTreg marker e.g. include glucocorticoid-induced TNFR family-related protein (GITR), OX40 (CD134), L-selectin (CD62L), and cytotoxic T lymphocyte-associated molecule 4 (CTLA-4) [46]. Furthermore, APCs are also capable of inducing peripheral tolerance. As already mentioned, DCs, e.g. when they mature in the presence of IL-10, can induce the conversion of naïve T cells towards pTres and give e.g. rise towards type 1 Tregs (T_R1 cells) that secrete high amounts of IL-10 and intermediated levels of TGF-ß, T_H3 cells which are induced by food antigens in the context of oral tolerance or other T cell subsets with regulatory capacity [46]. In addition, if an antigen is very abundant and constantly presented by an APC it may lead to apoptosis induction in the responding T cells [58]. Apoptosis induction also occurs by expression of Fas (CD95) upon T cell activation to prevent excessive immune responses [59].

1.3.3. Tumor-associated tolerance mechanisms

Since Rudolf Virschow proposed in 1863 that cancer may arise from sites of chronic inflammation a lot of effort has been done to reveal the complex interactions of tumor and immune cells leading to various hypothesis of those the aforementioned principle of “cancer immunoediting” by Robert D. Schreiber is the most commonly accepted [8,60]. After surviving elimination and slippage through the equilibrium phase, immune escape is the final stage of cancer immunoediting. It describes the modulation of the immune system by cancer cells to prevent being attacked, which then may lead to a clinical relevant tumor. Those tumor-associated tolerance mechanisms promote tumor growth and thereby limit the success of conventional therapies. Tumor escape may occur due to cell-intrinsic mechanisms like for example changes in tumor antigenicity, alteration in tumor cell metabolism or signal transduction events, and changes in the expression of MHC molecules [7]. Furthermore, tumor cells use host’s regulatory mechanisms to actively suppress immune responses (Figure 2). For instance, tumor cells secrete immunomodulatory cytokines like IL-6, IL-10, TGF-ß or vascular endothelial growth factor (VEGF) that may suppress T cell effector function, modulate DC maturation and induce Tregs (Figure 2) [61]. In addition, cancer associated immune cells in the tumor microenvironment like tolerogenic DCs, monocyte-derived suppressor cells (MDSCs) or Tregs greatly support and reinforce those immune regulating processes (Figure 2) [62]. IL-10, at least in the context of a tumor micromilieu, is one of the most potent anti-inflammatory cytokines that is secreted by many tumors for example stage-dependently in malignant melanoma [63,64]. In addition it is also secreted by tumor-associated immune cells, especially MDSCs, tolerogenic DCs or Tregs [65]. Major effects of IL-10 that signals through activation of the transcription factor (STAT3) are downregulation of MHC class I and II expression, downscaled co-stimulatory capacity and reduced secretion of pro-inflammatory cytokines by APCs [64]. In addition IL-10/STAT3 mediated tolerance reduces $CD8^+$ T cell mediated cytotoxicity and induces Tregs [66-69]. In tumor cells phosphorylated STAT3, which is additionally induced by IL-6, stimulation of epidermal growth factor receptors (EGFR), non-receptor tyrosine kinases like src or TLR stimulation, results in cell proliferation, inhibition of apoptosis, induction of angiogenesis and augments cell migration, which may lead to metastasis formation [70,71]. Finally, activation of STAT3 also leads to secretion of IL-10 creating a positive feedback loop of the immunosuppressive axis [71].

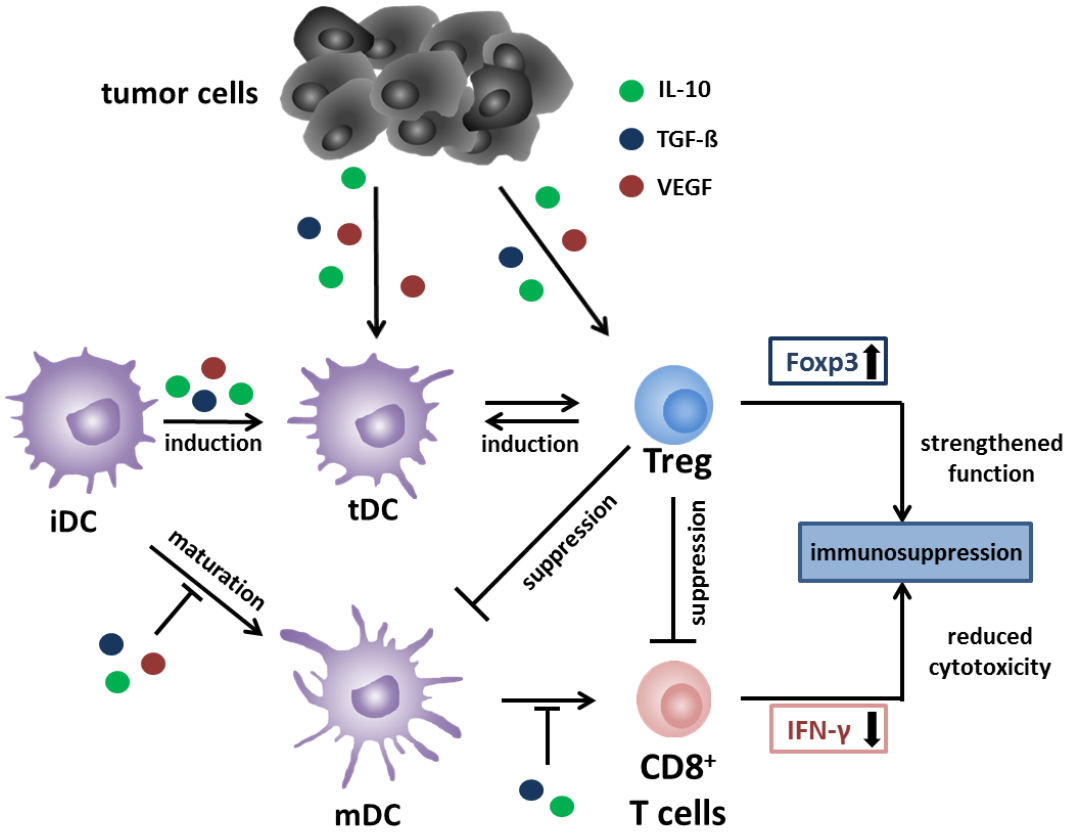

Figure 2: Tumor-associated tolerance mechanisms.
The figure illustrates the principle of immunosuppression induced by tumor cells and tumor-associated immune cells due to secretion of immunomodulatory cytokines which leads to induction of Tregs and tolerogenic DCs, but also inhibits DC maturation and generation of effector T cell function, leading to a broad spectrum of immunosuppression and tumor escape.

1.4. Requirement for targeted drug delivery for cancer immunotherapy

In recent years anti-cancer immunotherapy has become a clinically relevant therapeutic option for many late stage tumor patients with steady promotion of new drug approvals and an immense pipeline of lately developed immunomodulatory substances in clinical studies. Nonetheless, drugs that are designed to activate the immune system are prone to unintendedly disturb the tight balance of immune activation and immune tolerance in healthy tissues [12]. Therefore, directed drug delivery platforms appear to be a promising tool to avoid off-target effects while preserving or even improving anti-tumor properties [17].

1.4.1. Recent development in cancer immunotherapy

Although surgery, chemotherapy and radiation as cancer therapeutics are constantly improved in terms of accuracy and specificity, particularly metastatic cancer can hardly be controlled by those treatment options. Tumor immunotherapy offers distinct advantages over conventional therapies. Theoretically, tumor-antigen specific T cells are capable of reaching

tissues that are inaccessible for a surgeon and when appropriately stimulated can additionally attack distant metastasis, including undetectable microscopically small tumorous lesions without affecting other tissues. In addition, contrary to chemotherapy or radiation they are capable of killing slowly dividing cells, for example cancer stem cells and establish a memory response leading to long term protection [11]. Available immunotherapies include stimulatory cytokines, cell-based therapies or immune checkpoint inhibition [12].

The idea behind cytokines as targets in cancer immunotherapy is the direct stimulation of effector immune cells at the tumor site to induce anti-tumor immunity with durable responses. Especially IL-2, granulocyte-macrophage colony-stimulating factor (GM-CSF), and IFN-α have been used as potential candidates. However, low response rates, high-dose toxicity, serious systemic inflammation but also rather unexpected side effects like the vascular endothelial leakage syndrome during IL-2 therapy display major obstacles for cytokine therapies [72].

Cell-based immunotherapies can be divided into DC-based vaccinations or adoptive T cell transfer and represent excellent tools to produce a high anti-tumor T cell avidity thereby specifically targeting tumor antigens with low off-target effects. For approaches of DC-based vaccination DCs are obtained from the patient's PBMCs, loaded with a tumor-specific antigen plus an activation stimulus and then are reinjected. This attempt is characterized by low toxicity and led to the approval of sipuleucel-T by the Federal Drug Administration (FDA) in 2010 for the treatment of metastatic prostate cancer [73]. Adoptive T cell transfer describes techniques to either isolate tumor infiltrating lymphocytes (TILs) from the patient's tumor site expand them *ex vivo* and reinfuse them into the patient, genetic T cell engineering to introduce synthetic TCRs or chimeric antigen receptors (CARs) that are directed towards tumor antigens [74]. However, the expansion of TILs is limited to melanoma as the most immunogenic tumor. In addition for application of synthetic TCRs, the target antigen needs be presented on MHC class I molecules on the tumor. In contrast CARs that are generated by an antibody-variable region that is fused to the constant region of a TCR broaden adoptive T cell therapies to theoretically all malignancies and antigens [75]. So far the best clinical responses of CARs were obtained in B-cell related malignancies largely due to CD19 which is expressed across most of the B cell differentiation stages and serves as an excellent antigen. Thus, Kymriah (tisagenlecleucel) which targets CD19 together with a TNF receptor superfamily member 9 (4-1BB) co-stimulatory domain was approved as the first cell-based gene therapy by the FDA in 2017 [76,77]. For other malignancies the lack of tumor-specific, highly-expressed antigens that should preferably be indispensable for tumor survival due to possible tumor escape by downregulation is the greatest obstacle of all cell-based therapies [78,79]. In addition, tumor-associated tolerance mechanisms, lack of long lasting

responses and high costs impede the approval and further investigation of those promising therapy options [12].

Albeit, the most promising and advanced approach in cancer immunotherapy are immune-checkpoint blockades with the most established checkpoint inhibitors ipilimumab (anti-CTLA - 4 monoclonal antibody (mAb)) and pembrolizumab or nivolimumab (anti-programmed cell death protein (PD)1 monoclonal antibodies), which were approved for the treatment of melanoma by the FDA in 2011 and 2014, respectively, but also show clinical efficacy in other tumor types [80]. CTLA-4 is a surface molecule that is present on activated T cells or Tregs. In activated T cells, CTLA-4 dampens immune responses by outcompeting CD28 on binding CD80 and CD86 on APCs and preventing signaling downstream of the TCR, whereas Tregs use CTLA-4 as a suppressive mechanisms mainly to inhibit APC function [81]. In contrast, PD1 is expressed by antigen-experienced T cells and binds to PD-L1 or PD-L2 which are expressed by many tumors but also represent inhibitory ligands of APCs. PD1 activation leads to induction of apoptosis and to inactivation of the phosphoinositide 3-kinase (PI3K)/ protein kinase B (PKB) signal cascade, resulting in blockade of the production and secretion of cytotoxic mediators in T cells [82]. Blockade of either CTLA-4 or PD-1 or a combination of both exhibits potent anti-tumor responses, leading to a prolongation of overall survival. In some patients even long-lasting, sufficient clinical responses were observed. However, only a small subpopulation of patients gain benefits from immune checkpoint blockade and severe immune-related adverse effects (irAEs) can be observed greatly limiting its potential [78,80]. In addition, multiple other immune checkpoint pathways and furthermore activation of immunostimulatory receptors as for example the 4-1BB co-stimulus in Kymriah (tisagenlecleucel) are targets for tumor immunotherapy. Even though the immunotherapeutic options can also be combined, it becomes apparent that cancer immunotherapy would greatly benefit from targeted drug delivery.

1.4.2. Nanodimensional, polymeric therapeutics for tumor immunotherapy

The most relevant advantages of targeted therapies are the opportunity to specifically address tumor sites or distinct cell populations and to enhance the pharmaceutical properties for example protection of the drug and regulation of the release characteristics. Furthermore, nanoparticles offer the opportunity to deliver different therapeutics at once. These advantages lead to improvement of therapeutic efficacy and a reduction of side effects. In addition, nanoparticles also enable the delivery of poorly soluble agents and may increase blood half-life of the agents [83]. General requirements for nanomaterials in tumor immunotherapy are a long circulation time, meaning to avoid both clearance through the kidney but also minimize accumulation in the liver or undesired uptake by the reticuloendothelial system [84]. Hydrophilic Poly(ethylene-glycol) (PEG) is often used to

increase solubility and circulation time of proteins or nanoplatforms possibly by modulation of the formation of a protein corona after injection into the bloodstream [85,86]. PEG additionally causes shielding of the nanoparticles reducing immunogenicity and preventing unspecific uptake [87]. However, other biomaterials might also be used to achieve this effect like for example hydroxyethyl starch (HES) which is used in the clinic as volume expander or a combination of HES and PEG [88].

Leading immunotherapeutic agents directly to the tumor mainly depends on the enhanced permeability and retention (EPR) effect. It predicts that nanoparticles of a suitable size can enter a tumor through its primitive, leaking vascularity but prevent drainage through the defective tumorous lymph system resulting in a passive accumulation inside the tumor tissue. Particle sizes that are designed to exploit the EPR effect are usually around 10-100 nm in diameter but EPR also depends on shape, charge and potential protein absorption of the particles after injection [89,90]. Furthermore, not all tumor types initiate the formation of a primitive vasculature [91]. Still, in addition to induce accumulation of cytotoxic drugs in the tumor, the EPR effect has also been used to concentrate immunotherapeutics in the tumor proximity for example the STAT3 inhibitor sunitinib which successfully inhibited STAT3-mediated immune tolerance resulting in a pro-inflammatory remodeling of the tumor microenvironment [92].

In other approaches, immune cells (and also tumor cells) are also cell-specifically targeted *in vivo* by ligand-mediated drug delivery allowing cell-type specific accumulation of drugs [93]. Targeting of DCs, as initiators of adaptive immune responses, via antibodies, carbohydrates or peptides is the most frequently used approach [93,94]. However, the main obstacle for immune cell specific targeting is the quest for a targeting receptor that is exclusively expressed on the desired cell population. Promising receptors for DC-based vaccination are for example DEC-205, DC-SIGN, the mannose receptor, Fc receptors, CD40, or CD11c although they are not DC-specific [95]. In a phase 1 clinical trial nanoparticles targeting DCs by using anti-DEC205 antibodies initiated antigen presentation and robust humoral and cellular responses [96].

Following reaching their requested destination, the next requirement on directed drug delivery platforms is intracellular or intratumoral drug release. For instance, intracellular drug release is achieved by introducing reducible disulfide bounds (which can be cleaved inside the cytoplasm by reducing enzymes, for example the glutathione reductase) [97], pH responsive crosslinker (that get hydrolyzed in the acidic lysosomes)[98,99], or protein parts (which can be cleaved by intracellular proteinases into the nanoparticle shell)[100]. Tumor tissue specific release can be triggered by the synthesis of sensitive shells towards changes in pH, redox state and enzymes that are associated within the tumor microenvironment [101].

1.5. Biological function of IL-2 and the IL-2 receptor

The 15kDa protein IL-2 was discovered in 1976 as stimulatory *in vitro* growth factor for T lymphocytes [102]. However, following studies, especially with IL-2 and IL-2 receptor deficient mice that exhibit a breakdown of self-tolerance which is characterized by lymphoadenopathy, splenomegaly and severe inflammation in the gut due to lack of Tregs, demonstrated the crucial role of IL-2 in regulating immune homeostasis under non-inflammatory conditions [103].

IL-2 either signals through the dimeric or trimeric IL-2 receptor. The dimeric low affinity IL-2 receptor (K_d: 10^{-9}) that consists of the ß-chain CD122 (which is also used by IL-15) and the common γ-chain CD132 (which is additionally used by IL-4, IL-7, IL-9, IL-15 and IL-21) is mainly expressed on memory $CD8^+$ T cells and NK cells. The α-chain CD25 is the additional component of the high-affinity (K_d: 10^{-11}) trimeric IL-2 receptor, that is constitutively expressed on Tregs, transiently on activated $CD4^+$ and $CD8^+$ T cells and to a lower extent on activated B cells, NK cells and certain non-immune cells (like endothelial cells). Additionally, CD25 is expressed on DCs, yet without CD122 and CD132 and binds IL-2 with low affinity (K_d: 10^{-8}) which may be utilized to present IL-2 *in trans* to antigen-specific T cells [104]. IL-2 initially binds to CD25 leading to recruitment of CD122 and CD132 and internalization of the IL-2/IL-2 receptor complex followed by downstream signaling mainly via STAT5, PI3K/PKB and MAP kinases [105-108].

In steady state IL-2 is mainly produced by $CD4^+$ T cells and to a smaller extent by $CD8^+$ T cells and NK cells. Following immune activation, IL-2 is vigorously produced by activated $CD4^+$ and $CD8^+$ T cells and by DCs yet in much lower amounts [109]. The low but constant production of IL-2 under steady-state condition is indispensable for Treg development and homeostasis, whereas local high IL-2 concentrations during immune stimulation causes proliferation of recently activated or memory T cells, and NK cells [108]. According to these bifunctional characteristics of IL-2, low-dose therapy leads to expansion of Tregs and may be suitable for treatment of chronic inflammatory disease like for example type 1 diabetes, systemic lupus erythematosus and graft versus host disease by enhancing Treg function [110]. In contrast, high-dose IL-2 may be used for immunotherapy against cancer because of its stimulatory capacity of effector T cells and NK cells as shown for melanoma and renal cell carcinoma [111,112]. However, low-dose IL-2 also slightly activates effector T cells and high doses also influence Tregs. In addition, IL-2 therapy induced serious side effects including the life-threatening vascular leak syndrome [113]. This led to the development of two IL-2/mAb complexes to more preferentially target dimeric and trimeric IL-2 receptor-expressing immune cells, respectively. The antibody S4B6 targets the CD25 binding site of the IL-2 molecule resulting in a preferential engagement of IL-2 with dimeric IL-2 receptor-expressing cells like of memory T cells and NK cells, whereas the antibody JES6-1 mimics linkage to CD122 and therefore preferably addresses trimeric IL-2 receptor expressing Tregs [114].

1.6. Motivation

Even though anti-tumor therapies are constantly improving in terms of accuracy and efficacy, especially late stage cancer remains one of the leading causes of death worldwide [1]. Tumor-associated tolerance mechanisms promote tumor growth and critically dampen the success of conventional therapeutic interventions [115]. By secretion of immunomodulatory cytokines like IL-10 and TGF-ß, cancer cells induce or reinforce the function of various regulatory immune subsets, like for example tolerogenic DCs and Tregs, which then further enhance immunosuppression [61,62]. For instance, Tregs, that are also cancer associated within the tumor microenvironment, are capable of suppressing immune responses either cell contact-dependently or by secretion of anti-inflammatory cytokines such as IL-10 [46]. IL-10, which signals through the transcription factor STAT3, mondifies Tregs function in various ways. First, one of the suppressive mechanisms of Tregs is the secretion of IL-10 which then influences surrounding immune cells or tumor cells [116]. Second, Tregs are directly affected by IL-10 induced STAT3, reinforcing their immunosuppressive function [67,68]. Even though, being one of the most important cell types in the tumor microenvironment that greatly contribute to tumor immune escape, direct targeting of Tregs remains an obstacle due to low endocytic activity of T cells [117]. In their first description by Sakaguchi et al. in 1995, Tregs were defined as $CD25^+$ expressing $CD4^+$ T cells [55]. CD25 is the α chain of the high affinity IL-2 receptor that additionally consists of CD122 and CD132. After binding of IL-2, the ligand/receptor complex gets internalized [118,119]. The rationale behind of this study is to cell-type specifically target T cells with a focus on Tregs via the high affinity IL-2 receptor using human IL-2 functionalized hydroxyethyl starch (HES) nanocapsules (NC) for tumor immunotherapy. The cell type specific targeting may be used to inhibit Treg function that may be beneficial for establishing efficient, long lasting anti-tumor immune responses [120]. Targeting of Tregs should be combined with inhibition of Treg function by STAT3 blockade. For this purpose, ovalbumin protein NC are synthesized to efficiently carry the specific STAT3 inhibitor S3I-201 to inhibit IL-10- and STAT3-mediated tolerance mechanisms. Protection of the therapeutic agent and the possibility of cell-type specific targeting may lead to enhanced efficacy, as free, systemically applied STAT3 inhibitors induce serious side-effects, most prominently neurotoxicity [121]. Furthermore, low water solubility and insufficient accumulation at target tissues are main obstacles of anti-STAT3 cancer therapy [121].

II Material and Methods

2.1. Materials

2.1.1. Laboratory equipment

Autoclav	H+P Labortechnik GmbH, Oberschleißheim, Germany
Balance	MC1, Laboratory LC 2200P, Sartorius, Göttingen, Germany
Centrifuges	Megafuge 1.0.R, Thermo Fisher Scientific, Karlsruhe, Germany Centrifuge 5415D, Eppendorf, Hamburg, Germany
Cleanbench	HeraSafe, Thermo Fisher Scientific, Langenselbod, Germany
ELISA microplates reader	Medel 450, Bio-Rad Laboratories, München, Germany Software: KC Junior Bio-Tek Instruments GmbH, Bad Friedrichshall, Germany
Flow – cytometer	BD LSR Flow Cytometer, Becton Dickinson, Heidelberg, Germany Software: FACS Diva 6, Becton Dickinson, Heidelberg, Germany BD LSRFortessa, Becton Dickinson, Heidelberg, Germany Software: FACS Diva 6, Becton Dickinson, Heidelberg, Germany
Neubauer hemocytometer	Neubauer's hemocytometer, Merck, Wiesbaden, Germany
Incubator	HERAcell 240, Thermo Scientific, Karlsruhe, Germany
Microscope	Diaplan, Leitz, Wetzlar, Germany Olympus LH50A, Olympus, Tokia, Japan Confocal Leica TCS SP5, Leica Microsystems, Wetzlar, Germany
Semiautomatic cell harvester	SKATRONAS, SKATRON, Lier, Norway
ß-scintillation counter	LKB, Bromma, Sweden
Stiring Wheel	Thermo Fisher Scientific, Karlsruhe, Germany
Water bath	Julabo TW 12, Julabo Labortechnik GmBH, Seelbach, Germany

2.1.2. Plastic ware and consumables

8 well Nunc Lab-Tek Chamber Slides	Fisher Scientific, Schwerte, Germany
Assay plastic wrapping 102 x 258 mm	Wallac, Turau, Finland
Brand Handystep	Brand GmbH, Wertheim, Germany
Brand PD tips, 2.5 ml	Brand GmbH, Wertheim, Germany
Cannulas, single-use cannulas	B.Braun Melsungen AG, Melsungen, Germany
Cell culture plate, 6-wellcell culture plate	Costar, Bodenheim, Germany
Cell culture plate, 12-well cell culture plate	Costar, Bodenheim, Germany
Cell culture plate, 24-well cell culture plate	Costar, Bodenheim, Germany
Cell culture plate, 96-well cell culture plate, flat bottom	Costar, Bodenheim, Germany
Cell culture plate, 96-well cell culture plate, (unsterile)	Costar, Bodenheim, Germany
Cell Strainers 70µm	Fisher Scientific, Schwerte, Germany
Centrifuge tubes 15 ml / 50 ml tubes	Greiner GmbH, Frickenhausen, Germany
Corning cell culture flasks 75cm^2	Sigma-Aldrich, Darmstadt, Germany
Disposable fine dosage syringes, 1 ml	BRAUN, Melsungen, Germany
Filter paper A 120 x 258 mm	Wallac, Turau, Finland
Glass pipette, 10 ml	Greiner GmbH, Frickenhausen, Germany
Injekt-F, single-use syringes, 1 ml	B. Braun Medical AG, Melsungen, Germany
DynaMag-50 Magnet	Thermo Scientific, Karlsruhe, Germany
Greiner Cell Scrapers	Sigma-Aldrich, Darmstadt, Germany
MACS LD (depletion) column	Miltenyi Biotec GmbH, Bergisch Gladbach, Germany
MACS LS (enrichment) column	Miltenyi Biotec GmbH, Bergisch Gladbach, Germany
MidiMACS Separator	Miltenyi Biotec GmbH, Bergisch Gladbach, Germany
Pipette tips, 10 µl, 200 µl, 1000 µl	Greiner GmbH, Frickenhausen, Germany
Sterile filter 0.2 µm	Pall GmbH, Dreieich, Germany
M-Dish$^{35mm, low}$	ibidi GmbH, Planegg, Germany

2.1.3. Reagents

ACK Lysing Buffer	Lonza, Verviers, Belgium
Aqua dest.	B.Braun Melsungen AG, Melsungen, Germany
BD Phosflow Fix Buffer I	BD Bioscience, Heidelberg, Germany

BD Phosflow Permeabilization Buffer II	BD Bioscience, Heidelberg, Germany
BD Pharmingen Stain Buffer	BD Bioscience, Heidelberg, Germany
BSA	Bovine serum albumin, PAA Laboratories GmbH Pasching, Austria
C^3 [H]-thymidine	ICN Biomedicals GmbH, Eschwege, Germany
Cell Mask Deep Red	Thermo Fisher Scientific, Karlsruhe, Germany
Cell Mask Orange	Thermo Fisher Scientific, Karlsruhe, Germany
DPBS	Thermo Fisher Scientific, Karlsruhe, Germany
ebiosciences Foxp3 stainig buffer set	Thermo Fisher Scientific, Karlsruhe, Germany
EDTA	Serva, Heidelberg, Germany
Ethanol, 70%	Carl Roth GmbH, Karlsruhe, Germany
Ficoll	Lymphocyte separation medium, PAA Laboratories GmbH, Pasching, Austria
FBS	Fetal Bovine Serum, Thermo Fisher Scientific, Karlsruhe, Germany
HSA	Human serum albumin, Pharmacia, Erlangen, Germany
Human IL-2 ELISA Kit	BD Bioscience, Heidelberg, Germany
KCl	Carl Roth GmbH, Karlsruhe, Germany
KH_2PO_4	Carl Roth GmbH, Karlsruhe, Germany
NaCl	Carl Roth GmbH, Karlsruhe, Germany
NA_2HPO_4	Carl Roth GmbH, Karlsruhe, Germany
Paraformaldehyde (PFA)	Merck, Wiesbaden, Germany
Penicillin-Streptomycin	Thermo Fisher Scientific, Karlsruhe, Germany
S3I-201	Thermo Fisher Scientific, Karlsruhe, Germany
Scintillation cocktail	Carl Roth GmbH, Karlsruhe, Germany
Simulect (basiliximab)	Novartis, Basel, Switzerland
Tris	Carl Roth GmbH, Karlsruhe, Germany
Trypanblue	Sigma, Taufkirchen, Germany
Tween20	Sigma, Taufkirchen, Germany
Vybrant CFDA SE Cell Tracer Kit	Thermo FisherThermo Fisher Scientific Scientific, Karlsruhe, Germany

Media

Dulbecco's Modified Eagle Medium	Lonza, Verviers, Belgium
RPMI 1640	Lonza, Verviers, Belgium
X-VIVO 20	Lonza, Verviers, Belgium

Fluorochromes

Table1: Fluorochromes.
Table 1 displays the fluorochromes that were used in this study with their maximal excitation and emission plus their abbreviation which is used in the text.

Fluorochrome	Abbreviation	Excitation peak [nm]	Emmission peak [nm]
Allophycocyanine	APC	650	660
Allophycocyanine-Cyanine 7	APC-Cy7	650	785
AmCyan	-	457	491
Cell Mask Deep Red	-	649	666
Cell Mask Orange	-	554	567
Cell Trace Violet	-	405	450
Chloromethylfluorescein diacetate	CMFDA	492	517
Fluoresceinisothiocyanate	FITC	495	519
Fixable Viability Dye eFluor 780	Fix Dye	633	780
Hoechst 33342	Hoechst	343	483
Pacific Blue	PB	401	452
Peridinin chlorophyll protein	PerCP	482	678
Peridinin chlorophyll-Cyanine	PerCP-Cy5.5	480	695
R-Phycoerythrin	PE	496	578
R-Phycoerythrin-Cyanine 5	PE-Cy5	496	667
R-Phycoerythrin-Cyanine 7	Pe-Cy7	496	785
Sulforhodamine SR101	SR101	580	605

2.1.4. Antibodies (dilution)

Flow cytometry

anti-B220 FITC (1/1000)	Rat-anti-mouse-IgG2a, clone RA3-6B2 BioLegend, Fell, Germany
anti-CD3 APC-Cy7 (1/10)	Mouse-anti-human-IgG2a, clone HIT3a BioLegend, Fell, Germany
anti-CD4 APC (1/20)	Mouse-anti-human-IgG1, clone RPA-T4 BD Bioscience, Heidelberg, Germany
anti-CD4 FITC (1/30)	Mouse-anti-human-IgG1, clone 13B8.2 Beckman Coulter, Krefeld, Germany
anti-CD4 PE-Cy7 (1/20)	Rat-anti-human-IgG2a, clone SK3 BioLegend, Fell, Germany
anti-CD4 PerCP-Cy5.5 (1/400)	Rat-anti-mouse-IgG2a, clone RM4-5 Thermo Fisher Scientific, Karlsruhe, German

anti-CD8 FITC (1/30)	Mouse-anti-human-IgG1, clone B9.11 Beckman Coulter, Krefeld, Germany
anti-CD8 FITC (1/200)	Rat-anti-mouse-IgG2a, clone 53-6-7 BD Bioscience, Heidelberg, Germany
anti-CD8 PE (1/20)	Mouse IgG1, clone HIT8a BD Bioscience, Heidelberg, Germany
anti-CD11b PE-Cy7 (1/200)	Rat-anti-mouse IgG2b, clone M1/70 BioLegend, Fell, Germany
anti-CD11c APC (1/200)	Hamster-anti-mouse IgG, clone N418 Miltenyi Biotec, Bergisch-Gladbach, Germany
anti-CD25 APC (1/10)	Mouse-anti-human IgG2b, clone 4E3 Miltenyi Biotec, Bergisch-Gladbach, Germany
anti-CD25 APC (1/100)	Rat-anti-mouse IgG1, clone PC61.5 Thermo Fisher Scientific, Karlsruhe, Germany
anti-CD25 PE (1/10)	mouse anti-human IgG2b, clone 4E3 Miltenyi Biotec, Bergisch-Gladbach, Germany
anti-CD25 PE-Cy5 (1/2)	Mouse-anti human IgG1, clone M-A251 BD Bioscience, Heidelberg, Germany
anti-CD45 AmCyan (1/100)	Mouse-anti-human-IgG1, clone 2D1 BD Bioscience, Heidelberg, Germany
anti-CD45RA FITC (1/20)	Mouse-anti-human-IgG2b, clone HI100 BD Bioscience, Heidelberg, Germany
anti-CD45RO PE (1/20)	Mouse-anti-human-IgG2a, clone UCHL1 BD Bioscience, Heidelberg, Germany
anti-CD90.2 eFluor 450 (1/200)	Rat-anti-mouse-IgG2a, clone 53-2.1 Thermo Fischer Scientific, Karlsruhe, Germany
anti-CD122 APC (1/20)	Mouse-anti-human-IgG1, clone TU27 BioLegend, Fell, Germany
anti-CD132 PE (1/4)	Mouse-anti-human-IgG2b, clone TUGh4 BD Bioscience, Heidelberg, Germany
anti-F4/80 PerCP-Cy5.5 (1/100)	Rat-anti-mouse-IgG2a, clone BM8 BioLegend, Fell, Germany
anti-FoxP3 PE (1/2)	Mouse-anti-human-IgG2a, clone PCH101 Thermo Fisher Scientific, Karlsruhe, Germany
anti-MHC class II eFluor 450 (1/800)	Rat-anti-mouse IgG2b, clone M5/114.15.2 BD Bioscience, Heidelberg, Germany
anti-NK1.1 (1/400)	Rat-anti-mouse-IgG2a, clone PK136

	Thermo Fisher Scientific, Karlsruhe, Germany
anti-STAT3 PE (1/5)	Mouse-anti-human-IgG2a, clone M59-50
	BD Bioscience, Heidelberg, Germany
anti-pSTAT3 PE (1/10)	Mouse-anti-human-IgG1, clone 4/P-STAT3
	BD Bioscience, Heidelberg, Germany
T cell stimulation	
anti-CD3	OKT3 hybridome, lab-made
anti-CD28	Mouse IgG1, clone CD28.2
	BD Bioscience, Heidelberg, Germany
Micro Beads	
CD4 MicroBeads	Miltenyi Biotec, Bergisch Gladbach, Germany
CD14 MicroBeads	Miltenyi Biotec, Bergisch Gladbach, Germany
CD25 MicroBeads	Miltenyi Biotec, Bergisch Gladbach, Germany
CD45RO MicroBeads	Miltenyi Biotec, Bergisch Gladbach, Germany
Dyna Beads	
CD8 Dyna Beads	Miltenyi Biotec, Bergisch Gladbach, Germany
CD14 Dyna Beads	Miltenyi Biotec, Bergisch Gladbach, Germany
CD19 Dyna Beads	Miltenyi Biotec, Bergisch Gladbach, Germany

2.2. Methods

All experiments were performed under sterile conditions inside a cleanbench. Cells were cultured in an incubator at 37 °C with 5% CO_2 content and 95% humidity. In general, cells were counted using a Neubauer hemocytometer counting chamber. To exclude dead cells they were first stained with trypanblue (1/10 diluted in phosphate buffered saline (PBS)) which passes damaged membranes and resulting in staining of the DNA. To wash the different cell populations, they were resuspended in ice-cold 1 x PBS (137 mM NaCl, 2.7 mM KCl, 8.1 mM Na_2HPO_4 and 1.5 mM KH_2PO_4) and subsequently spun down by 400 x g for 10 min at 4 °C. After each isolation process, cells were phenotypically analyzed using flow cytometry to investigate the purity and exclude contamination with other cell types.

2.2.1. Nanocapsule generation and characterization

2.2.1.1. Miniemulsion polymerization

Emulsions are defined as a dispersed system of two immiscible liquids by which the liquid of the dispersed phase forms droplets in the other liquid that is called the continuous phase [122]. Miniemulsions are understood as emulsions in which the droplets of the dispersed phase range from 50nm to 1µm in size, usually have to be stabilized and exhibit a reduced polydispersity compared to macro- or microemulsions [123]. In contrast to oil-in-water systems that are called direct miniemulsions, inverse miniemulsion describes the formation of water droplets in oil. The design of a miniemulsion starts with mixing of the dispersed phase with a monomer and a osmotic pressure together with the continuous phase containing a surfactant. Subsequently, a high shear force using ultrasonification or a high pressure homogenizer needs to be initialized. For the formation of NC, a crosslinker is added to initiate the polymerization at the droplets interface [122,124,125]. Since droplets are sensitive towards molecular diffusion degradation (Ostwald ripening) and coalescence caused by collision. They need to be stabilized by an osmotic pressure agent and by a surfactant to provide steric colloid stability [122]. Ostwald ripening is understood as the dissolving of small droplets and redisposition on larger ones due to different solubilities depending on the droplet size [126]. In contrast, coalescence describes the process of two particles melting to a single droplet. Ostwald ripening and coalescence lead to reduction of conventional emulsion steadiness and enlargement of the droplet size [127].

Surfactants are amphiphilic compounds that adsorb to the droplets surface, thereby lowering the surface tension between the two immiscible liquids. In addition to stability, the amount of surfactant influences the droplet size which may be useful for capsule engineering [122]. In the present study, NC were generated by inverse (water-in-oil) miniemulsion polymerization which offers the advantage of encapsulating hydrophilic compounds.

2.2.1.2. Generation of HES-D-IL-2 nanocapsules

HES-D-IL-2 NC were kindly manufactured and characterized in the working group of [redacted] by [redacted] from the Max Planck Institute for Polymer Research in Mainz. First, hydroxyethyl starch capsules were generated by a polyaddition reaction in an inverse miniemulsion as previously described [88,128]. The aqueous dispersed phase consisted of water-soluble hydroxyethyl starch that was mixed with the fluorescent dye sulforhodamine SR101 which was used for NC tracking. Alongside, the oil soluble surfactant poly(ethylene-co-butylene)-b-(ethylene oxide) (PB/E-*b*-PEO) was mixed with the co-stabilizer cyclohexane representing the continuous phase. After mixing the two phases by stiring the emulsion, the homogenization step was initiated by ultrasonication

under ice-cooling conditions. Subsequently, the polymerization was started by the addition of the crosslinker toluol-2,4-diisocyanate (TDI) at 25° C under mechanical steering. The reaction takes place between the hydroxyl groups of the hydroxyethyl starch and the isocyanate groups of the TDI. After synthesis, nanocapsules were purified by dialysis and centrifugation in order to remove residual amounts of TDI and redispersed in cyclohexane [88]. To introduce amine groups on the NC surface for further modification, the capsules were mixed with TDI and stirred. Following, the NC were redispersed in aqueous solution by sonification and addition of the water-soluble surfactant sodium dodecylsulfat (SDS). After redispersion in aqueous solution, the HES-NC were dialyzed and centrifuged for purification and removal of residual SDS.

Afterwards, HES-NC were functionalized with dibenzylcyclooctyne (DBCO) to obtain reactive, ring-strained alkyne groups. Therefore, the NC solution was mixed with a DBCO-PEG_5-NHS ester to initiate a NHS ester reaction between the amine groups of the capsules and the NHS ester and residual DBCO was removed by centrifugation. Those DBCO functionalized HES NC (HES-D) served as controls in some of the *in vitro* and *in vivo* experiments.

For simultaneous N-terminal azid functionalization of IL-2, human recombinant IL-2 was mixed with a NHS-ester-PEG_4 azide to conduct a NHS ester reaction resulting in IL-2-N3. IL-2-N3 was subsequently linked to alkyne functionalized HES-D by copper-free click reaction. Copper free click reaction is a very specific, fast reaction because of the high ring-strain of the alkyne group in the DBCO molecule and it is biocompatible because no toxic catalyst is required [129]. The azide-alkyne cycloaddition reaction takes place between the alkyne-bearing ring of the cyclooctine and the azide-bearing IL-2, resulting in the formation of a triazole ring [129]. After the reaction, NC were dialyzed twice and transferred into isotonic NaCl (0.9%). For some experiments, in addition to the IL-2 functionalized NC (HES-D-IL-2), NC with a twofold (HES-D-IL-$2_{/2}$) an tenfold reduced (HES-D-IL-$2_{/10}$) amount of IL-2 on the NC surface were generated by adding the respective amount of IL-2 during copper-free click reaction.

2.2.1.3. Generation of ovalbumin protein nanocapsules

The ovalbumin protein NC were kindly generated and characterized by [redacted] in the working group of [redacted] at the Max Planck Institute for Polymer Research Mainz. Similar to the HES-D-IL-2 NC they were generated by inverse (water-in-oil) miniemulsion polymerization similar to previously published protocols [130]. The dispersed phase consisted of ovalbumin, the STAT3 inhibitor S3I-201 and 5-chloromethylfluorescein diacetate (CMFDA) cell tracker green respectively which were previously dissolved in DMSO. S3I-201 is a specific inhibitor of STAT3 activation which binds to the SH2 domain of STAT3 thereby preventing phosphorylation, dimerization and DNA binding [131]. CMFDA cell tracker

served to confirm uptake and release properties which were already described [100,132]. The oil-soluble continuous phase consisted of cyclohexane and the surfactant PB/E-*b*-PEO. After stiring and ultrasonification, the polyaddition reaction was initiated by dropwise addition of TDI. Following purification of the NC by dialysis and centrifugation, they were redispersed in cyclohexane and transferred into an aqueous solution by using SDS and dissolved in 0.9% NaCl.

2.2.1.4. Nanocapsule characterization

Morphological studies of the NC were performed using transmission electron microscopy (TEM) and scanning electron microscopy (SEM). In contrast to light microscopes which are usually limited by diffraction to around 200nm of resolution, electron microscopes use a beam of accelerated electrons as source which results in a resolution up to 50 pm [133]. In a TEM microscope, electrons are transmitted through a sample that needs to be thinner than approximately 100 nm. The detection of the sample structure arises from variations of different sample parts in electron transmission. Electrons that emerge from the specimen thus carry information about its structure [134].

In contrast, SEM images develop from raster scanning of the sample's surface. The sample emits secondary electrons which can then be detected and provide information about the topography and composition of the specimen's surface [135].

Size, size distribution and aggregation behavior of the NC in solution were assessed by dynamic light scattering (DLS) [136]. For DLS a laser light is shot through the solution and each molecule that is hit, diffracts light in all directions (Rayleigh-scattering). The fluctuation of the scattered light is then collected and projected onto a screen [137].

The zeta potential (ζ-potential) is understood as the electric potential of the droplets in colloidal dispersions. Charged particles in a suspension are overlaid by an ion layer (Helmholtz double layer) which results in electric neutral appearing particles. However, shearing forces that arise during particle movement may remove some of the complexed ions, shifting the electric potential [138]. The potential at the slipping plane is the zeta potential which describes the colloidal stability of the system and was analyzed by a zeta nanosizer [138].

The amount of IL-2 after azidification was investigated using Pierce BCA Protein Assay. In addition, matrix-assisted laser desorption and ionization time-of-flight (MALDI-TOF) analysis were conducted to evaluate the azidification rate of the IL-2 molecule. In principle, during MALDI molecules are ionized and subsequently their time-of-flight is analyzed by mass spectroscopy. First the specimen is embedded in a suitable matrix, then a laser is applied on the sample, absorbed by the matrix and converted to heat energy. Part of the matrix and the

sample heat up and vaporize in a process called ablation. Thereby, charged ions of differing sizes are generated out of the sample which are accelerated by a mass spectrometer and analyzed upon their time-of-flight.

To determine and quantify the amount of DBCO groups and NC-functionalized IL-2, 9-(azidomethyl)anthracene was synthesized and used [139]. Following binding to free DBCO groups via copper free click reaction, 9-(azidomethyl)anthracene is quenched via electron transfer which leads to an increase of the quantum yield, resulting in a fluorescence enhancement [140]. The signal can be scaled and re-calculated to the amount of free DBCO surface groups and surface coupled IL-2.

2.2.2. Isolation and preparation of human immune cells and cell culture

For the isolation of human T cell subsets, peripheral blood mononuclear cells (PBMCs) were isolated from buffy coats or leukapheresis products by Ficoll density gradient centrifugation. The apharesis products were obtained from healthy, adult volunteers according to an approval of the local ethics committee of Rhineland-Palatinate. Therefore, the respective blood components were mixed with DPBS (Dulbecco's phosphate buffered saline without $CaCl_2/MgCl_2$) in a 1/1 ratio and always 30 ml per 15 ml Ficoll were placed on the Ficoll gradient. After centrifugation at 400 x g and 25° C for 30 min without break, PBMCs were obtained from the emerging whitish interphase. After 3-4 washing steps with 1 x PBS, to remove remaining platelets, PBMCs were used for further isolation procedures. The generation and isolation of human activated $CD4^+CD25^+$ T cells, naïve $CD4^+CD25^-$ T cells and $CD4^+CD25^{high}$ Tregs is summarized in Figure 3.

2.2.2.1. Generation of human activated $CD4^+CD25^+$ T cells

To generate human activated $CD4^+CD25^+$ T cells, PBMCs were incubated with paramagnetic CD4 Microbeads for 15 min on ice at a density of 4 mikroliter (µl) Micro Beads and 16 µl MACS Buffer (1 x PBS supplemented with 0.5 % HSA and 3 mM EDTA) per $1x10^7$ PBMCs. After a washing step with MACS buffer, PBMCs were resuspended in 1ml MACS buffer and placed on a LS column (capacity of $2x10^9$ cells) in a MidiMACS separator. To remove unbound cells, the column was washed 3 times with 3 ml MACS Buffer and subsequently removed from the MidiMACS separator to isolate the coupled $CD4^+$ T cells by strongly rinsing the column with 4 times 5 ml MACS buffer. For evaluation of T cell proliferation by flow cytometry, isolated $CD4^+$ T cells were additionally stained with Cell Trace Violet (CTV) according to the manufacturer's protocol. Briefly, T cells were incubated with 0.5 µM CTV in 1 x PBS for 20 min at 37 °C and 5 min at room temperature at a density of $1x10^6$/ml and thereafter washed 2 times with 1 x PBS. CTV is a stable, intense fluorescent dye that stains free amines inside the cytoplasm. During cell division CTV is equally distributed to the

daughter cells resulting in thinning of the fluorescence intensity which can be visualized by flow cytometry [141]. For competition assays with naive $CD4^+$ T cells, activated T cells were stained with (5-(and-6))-carboxyfluorescein diacetate (CFDA) instead of CTV. For that purpose, activated T cells were incubated in 1 µM CFDA for 20 min at 37 °C with $1x10^7$/ml in 1 x PBS. To terminate the staining, 30 ml XVIVO20 supplemented with 10% fetal calf serum (FCS) were added. Similar to CTV, CFDA stains free amines inside the cell and gets diluted during cell proliferation. For induction of the expression of the high affinity IL-2 receptor, isolated T cells were incubated in XVIVO20 supplemented with 1 µg/ml anti-CD3 mAb and 0.5 µg/ml anti-CD28 mAb for 16 h at a density of $2x10^6$ /ml/well in a 12 well well plate. Anti-CD3 mAb stimulates the TCR, whereas anti-CD28 mAb mimics co-stimulation [142]. To control the purity and activation state of the isolated activated T cells, they were stained for CD4, CD8 and CD25 expression directly after isolation and following activation and analyzed by flow cytometry.

2.2.2.2. Isolation of human naïve $CD4^+CD25^-$ T cells

Naïve $CD4^+$ T cells were isolated as described by Kryczanowsky et al. [143] In a first step, PBMCs were incubated for 15min on ice with 5 µl CD14 Microbeads 4 µl CD25 Microbeads, and 6 µl CD45RO Microbeads plus 15 µl MACS buffer per $1x10^7$ cells. Thereafter, for depletion of $CD14^+$ monocytes, antigen-experienced $CD45RO^+$ and Tregs plus activated $CD25^+$ T cells respectively, cells were spun down, incubated in 300 µl MACS buffer and placed on a magnetic LD column (capacity of $5x10^8$ cells) that is located in a MidiMACS separator. The flow-through and 3 times 1 ml washing eluates were collected and washed 1 time with MACS buffer. To additionally enrich $CD4^+$ T cells, pelleted cells were incubated with 16 µl MACS buffer supplemented with 4 µl CD4 Mircobeads per $1x10^7$ cells for 15 min at 4 °C. Cells were centrifuged, resuspended in 1 ml MACS buffer and put on a LS column. After washing and elution, naïve T cells were stained with CTV as described for activated T cells. Purity and maturation state of the isolated naïve T cells were addressed by staining of CD4, CD8, CD25, CD45RA and CD45RO.

2.2.2.3. Isolation of human $CD4^+CD25^{high}$ Tregs

Tregs were isolated as previously described [144]. In contrast to activated and naïve T cells that derived from buffy coats, Tregs were obtained from leukapheresis products to increase the isolation yield. Initially, PBMCs were incubated with 10 µl MACS buffer supplemented with 1 µl CD25 microbeads per $1x10^7$ cells for 15 min at 4°C. Thereafter, to obtain $CD25^+$ T cells PBMCs were washed with MACS buffer, spun down by centrifugation and after resuspension in 1 ml put on a LS enrichment column which is placed on the MidiMACS separator. After washing 3 times with 3 ml MACS buffer, $CD25^+$ cells were collected by replacing the column

and rinsing of the coupled cells. Subsequently, after a washing step with MACS Buffer, cells were incubated in 10 ml MACS buffer, supplemented with $2x10^6$ CD8, $2x10^6$ CD19 dynabeads, and $1x10^6$ CD14 Dynabeads per 10^6 cells and set on a stirring wheel for 20 min at 4 °C. After addition of 30 ml XVIVO20 and another 5 min on the stirring wheel, the cell/bead mixture was put on a Dyna-Mag50 magnet, washed 3 x with MACS buffer and the particular supernatant was taken to obtain $CD4^+CD25^{high}$ Tregs. Thereafter, the cells were stained with CTV to investigate their proliferative behavior during the experiments. Subsequently, they were activated for 12-14 h overnight in XVIVO20 enriched with 0.5 µg/ml anti-CD3 and 0.25 µg/ml anti-CD28 plus 2 Units/ml (U/ml) IL-2 in 12 well plates at a density of $2x10^6$ /ml/well to obtain activated $CD4^+CD25^{high}$ Tregs that were used in further experiments. After activation, the purity of the cells was evaluated by staining of CD4, CD25, CD122, CD132 and Foxp3.

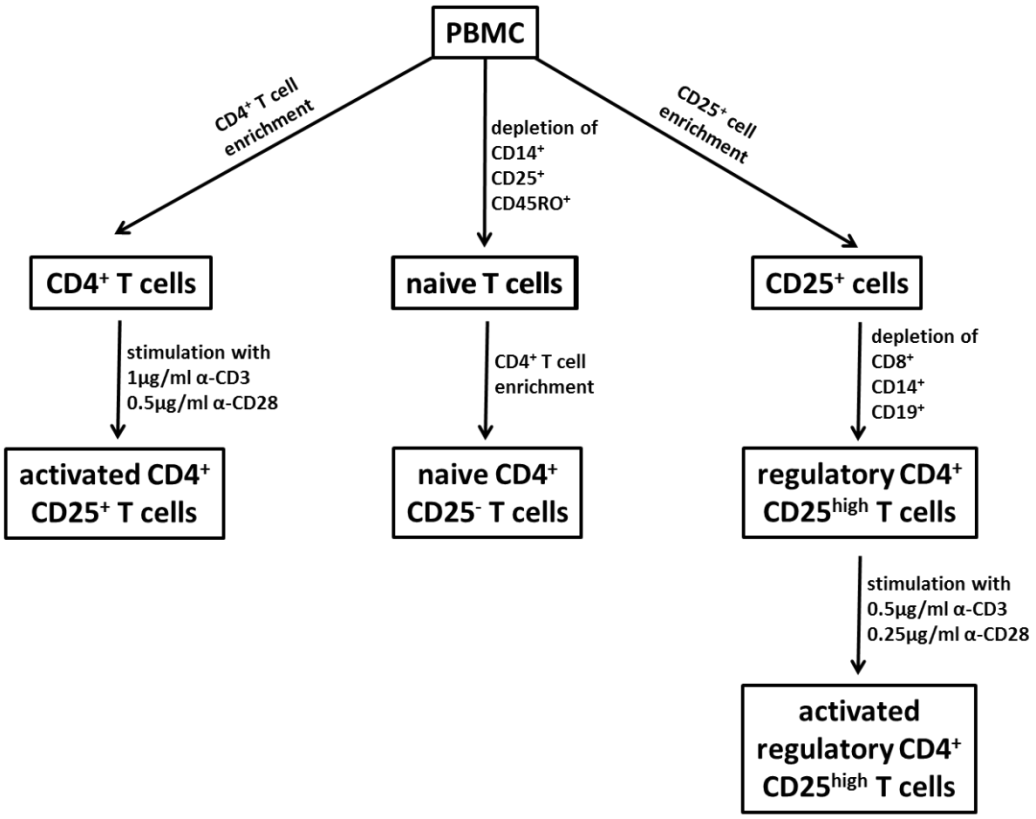

Figure 3: T cell generation and isolation.
Isolation and generation of the different human T cell subset from PBMCs that were used for uptake experiments of HES-D-IL-2 were isolated by MACS or Dyna Beads. Activated $CD4^+$ T cells were generated by $CD4^+$ T cell enrichment and stimulation with anti-CD3 mAb, anti-CD28 mAb, whereas naïve T cells were isolated by depletion of CD14, CD25 and CD45RO and subsequent enrichment of $CD4^+$ T cells. Additionally, Tregs were generated by CD25 enrichment, following depletion of CD8, CD14 and CD19 and stimulation with anti-CD3 mAb and anti-CD28 mAb.

2.2.2.4. Cell culture

HeLa cells (cervical cancer, adenocarcinoma)

The immortal HeLa cell line was isolated from a glandular cervical cancer of Henrietta Lacks in 1951 and since serves as an essential tool in Cancer Res [145]. For cell culture maintenance, HeLa cells were cultured in 75 cm^2 flasks in 15 ml Dulbecco's Modified Eagle Medium (DMEM) supplemented with 10% heat-inactivated FCS (HeLa medium) and passaged twice a week after trypsin treatment in a 1/10 ratio.

CTLL-2 cells (cytotoxic T lymphocyte)

CTTL-2 cells have derived from a subclone of T cells, that was isolated from a C57Bl/6 mouse. CTLL-2 cells depend on IL-2 for their growth [146]. For cultivation, CTLL-2 cells were grown in 6 well plates in 3 ml RPMI1640 supplemented with 10% heat-inactivated FCS, 2 mM L-glutamine and 50 µM β-mercaptoethanol (CTLL-2 medium). For cell culture maintenance 50 U/ml Proleukin (human IL-2) was additionally added. Three times a week cells were diluted to a density of approximately $1x10^4$/ml.

2.2.3. Nanocapsule uptake and release studies

2.2.3.1. Uptake/binding studies of HES-D-IL-2

Activated $CD4^+CD25^+$ T cells

The uptake/binding of HES-D-IL-2 and control capsules, respectively, and their induction of T cell proliferation, were evaluated by use of activated T cells. For this purpose, CTV^+ T cells were harvested after generation, washed twice with 1 x PBS and subsequently incubated in 750 µl XVIVO20 supplemented with 10.000 U/ml Penicillin/Streptomycin in 24 well plates with $7.5x10^5$ cells/well. The corresponding NC were added at a concentration of 1 µg/ml (in some experiments), 12.5 µg/ml (in some experiments), 25 µg/ml and 75 µg/ml. As controls, activated T cells alone and activated T cells with the addition of 50 U/ml Proleukin were additionally investigated to stimulate maximal proliferative capacity [147]. After 72 h, cells were flushed of the plates by vigorous rinsing, washed with 1 x PBS and stained with Fixable Viability Dye eFluor780 (1/1000 in 1xPBS) for 30 min at 4° C to determine viability of the examined cells. Fixable Viability Dye stains free amines inside the cell. However, the dye will only penetrate the damaged membrane of dead cells [148]. After a washing step with 1 x PBS cells were fixed with 4 % paraformaldehyde (PFA) for 10min on ice, washed with 1 x PBS, and resuspended in MACS buffer for flow cytometric analysis.

To supplementary investigate the high affinity IL-2 receptor specificity of the uptake or binding, T cells were additionally stained with anti-CD25, which is the most regulated chain of

the high affinity IL-2 receptor complex on T cells (CD25 is constitutively expressed on Tregs and upregulated upon activation on other T cell subsets) [104]. Therefore, activated T cells were stained with anti-CD25 mAb in MACS buffer prior to fixation and flow cytometry analysis.

In other experiments, confirming IL-2 receptor specificity, 20 µg/ml of the anti-CD25 mAb Simulect (basiliximab) was additionally added during cultivation of activated T cells with NC to inhibit high affinity IL-2 receptor-mediated uptake [149] and then handled equally.

Naïve $CD4^+CD25^-$ T cells

After isolation, CTV^+ naïve T cells were washed with 1 x PBS and $7.5x10^5$ naïve T cells were incubated in 750 µl XVIVO20, supplemented with 10.000 U/ml Penicillin/Streptomycin in a 24 well plate at a density of $1x10^6$ /ml similar to activated T cells. IL-2 functionalized NC at concentrations of 1 µg/ml, 25 µg/ml and 75 µg/ml and control NC without further stimulus and with 50 U/ml IL-2 as positive control were added to the cells for 48 h and 72 h, respectively. After harvesting, cells were stained with Fixable Viability Dye eFluor 780, anti-CD25 mAb, fixed, and subsequently analyzed by flow cytometry.

$CD4^+CD25^{high}$ Tregs

After isolation and stimulation, CTV^+ Tregs were obtained by strong rinsing and a following washing step with 1 x PBS. Thereafter, $7.5x10^5$ cells were incubated in 750 µl XVIVO20, supplemented with 10.000 U/ml Penicillin/Streptomycin in 24 well plate at a density of $1x10^6$ /ml. NC were added at a concentration of 1 µg/ml, 25 µg/ml and 75 µg/ml. In addition, the control NC, without stimulation and a positive control of optimally proliferating T cells induced by 50 U/ml IL-2 were also included. After 4 h, 24 h, and 72 h ,respectively, Tregs were harvested, stained with Fixable Viability Dye eFluor 780 plus anti-CD25 mAb, fixed, and analyzed by flow cytometry.

Competition assays with activated $CD4^+CD25^+$ and naïve $CD4^+CD25^-$ T cells

Competition assays were performed to further inspect the specificity of the high affinity IL-2 receptor-dependent uptake. Activated CFDA stained and naïve CTV stained T cells were harvested, washed twice with 1 x PBS and incubated together in a 24 well plate at a density of $3.75x10^5$ each in 750 µl. After 72 h, T cells were harvested, stained with Fixable Viability Dye and anti-CD25 mAb. After Fixation with 4 % PFA, T cells were analyzed by flow cytometry.

2.2.3.2. Uptake and release studies with ovalbumin protein nanocapsules

To investigate the uptake and release properties of ovalbumin protein NC, HeLa cells were harvested by trypsin treatment and seeded at a density of $2x10^5$ /ml in 12 well plates in HeLa medium. After 24 h the supernatant was removed and HeLa cells were further cultivated in 1ml fresh medium. Furthermore, the ovalbumin protein NC were added at a concentration of 50 µg/ml. Uptake and release was investigated 4 h and 24 h after incubabtion by the release of the Cell tracker Dye CMFDA, that can only be detected after clevage by intracellular esterases [150]. To exclude free CMFDA dye in nanocapsule's medium, NC were spun down by 2600 x g for 20 min and cells were additionally incubated with the supernatant in equal volumes. After 24 h, cells were additionally stained with Fixable Viability Dye to ascertain toxicity of the NC and then analyzed by flow cytometry.

2.2.4. Evaluation of phosphorylated STAT3 inhibition by ovalbumin protein nanocapsules

HeLa cells were used to evaluate the inhibitory effect of the soluble and encapsulated STAT3 inhibitor S3I-201 on STAT3 phosphorylation [131]. For that reason, HeLa cells were harvested via trypsin treatment and $5x10^5$ HeLa cell were disseminated in 6 well plates in 2 ml HeLa medium. After 24 h, medium was removed by 1 ml fresh HeLa medium and the soluble or NC-encapsulated inhibitor was added for 4 h. In the last 15 min of culture, 100 U/ml IL-6 was added to stimulate STAT3 phosphorylation [151] and pSTAT3 and STAT3 expression were analyzed by flow cytometry.

2.2.5. T cell proliferation assays

T cell proliferation was either assessed by CTV dilution during uptake/binding experiments or by using ^{3}[H]-thymidine incorperation assays. ^{3}[H]-thymidine is a radioactively labeled (ß-radiation) thymidine that interacts with adenosine in the DNA replication step during the S-phase of the cell cycle which is essential for proliferation [152]. For the last 16-18 h of culture in 96 well plates, T cells were pulsed with 1 drop of 1/10 diluted ^{3}[H]-thymidine per well. ^{3}[H]-thymidine then intercalates in the DNA strands proportional to cell proliferation. Subsequently, T cells were harvested on a fiberglass filter paper, DNA bound radioactive thymidine was visualized by addition of a scintillation cocktail and electron emission was subsequently assessed in a liquid ß-scintillation counter. The proliferation rate of the T cells in that 16-18 h time period is then expressed as counts per minute.

2.2.5.1. CTLL-2 proliferation

To investigate the biological activity of the nanocapsule-coupled IL-2 in comparison to soluble, unmodified IL-2, to exclude residual IL-2 in the capsules supernatant and to evaluate

the differently IL-2 functionalized HES-D-IL-2 NC, CTLL-2 proliferation assays were performed. For this purpose, CTLL-2 were harvested, washed 2 x with 1 x PBS, and cultured at a density of $3x10^3$ /well in 200 µl in 96 well plates together with HES-D-IL-2 and the corresponding supernatants. To obtain supernatants, HES-D-IL-2 were centrifuged at 2600 x g for 20 min. HES-D-IL-2 were titrated at concentrations of 75, 25, 10, 1, 10^{-1}, 10^{-2}, 10^{-3}, and 10^{-4} µg/ml. For the supernatants the corresponding equal volume was added. For comparison of NC-bound IL-2 to soluble IL-2, the exact amount of IL-2 on the NC was calculated and additionally applied in soluble form to the CTLL-2 cells. In T cell proliferation assays, each experimental approach was set up as triplicates. Titration of Proleukin (human IL-2) in concentrations of 200, 100, 50, 25, 12.5, 6.25, 3.13, 1.57, 0.78, and 0 U/ml served as control for testing of the proliferative capacity of the CTLL-2 cells. After 48 h of culture, CTLL-2 cells were pulsed with ^{3}[H]-thymidine and proliferation was assessed.

2.2.5.2. Activated human CD4$^+$ T cell proliferation

Proliferation assays of activated CD4$^+$ T cells were conducted to examine the effect of the anti-CD25 mAb basiliximab [149] on HES-D-IL-2-induced T cell proliferation and to evaluate differences between the varying amounts of IL-2 on the NC surface of different IL-2 NC. Activated CD4$^+$ T cells were harvested, washed 2 x with 1 x PBS and incubated in 200 µl XVIVO20 in 96 well plates at a density of $2.5x10^4$ cells/well. NC were added in concentrations of 25, 10, 1, 10^{-1}, 10^{-2}, 10^{-3} and 10^{-4} µg/ml with or without 10 µg/ml basiliximab. Similar to CTLL-2 assays, titration of Proleukin served as a control to quantify the T cell proliferative capacity. After 72 h cells were pulsed for 16-18 h with ^{3}[H]-thymidine to assess T cell proliferation.

2.2.6. ELISA

The amount of IL-2 on the NC surface and as soluble form in the corresponding supernatants was evaluated by enzyme-linked immune-sorbent assay (ELISA) [153]. The principle of ELISA was first described by Engvall and Perlmann in 1971 and enables quantitative detection of substances in different solutions. In summary, sandwich ELISA is performed by coating a capture antibody against the target antigen onto an unsterile 96 well plate. After blocking unspecific binding sizes by irrelevant proteins, the sample is added and another enzyme-linked antibody against another epitope plus the streptavidin horseradish peroxidase reagent are appended. After addition of an initially blank substrate, the enzymatic activity converts the blank substrate into a detectable dye, hence resulting in a quantitative detection of the antigen [154].

IL-2 ELISA was conducted according to manufacturing protocols. The IL-2 capture antibody (1/250 diluted) was incubated on 96 well microplates at 4° C overnight. After a washing step,

unspecific epitopes were saturated by incubation of blocking buffer (1 x PBS supplemented with 10 % FCS) for 1 h. Then NC and supernatants were incubated at dilutions ranging from 1/1.000 to 1/10.000.000 for 2 h at room temperature. After another washing step, an enzyme-linked detection antibody, (1/250), and the streptavidin horseradish peroxidase reagent (Streptavidin-HRP conjugate 1/250) were added for 1 h at room temperature. Then, plates were washed again and the substrate was added. After 20-30 min enzymatic activity was stopped by addition of 1N H_2SO_4 and extinction was detected with a photometer at 450 nm.

2.2.7. Flow cytometry analysis

Flow cytometry or fluorescence activated cell sorting (FACS) is a method to discriminate different cell types based on different proteins. Those proteins can either be located on the surface, intracellular or intranuclear and are first tagged with fluorescently-labeled antibodies. Following labeling of the cells, they pass different argon lasers and then depict signals on different detectors that represent size, granularity, and fluorescence of single cells. First two detectors assess size and granularity which is determined by the forward scattered (FSC) and sideward scattered (SSC) light. In addition different laser emit light of distinct wavelength that excites the fluorochromes on the cells which then emit light of different wavelengths which is detected by various detectors (Figure 4) [155]. For flow cytometry experiments, debris by FSC/SSC exclusion and duplets (for all uptake/binding experiments), by plotting SSC-area against SSC-width, were excluded. Flow cytometry experiments can either be evaluated by the percentage of detected positive cells or by the mean fluorescence intensity (MFI) that expresses the average amount of fluorescence intensity per cell. In this study, the BD LSR II™ which is equipped with a blue Argon laser (488 nm), a red HeNe diode laser (633 nm), and a violet laser (405 nm) or the BD LSRFortessa™ cell analyzer which additionally

on the BD LSRFortessa™ cell analyzer were greatly assisted and supported by the Core Facility Cytometry and most notably by [redacted] and [redacted] at the Institute for Molecular Biology Mainz.

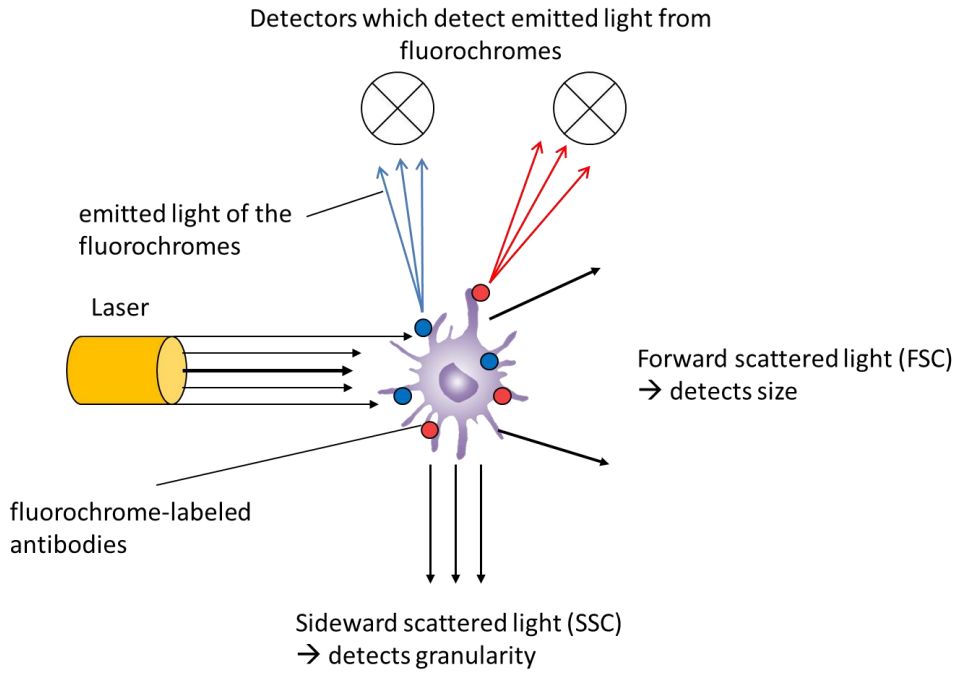

Figure 4: Principle of flow cytometry.
During flow cytometry, size and granularity of the passing cells are detected by the forward and sideward scattered light, respectively. In addition fluorochrome-labeled antibodies that were coupled cell surface/intracellular/intranuclear proteins get excited at certain wavelength and then emit light of distinct different wavelength, which is detected by different detectors to verify different surface marker.

Surface marker

For the analysis of surface molecules, cells were harvested, seeded at a density of $1x10^5$-$1x10^6$ in a 96 well plate and washed twice with FACS Buffer (1 x PBS supplemented with 0.5% HSA and 3 mM EDTA) by 3 min centrifugation at 4 °C using 400 g. Subsequently, the supernatant was removed and cells were stained with the corresponding fluorochrome-conjugated antibodies and incubated for 15 min at 4° C. After two more washing steps, cells were resuspended in 150 µl FACS buffer and analyzed by the BD LSR II™ or the BD LSRFortessa™ cell analyzer.

Intranuclear staining of Foxp3

Foxp3 intranuclear staining was performed by the Foxp3 staining kit, according to manufactor's instructions. Briefly, after Treg isolation and activation $1x10^6$ cells/well were incubated in 96 well plates in 200 µl Fixation/Permeabilization working solution (1 x Fixation/Permeabilization Concentrate with 3x Foxp3 Fixation/Permeabilization Diluent) for 30min at room temperature. After 2 washing steps with 1 x Permeabilization Buffer, cells were stained with anti-Foxp3 mAb for 30min at room temperature. Following 2 more washing steps with Permeabilization Buffer, cells were resuspended in MACS buffer and analyzed by flow cytometry.

Intracellular staining of pSTAT3 and STAT3

To investigate the phosphorylated and total STAT3, cells were stained according to BD Phosflow Protocol III. For fixation, pre-warmed BD Phoflow Fix Buffer was added to the HeLa cell medium at a 1/1 ratio for 10 min at 37 °C. Afterwards, cells were harvested by gently scraping the bottom of the plate with a Greiner cell scraper and collected in tubes. After centrifugation HeLa cells were permeabilized by addition of 1 ml ice-cold BD Phosflow Permeabilization Buffer III and incubated for 30 min on ice. Following 3 washing steps with MACS Buffer, cells were stained with anti-STAT3 mAb and anti-pSTAT3 mAb, respectively, in BD Pharmingen Stain Buffer for 30 min at room temperature, washed 1 x with MACS buffer and analyzed in 150 µl MACS Buffer using the BD LSR II^{TM}.

2.2.8. Confocal laser scanning microscopy

Confocal laser scanning microscopy (CLSM) is a specific form of light microscopy. In contrast to ordinary light microscopy, a confocal laser scanning microscope provides the opportunity of sequentional screening a three dimensional sample by pointwise rastering of the light source through the specimen. The intensities of the reflected or fluorescent light emission in all areas are thus successively assessed and merged to a single picture. A spatial pinhole filters the out of focus light which increases optical resolution and contrast.

CLSM was conducted at the Institute for Molecular Biology (IMB) Mainz using the Confocal Leica TCS SP5 microscope with great support by the Microscopy Core Facility in particular by [redacted] and [redacted]. The Leica TCS SP5 is equipped with 4 different photomultipliers and different laser lines (UV OPSL 355 nm, Diode 405/458 nm, Diode 442 nm, Ar 458/476/488/496/514 nm, DSS 561 nm, HeNe 594 nm, HeNe 633 nm) and a white-light laser.

Confocal laser scanning microscopy of HES-D-IL-2

Confocal laser scanning microscopy of HES-D-IL-2 was performed to confirm the flow cytometry results and to additionally distinguish between uptake of HES-D-IL-2 or attachment to the cell membrane. For this purpose, $2x10^5$ activated $CD4^+$ T cells were cultured in 200 µl XVIVO 20 supplemented with 10.000 U/ml Penicillin/Streptavidin in 8-well chamber slides. HES-D-IL-2 and IL-2 as control were added at 75 µg/ml and 50 U/ml respectively in different chambers. After 72 h, cell membranes were stained with 1 µg/ml Cell Mask Deep Red and cell nuclei were visualized by 1 µg/ml Hoechst 33342. Directly after addition of the dyes, samples were quantified.

Confocal laser scanning microscopy of ovalbumin protein nanocapsules

Confocal laser scanning microscopy of the ovalbumin protein NC was performed to confirm the flow cytometry results. $4x10^4$ HeLa cells were harvested via trypsinization, and seeded in 200 µl HeLa medium supplemented with 10.000 U/ml penicillin/streptavidin in 8-well chamber slides. After 24 h, medium was removed, 200 µl of fresh medium and 50 µg/ml of the ovalbumin protein NC with encapsulated CMFDA were incubated with the cells for 24 h. The supernatant of the NC served as control. Prior to microscopy, cells were stained with 1 µg/ml Cell Mask Orange and analyzed directly after addition of the dye.

2.2.9. *In vivo* application of HES-D-IL-2

All animal experiments were performed after approval of the Landesuntersuchungsamt of the state Rhineland-Palatinate according to the German Animal Welfare Act (Tierschutz-Versuchstierverordnung) from 2013. The mouse models that were used to evaluate the *in vivo* targeting of murine and human T cells are summarized in Figure 5.

2.2.9.1. Targeting of murine $CD25^+$ T cells *in vivo*

The uptake/binding of HES-D-IL-2 by murine T cells *in vivo* was investigated in adult (8-10 weeks old) wild-type C57BL/6J mice, which were intravenously injected with 30 µg NC (HES-D-IL-2 and HES-D respectively), diluted in 150 µl NaCl. In addition, 150 µl NaCl solution without NC addition served as control. After 24 h, mice were sacrificed and cervical, axillar, and inguinal lymph nodes were obtained and temporary stored in ice-cold RPMI complete (RPMI supplemented with 200 mM L-Glu, 50 µM β-mercaptoethanol, 10.000 U/ml Penicillin/Streptomycin, 1 M 2-(4-(2-Hydroxyethyl)-1-piperazinyl)-ethansulfonsäure (Hepes) and 10 mM Non-essential amino acids). To obtain single cell suspensions, lymph nodes were squeezed through a 70 µm cell strainer and for the removal of residual erythrocytes, lymph node cells were incubated in 300 µl ACK lysis buffer for 3 min at room temperature. After terminating the lysing procedure by addition of 30 ml RMPI complete, cells were spun down and $1x10^6$ cells/well were incubated in 96 well plates for FACS staining. Following another washing step with 150 µl FACS Buffer, cells were either stained with antibodies against murine CD4, CD8α, NK1.1, Thy1.1 and CD25 or B220, CD11b, CD11c, and F4/80 and analyzed by the BD LSR Fortessa.

2.2.9.2. Human T cell reconstituted $RAG2^{-/-}\gamma c^{-/-}$ mice for local targeting of human $CD25^+$ T cells *in vivo*

In addition to evaluate the uptake/binding behavior of the IL-2 functionalized NC by human T cells in an *in vivo* environment adult immunodeficient $RAG2^{-/-}\gamma c^{-/-}$ that lack B cells, T cells and displayed reduced NK cells number [156-158] were intraperitoneally reconstituted with human

$CD4^+$ T cells. For this purpose, human $CD4^+$ T cells from buffy coats were isolated using Ficoll density gradient centrifugation and MACS separation as described for the generation of activated $CD4^+$ T cells. Subsequently, $10x10^6$ $CD4^+$ T cells in 150 µl PBS were intraperitoneally injected into $RAG2^{-/-}\gamma c^{-/-}$ mice. Immediately after, 150 µg of HES-D-IL-2 or HES-D (in 150 µl NaCl solution) or 150 µl NaCl without NC, respectively, were intraperitoneally injected. After 4 h, T cells were obtained by an intraperitoneal lavage. Therefore, ice-cold PBS was injected into the peritoneum, the abdomen was gently massaged for several seconds to induce cell detachment from the peritoneum. After aspiration of the cell/PBS solution, they were centrifuged and incubated in 300 µl ACK lysis buffer for 3 min at room temperature to remove residual erythrocytes. The osmotic stress was terminated by addition of 30 ml RPMI complete supplemented with 10% FCS. Subsequently, $1x10^6$ cells were stained with antibodies against human CD3, CD4, CD25, and CD45 and measured by the LSR Fortessa.

2.2.9.3. Xenogeneic GvHD for systemic targeting of human $CD25^+$ T cells *in vivo*

In general, human PBMC-reconstituted immunodeficient $RAG2^{-/-}\gamma c^{-/-}$ mice are a useful tool for the investigation of xenogeneic graft versus host disease (GvHD) [157,159]. For this study however, this mouse model was used to endow these mice with a human immune system without inducing any clinically visible GvHD symptoms. The development of GvHD symptoms was carefully monitored by evaluation of weight loss, posture, activity, fur texture and skin integrity [160]. For human T cell engraftment, human PBMCs were isolated by Ficoll Density gradient centrifugation and $20x10^6$ PBMCs in 150 µl PBS were intraperitoneally injected into 2-3 week old $RAG2^{-/-}\gamma c^{-/-}$ mice. After 4 weeks, 150 µg of HES-D-IL-2 and HES-D in 150 µl NaCl solution were intravenously injected and after 24 h the spleen was isolated and temporary stored in 20 ml RPMI complete + 10% FCS. Subsequently, spleen cells were squeezed through a 70 µm cell strainer and incubated in 500 µl ACK buffer for 5 min. The lysis was stopped by addition of 30 ml RPMI complete supplemented with 10% FCS and $1x10^6$ cells were incubated in FACS buffer for flow cytometry staining. Cells were either stained with antibodies against human CD3, CD4, CD8, CD25, and CD45 or against human CD45, murine CD11b, CD11c, F4/80 and CD45 and evaluated by a BD LSR Fortessa.

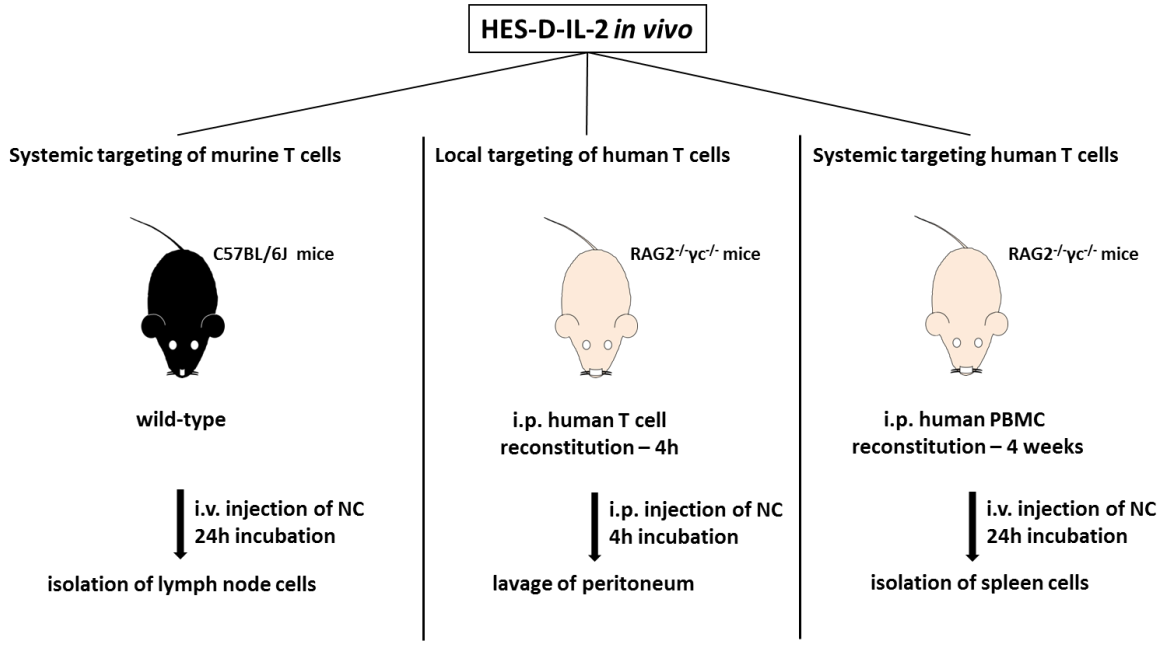

Figure 5: HES-D-IL-2 in vivo.
The figure displays the different mouse models that were used to evaluate the uptake/binding of HES-D-IL-2 by murine and human T cells *in vivo*. Systemic targeting of murine T cells was evaluated after i.v. injection of the NC and harvesting and analyzing of the lymph node cells after 24 h. In contrast, local targeting of human T cells was assessed by i.p. injection of human $CD4^+$ T cells and NC into $RAG2^{-/-}\gamma c^{-/-}$ mice. After 24 h, i.p. cells were obtained and analyzed. For the systemic targeting of human T cells, human PBMCs were i.p. injected into RAG2-/-γc-/- mice. After engraftment, NC were i.v. injected and spleen cells were isolated and analyzed 24 h later.

III Results

3.1. IL-2 functionalized hydroxyethyl starch nanocapsules

HES-D-IL-2 were used in this study to cell-specifically target different T cell populations *in vitro* and *in vivo* via the high affinity IL-2 receptor with focus on Tregs. Those experiments are reproduced in part with permission from Frick S.U., Domogalla M.P., Baier G., Wurm F.R., Mailänder V., Landfester K., Steinbrink K. (2016) Interleukin-2 functionalized Nanocapsules for T cell-based Immunotherapy. ACS Nano 10 (10): 9216–26. DOI: 10.1021/acsnano.5b07973. Copyright 2016 American Chemical Society.

3.1.1. Quality control of HES-D-IL-2

After generation, the quality of HES-D-IL-2 was investigated by various, different physical, chemical, and biological assays.

Physico-chemical properties of HES-D-IL-2

In all preparations that were used for further experiments, the diameter (D_Z) of the HES-D control capsules and HES-D-IL-2 in water ranged from 210-220 nm as determined by dynamic light scattering. The relative size distribution (rSD) was ≤30% demonstrating the generation of capsules of on average 215 nm in diameter with a narrow size distribution and low aggregation behavior (Figure 6a). Those results were confirmed by TEM and SEM microscopy that additionally demonstrated capsule-like shape and relative homogenous shape of the miniemulsion products and is displayed in Figure 6b. The zeta potential of the NC was slightly negative, -22 mV for HES-D and -7 to -10 for HES-D-IL-2, respectively. MALDI-TOF analysis of the azid-functionalized IL-2 demonstrated coupling of either one, two or three azide groups per IL-2 molecule with approximately 15 % of unmodified IL-2 remaining in the product (Figure 6c).

To indirectly calculate the number of IL-2 molecules on the NC surface, free DBCO molecules on the NC were quantified with a chemical reaction involving 9-azidomethylanthracene. Those experiments revealed 3.885±195 DBCO groups/NC resulting in 1.660, 1.020 and 180 IL-2 molecules per NC for HES-D-IL-2, HES-D-IL-$2_{/2}$ and HES-D-IL-$2_{/10}$ (Figure 6a). The analysis of the NC were kindly performed by [redacted] (Max Planck Institute for Polymer Research Mainz) reproducibly for each preperation.

a

	size [nm]	rSD [%]	ζ-potential [mV]	SD [mV]	DBCO groups/ NC	IL-2 molecules/ NC
HES-D	220	30	-22	2	3885±195	0
HES-D-IL-2	215	28	-7	1	3885±195	1660±90
HES-D-IL-$2_{/2}$	215	30	-9	2	3885±195	1020±90
HES-D-IL-$2_{/10}$	215	30	-10	2	3885±195	180±50

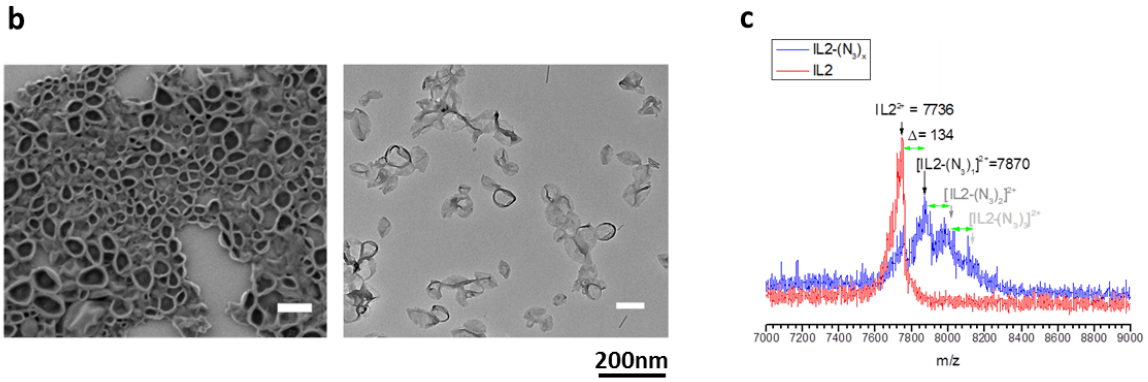

Figure 6: Physico-chemical characterization of IL-2 functionalized NC.
a) Size and size distribution (rSD) was assessed by using DLS. Electrophoretic mobility, which is demonstrated by the zeta potential (ζ-potential + SD), was assessed by a zeta nanosizer. Furthermore, DBCO groups/NC and the number of IL-2 molecules per/NC were quantified by 9-azidomethylanthracene. Pooled data of 3 independent experiments are depicted.
b) The figure illustrates TEM (left) and SEM (right) images of the IL-2 functionalized NC as one representative of 3 independent experiments. Scale bar represents 200 nm.
c) The number of azid modifications per IL-2 molecule was examined by MALDI-TOF. Representative data of 3 independent experiments are depicted.

ELISA

An IL-2 ELISA was performed after each NC preparation to determine the amount of coupled IL-2 on the NC surface and residual IL-2 in the NC supernatant. Table 2 displays one representative result of 4 independent capsule preperations. IL-2 ELISA revealed that amounts between 10^7-10^8 ng/ml IL-2 were present on the HES-D-IL-2 NC surface, whereas only a residual, 100-fold reduced concentration of around 10^5 ng/ml IL-2 was detected in the supernatant. In addition, ELISA was utilized as a quality control for the IL-2 functionalized NC with twofold (HES-D-IL-$2_{/2}$) and tenfold (HES-D-IL-$2_{/10}$) reduced amounts of IL-2 molecules on their surface. Those results demonstrated a 100-fold decreased amount ($5x10^6$ to $2x10^4$ and $3x10^6$ to $6x10^4$, respectively) in the supernatants and reduced levels of IL-2 bound to HES-D-IL-$2_{/2}$ and HES-D-IL-$2_{/10}$.

Table 2: ELISA of HES-D-IL-2.
The amount of IL-2 on the NC surface was assessed by ELISA. One representative result of 4 independent experiments for HES-D-IL-2, HES-D-IL-$2_{/2}$ and HES-D-IL-$2_{/10}$ and their corresponding supernatants, respectively is displayed.

	capsule IL-2 [pg/ml]	**supernatant IL-2 [pg/ml]**
HES-D-IL-2	4×10^7 pg/ml	2×10^5
HES-D-IL-$2_{/2}$	5×10^6 pg/ml	2×10^4
HES-D-IL-$2_{/10}$	3×10^6 pg/ml	6×10^4

CTLL-2 cells

IL-2 dependent CTLL-2 proliferation was exploited to investigate the biological activity of the IL-2 after azidification and coupling to the NC surface. For that purpose, the theoretical biological activity of the NC IL-2 on the NC surface was calculated and proliferation induction was compared to the same amount of soluble, unmodified IL-2. As displayed in Figure 7a only negligible differences between IL-2 on HES-D-IL-2 and soluble IL-2 were observed. These experiments indicate the generation of IL-2 functionalized NC with different amounts of covalently bound, biologically active IL-2 on the surface and no loss of biological IL-2 activity during the functionalization process.

Furthermore, the amount of biologically active IL-2 on the IL-2 functionalized NC in comparison to their corresponding supernatants was investigated by proliferation of the IL-2 dependent cell line CTLL2. EC50 values of CTLL-2 cells are defined as half-maximal proliferation induction and were calculated by first log scaling of the x-axis (which depicts the concentration of HES-D-IL-2) and then calculating the EC50 by using GraphPad Prism 7. As depicted in Figure 7b, HES-D-IL-2 induced vigorous proliferation of CTLL-2 cells with an EC50 value of 0.004 µg/ml. In contrast, the supernatant of HES-D-IL-2 revealed a negligible induction of proliferation with an EC50 value of 26.5 µg/ml. Additionally, HES-D did not induce any proliferation. CTLL-2 cells were also used to evaluate the differences between the biological active IL-2 on HES-D-IL-2, HES-D-IL-$2_{/2}$ and HES-D-IL-$2_{/10}$ which is determined in Figure 7v. All preperations of IL-2 functionalized NC induced a proliferation proportional to the amount of IL-2 on the capsule's surface as shown by reduced proliferation induction by HES-D-IL-$2_{/2}$ and HES-D-IL-$2_{/10}$.

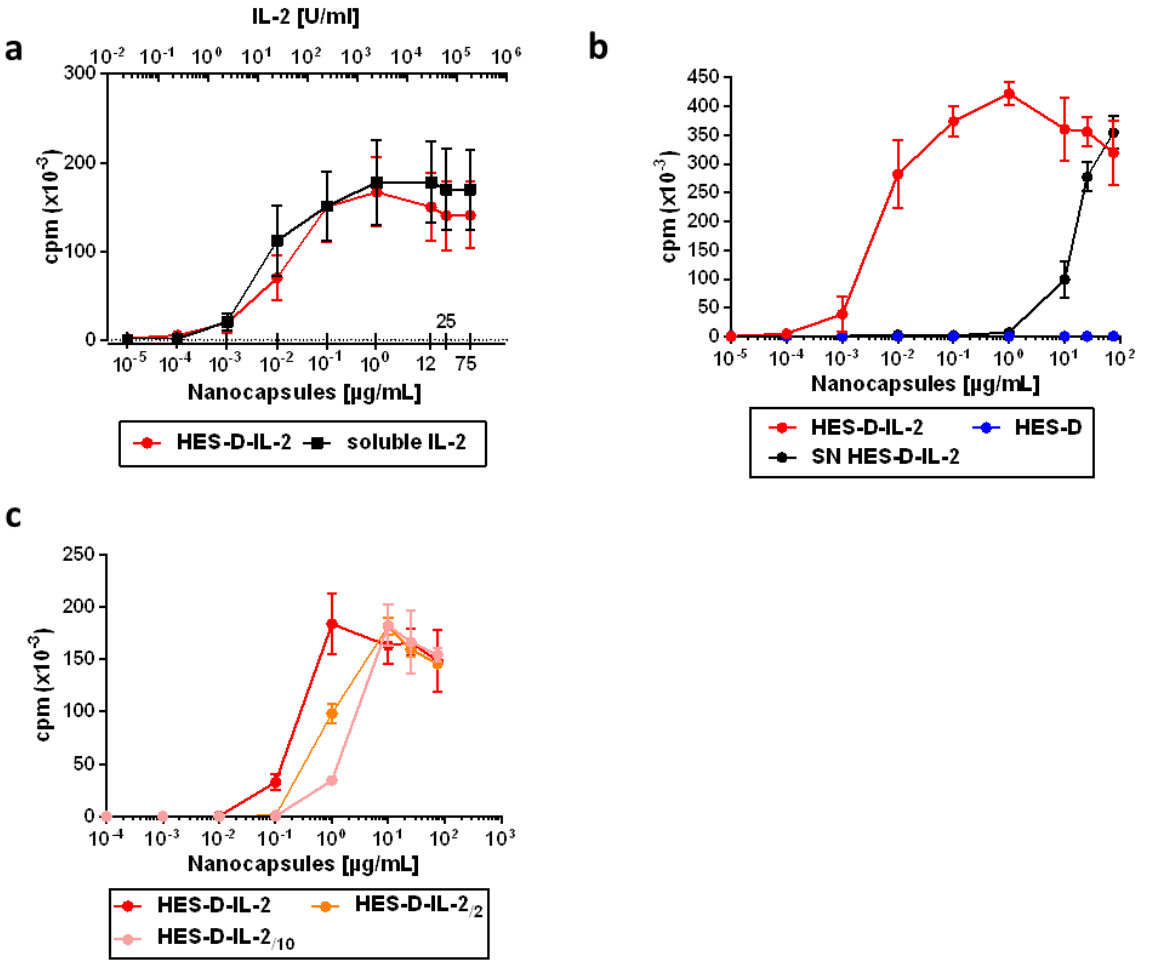

Figure 7: CTLL-2 assay of HES-D-IL-2.
The figure displays CTLL-2 assays that were performed for the quality control of HES-D-IL-2.
a) CTLL-2 proliferation induced by HES-D-IL-2, HES-D and the supernatant of HES-D-IL-2 was assessed in the figure illustrating the mean ± SD from triplicates of one representative experiment of 5 independent replications.
b) The figure shows the induction of proliferation by HES-D-IL-2, HES-D-IL-$2_{/2}$ and HES-D-IL-$2_{/10}$ respectively, as mean ± SD of triplicates of one representative result of 4 independent experiments.
c) Comparison of the biological activity of IL-2 coupled to HES-D-IL-2 and soluble IL-2 is depicted in the figure as mean ± SD of pooled data of 5 independent experiments.

3.1.2. Uptake/binding studies of HES-D-IL-2 by human T cells

To investigate the uptake/binding of HES-D-IL-2 by human T cells, different T cell populations were investigated. During all uptake/binding experiments, toxicity of the HES NC was excluded by Fixable Viability Dye staining.

3.1.2.1. Uptake/binding of HES-D-IL-2 by activated human $CD4^+CD25^+$ T cells

Uptake/binding of HES-D-IL-2 compared to HES-D

Activated, human $CD4^+CD25^+$ T cells were used to investigate the uptake/binding of $SR101^+$ HES-D-IL-2 in comparison to $SR101^+$ HES-D control capsules by use of flow cytometry analysis. After isolation and stimulation, activated $CD4^+$ T cells were first analyzed in respect to their expression of the surface marker CD4, CD8 and CD25 by flow cytometry. As depicted in Figure 8a stimulated $CD4^+$ T cells demonstrated a high purity (> 98% $CD4^+$) whereas just a few $CD8^+$ cells (< 2%) were detected. The α-chain of the IL-2 receptor CD25 was expressed on up to 60-70% following stimulation, demonstrating a successful activation by anti-CD3 anti-CD28 mAb engagement.

To evaluate the uptake/binding expression of SR101 was plotted against CTV which is used as a dye to detect proliferation. The gate for the uptake/binding was set with regard to the proliferation of T cells by 50 U/ml IL-2 as control (Figure 2b). 50 U/ml IL-2 was used as it induced the maximal proliferation of activated T cells (data not shown). After 72 h incubation of activated $CD4^+$ T cells with HES-D and HES-D-IL-2, respectively, the IL-2 functionalized NC exhibited a significantly enhanced uptake/binding by activated T cells compared to HES-D illustrated in Figure 8b as demonstrated by the percentage of $SR101^+$ cells. Additionally, pooled data are summarized in Figure 8c.

To verify the uptake of NC by T cells and to investigate the intracellular localization of the NC within the T cells, CLSM microscopy was performed. As shown in Figure 8d, after 72 h, HES-D-IL-2 were indeed preferentially located inside the cytoplasm of the T cells.

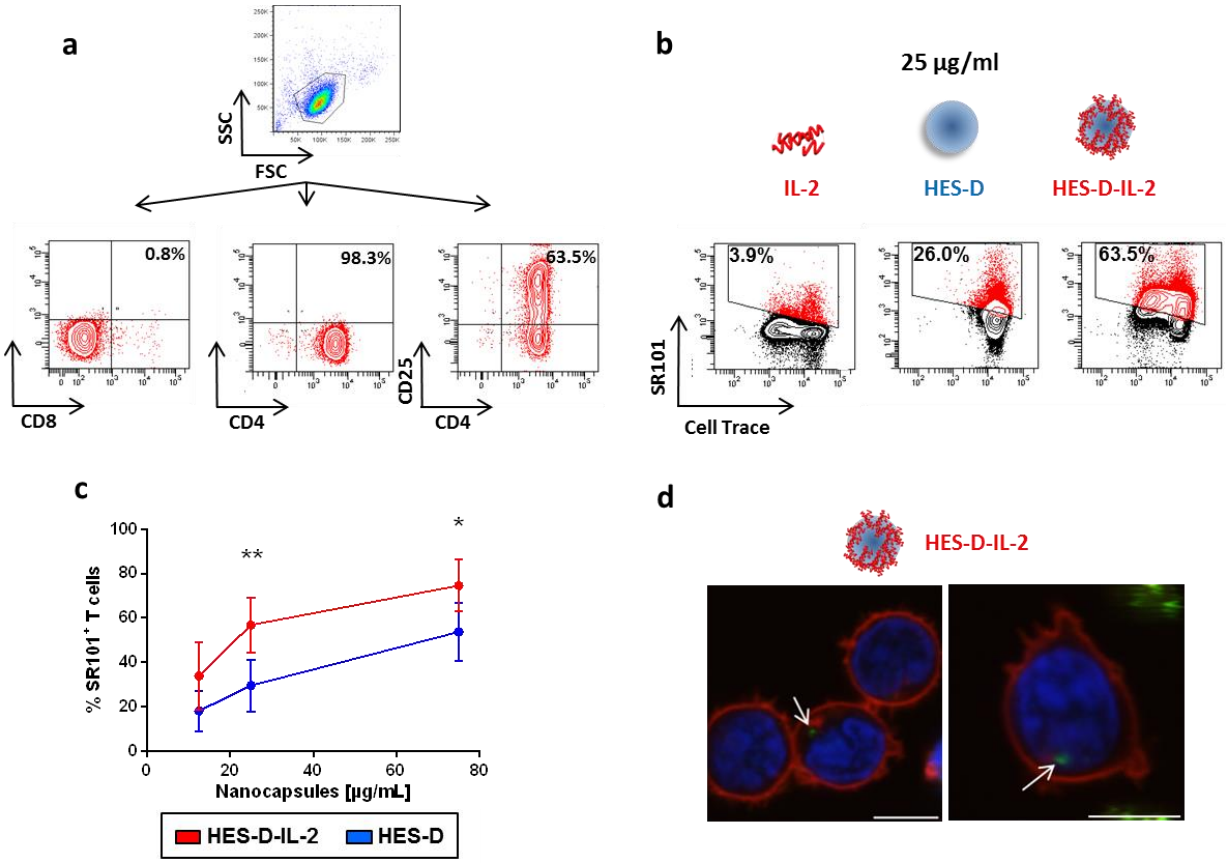

Figure 8: Uptake of HES-D-IL-2 by activated T cells.
a) To ascertain the purity and activation status after isolation and anti-CD3/anti-CD28 mAb stimulation, human activated T cells were stained for their expression of CD4, CD8 and CD25. A representative result of 17 independent experiments is depicted.
b) To assess the uptake/binding by human activated T cells, anti-CD3/anti-CD28 mAb stimulated $CD4^+CD25^+$ T cells were incubated with HES-D-IL-2 and HES-D for 72 h. SR101 expression was plotted against CTV and the percentage of $SR101^+$ T cells was detected. One representative result of 5 independent experiments at a NC concentration of 25 µg/ml is shown.
c) The figure indicates uptake/binding results of 5 independent experiments from *b)* which are summarized as mean ± SD. The statistics of those experiments were calculated by two-sided, ungrouped student t tests (*p < 0.05, **p < 0.01, ***p < 0.001).
d) After incubation with HES-D-IL-2 for 72 h, activated $CD4^+CD25^+$ cells were also evaluated by CLSM. The cell membrane was stained with CellMask Deep Red (which is depicted in red), the cell nucleus was visualized by Hoechst33342 (which is shown in blue) and the $SR101^+$ HES-D-IL-2 NC are visualized in green and highlighted with arrows. Scale bars represent 5 µm and the figure illustrates one representative result of 3 independent experiments.

Furthermore, CTV dilution was used to investigate the induced proliferation of the activated $CD4^+$ T cells by HES-D-IL-2 and HES-D, respectively. As demonstrated in Figure 9, HES-D-IL-2 induced a strong proliferation of 20-30 % proliferating T cells, whereas incubation with HES-D did not result in T cell proliferation, indicating that T cell proliferation is induced by IL-2 on the NC surface and not by the capsules alone.

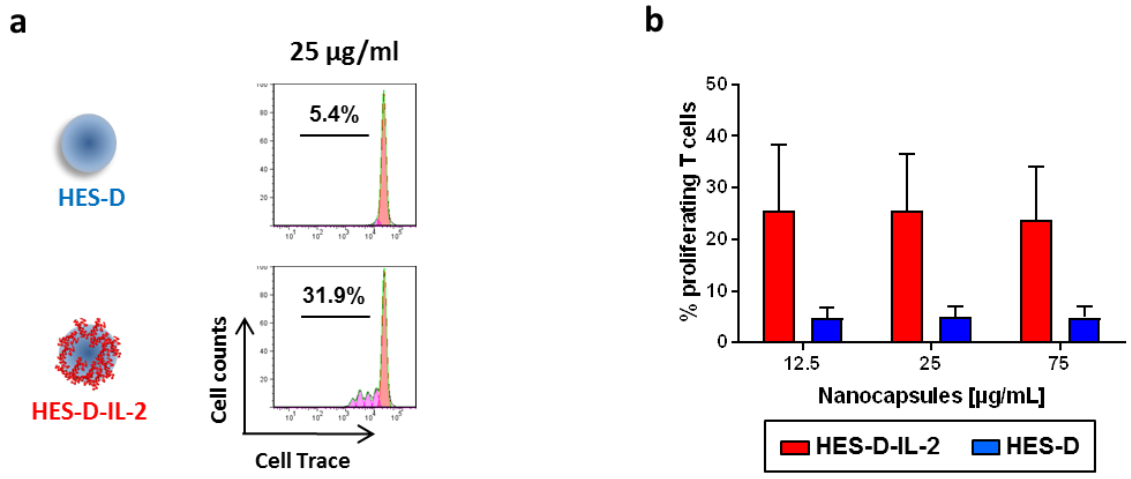

Figure 9: Induction of T cell proliferation by HES-D-IL-2.
To evaluate the induction of T cell proliferation by NC, activated $CD4^+CD25^+$ T cells were incubated with HES-D and HES-D-IL-2, respectively, for 72 h. Proliferation was assessed as percentage of CTV^+ T cells after dye dilution.
a) CTV expression was plotted against cell counts. One representative result of 5 independent experiments at a NC concentration of 25 µg/ml is depicted.
b) The figure illustrates pooled T cell proliferation data of 5 independent experiments from *a)* as mean ± SD.

Uptake/binding and induced proliferation by HES-D-IL-2, HES-D-IL-$2_{/2}$ and HES-D-IL-$2_{/10}$

To investigate whether the uptake/binding of HES-D-IL-2 by activated $CD4^+CD25^+$ T cells is dependent on the amount of IL-2 on the NC surface, the uptake/binding of HES-D-IL-2, HES-D-IL-$2_{/2}$ and HES-D-IL-$2_{/10}$ was assessed. To prevent a bias which may occur by different NC/T cell ratios due to different T cell numbers induced by different IL-2 functionalized NC (HES-D-IL-2, HES-D-IL-$2_{/2}$ and HES-D-IL-$2_{/10}$). The percentage of $SR101^+$ T cells was normalized to the number of cells after maximal proliferation after incubation with 50 U/ml IL-2. For this purpose, instead of recording a determined number of cells on the flow cytometer, cells were measured for 45 s at medium flow rate. As illustrated in Figure 10, the uptake of IL-2 functionalized NC by activated $CD4^+$ T cells after 72 h is depended on the amount of IL-2 present on the NC surface, as HES-D-IL-2 revealed a significantly enhanced incopropration compared to HES-D-IL-$2_{/2}$ and HES-D-IL-$2_{/10}$. Those differences were most pronounced at 25 µg/ml as shown by percentage of NC positive cells in Figure 10a and the amount of NC per cell which is depicted as MFI in Figure 10b.

Moreover, in order to investigate the induction of activated $CD4^+$ T cell proliferation by HES-D-IL-2 in comparison to HES-D-IL-$2_{/2}$ and HES-D-IL-$2_{/10}$, the amount of proliferating cells were quantified by CTV dilution, which was assessed by flow cytometry. Figure 10c shows the induction of T cell proliferation which significantly depended on the amount of IL-2 on the NC surface as HES-D-IL-2 induced the highest percentage of proliferating T cells compared to HES-D-IL-$2_{/2}$. In line with that, HES-D-IL-$2_{/10}$ exhibited the significantly lowest capacity of T cell proliferation.

Furthermore, a [^{3}H] thymidine assay was conducted to evaluate the proliferative capacity of T cells after cultivation with HES-D-IL-2, HES-D-IL-2$_{/2}$ and HES-D-IL-2$_{/10}$, respectively. The observed results confirmed the data assessed by flow cytometry. The induced T cell proliferation was dependend on the amount of IL-2 present on the NC surface. Thus, treatment by HES-D-IL-2 induced the most pronounced, whereas culture with HES-D-IL-2$_{/2}$ and in particular HES-D-IL-2$_{/10}$ resulted in T cell proliferation only at higher concentrations as illustrated in Figure 10d.

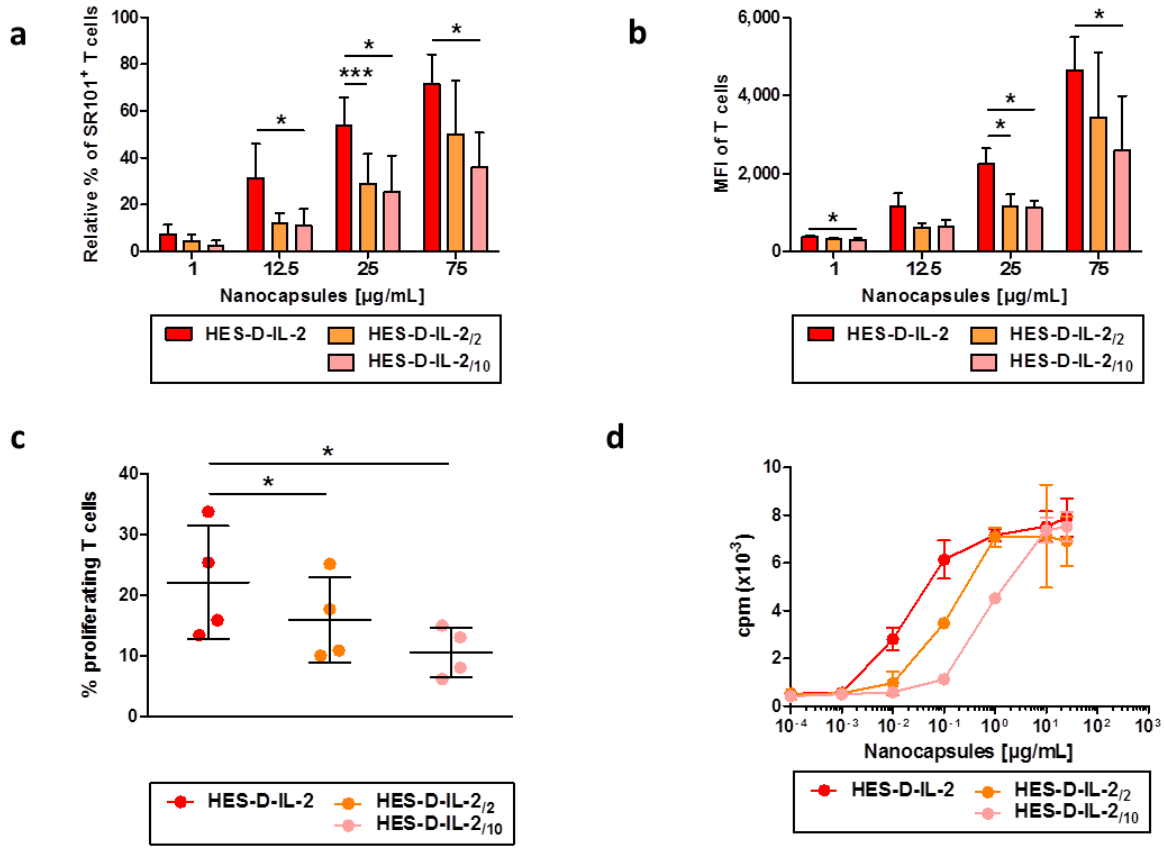

Figure 10: Incubation of HES-D-IL-2, HES-D-IL-2$_{/2}$ and HES-D-IL-2$_{/10}$ with activated CD4$^+$CD25$^+$ T cells
a)/b) To assess the uptake/binding by activated T cells, anti-CD3/anti-CD28 stimulated CD4$^+$CD25$^+$ T cells were incubated with HES-D-IL-2, HES-D-IL-2$_{/2}$ and HES-D-IL-2$_{/10}$ for 72 h and SR101 expression was plotted against CTV expression. Uptake/binding was investigated as relative percentage of SR101$^+$ T cells, calculated to maximal T cell proliferation induced by 50 U/ml IL-2 (= 100%) *(a)* and as MFI *(b).* The figure illustrates summarized data of 5 independent experiments as mean ± SD.
c)/d) To evaluate the induction of T cell proliferation by HES-D-IL-2, HES-D-IL-2$_{/2}$ and HES-D-IL-2$_{/10}$ human, activated CD4$^+$CD25$^+$ T cells were incubated with the NC for 72 h. Proliferation was assessed as percentage of proliferating cells by CTV dilution as mean ± SD of pooled data of 4 independent experiments *(c)* or ^{3}[H] thymidine incorporation for 16 h after 72 h of cell culture as one representative result of 3 independent experiments that were set up as triplicates *(d).*
Statistics were calculated by two-sided, ungrouped student t tests (*p < 0.05, **p < 0.01, ***p < 0.001).

3.1.2.2. Uptake/binding of HES-D-IL-2 by human naive CD4$^+$CD25$^-$ T cells

The uptake of the IL-2 functionalized NC and its dependence on different amounts of IL-2 bound on the NC surface was also investigated for human naïve CD4$^+$CD25$^-$ T cells. After isolation, purity and activation state of the naïve T cells was assessed using flow cytometry

by staining of the surface molecules CD4, CD8, CD25, CD45RA and CD45RO. Depicted in Figure 11, naïve T cells were $CD4^+$ (> 98%), $CD8^-$ (< 2%) and exhibited a very low CD25 expression (< 5%). In addition, they strongly expressed the CD45 isoform CD45RA to a purity of > 95%, whereas a low amount of > 5 % of $CD45RO^+$ cells was detected, indicating a high purity and low activation status of the naïve $CD4^+$ T cells.

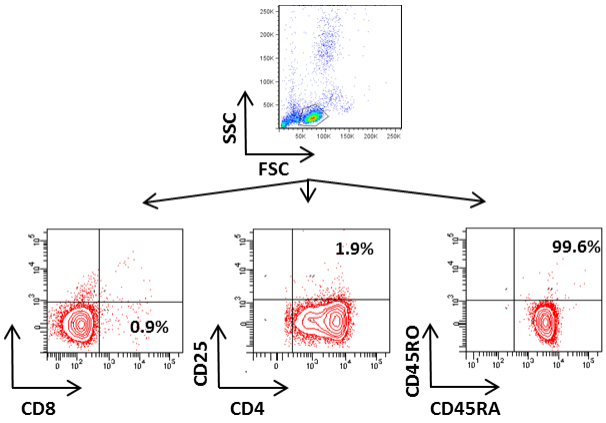

Figure 11: Purity and activation state of naïve T cells.
To ascertain their purity and activation state after isolation, human naive T cells were stained for expression of CD4, CD8, CD25, CD45RA and CD45RO. One representative of 8 independent experiments is depicted.

After incubation of naïve T cells with HES-D-IL-2, HES-D-IL-$2_{/2}$ and HES-D-IL-$2_{/10}$ for 72 h, flow cytometry experiments revealed a detectable uptake/binding of the IL-2 functionalized NC by naïve T cells resulting in up to 25% NC-positive cells. Furthermore, comparative studies of HES-D-IL-2, HES-D-IL-$2_{/2}$ and HES-D-IL-$2_{/10}$ demonstrated a significantly increased incorporation of HES-D-IL-2 by naïve T cells, in contrast to reduced binding/uptake of HES-D-IL-$2_{/2}$ and HES-D-IL-$2_{/10}$, respectively. These results are summarized in Figure 12 as percentage of $SR101^+$ T cells (Figure 12a) and as MFI of the NC dye SR101 (Figure 12b).

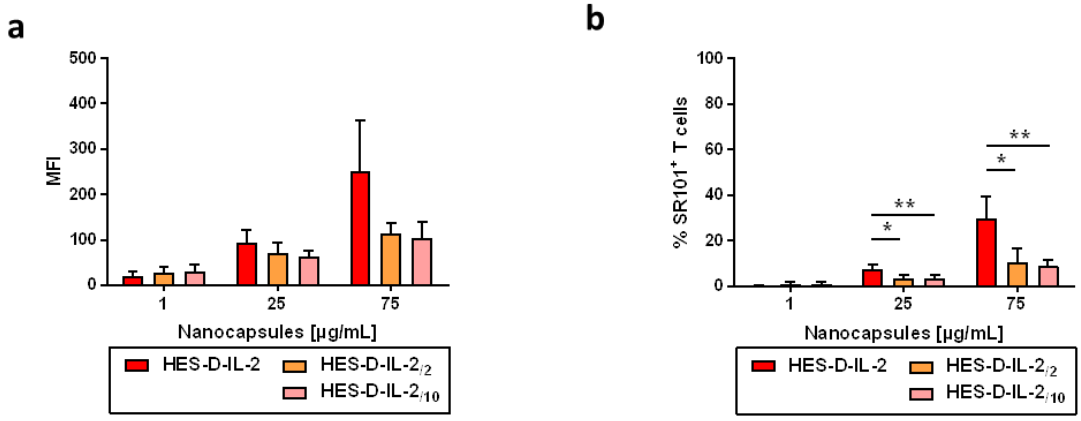

Figure 12: Uptake/binding of HES-D-IL-2, HES-D-IL-$2_{/2}$ and HES-D-IL-$2_{/10}$ by naïve $CD4^+CD25^-$ T cells a)/b) To assess the uptake/binding by human naïve T cells, isolated naïve $CD4^+CD25^-$ T cells were incubated with HES-D-IL-2, HES-D-IL-$2_{/2}$ and HES-D-IL-$2_{/10}$ for 72 h and SR101 expression was plotted against CTV expression. Uptake/binding was investigated as percentage of $SR101^+$ T cells *(a)* and as MFI *(b).* The figure illustrates summarized data of 4 independent experiments as mean ± SD. The statistics were calculated GraphPad Prism using a two-sided, ungrouped student t tests (*p < 0.05, **p < 0.01, ***p < 0.001).

3.1.2.3. Uptake/binding of HES-D-IL-2 by human $CD4^+CD25^{high}$ Tregs

In addition to the investigation of the uptake/binding of HES-D-IL-2, HES-D-IL-$2_{/2}$ and HES-D-IL-$2_{/10}$ by activated and naïve T cells, uptake/binding behavior of human $CD4^+CD25^{high}$ Tregs was examined. After isolation and stimulation, Tregs were analyzed based on their expression of CD4, CD25 and Foxp3. As shown in Figure 13, Tregs revealed a strong expression of CD4 (> 98%), CD25 (> 95%) and Foxp3 (> 95%), indicating a high purity of the isolated Tregs.

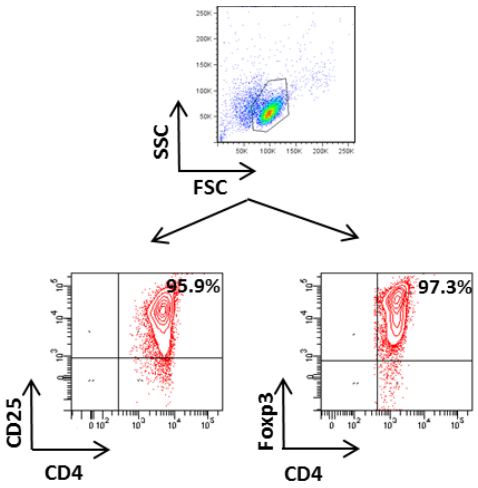

Figure 13: Purity and activation state of Tregs.
To ascertain their purity and activation state after isolation, human Tregs were stained for their expression of CD4, CD25 and Foxp3. A representative of 4 independent experiments is depicted.

After 72h of NC incubation, IL-2 functionalized NC revealed a strong uptake/binding by Tregs. This uptake was not dependend on the amount of IL-2 on the NC surface as HES-D-IL-2, HES-D-IL-$2_{/2}$ and HES-D-IL-$2_{/10}$ exhibited similar percentages of $SR101^+$ T cells illustrated in Figure 14a. Furthermore, the MFI confirmed no significant differences in the uptake/binding (Figure 14b). To exclude a time-dependent uptake behavior of the IL-2 functionalized NC by Tregs which may reveal possible differences between HES-D-IL-2, HES-D-IL-$2_{/2}$ and HES-D-IL-$2_{/10}$, the uptake of Tregs was also investigated after 4 h and 24 h. However, as depicted in Figure 14c and 14d, differences were also absent at earlier time points excluding differential IL-2 dependent uptake in a time-related manner.

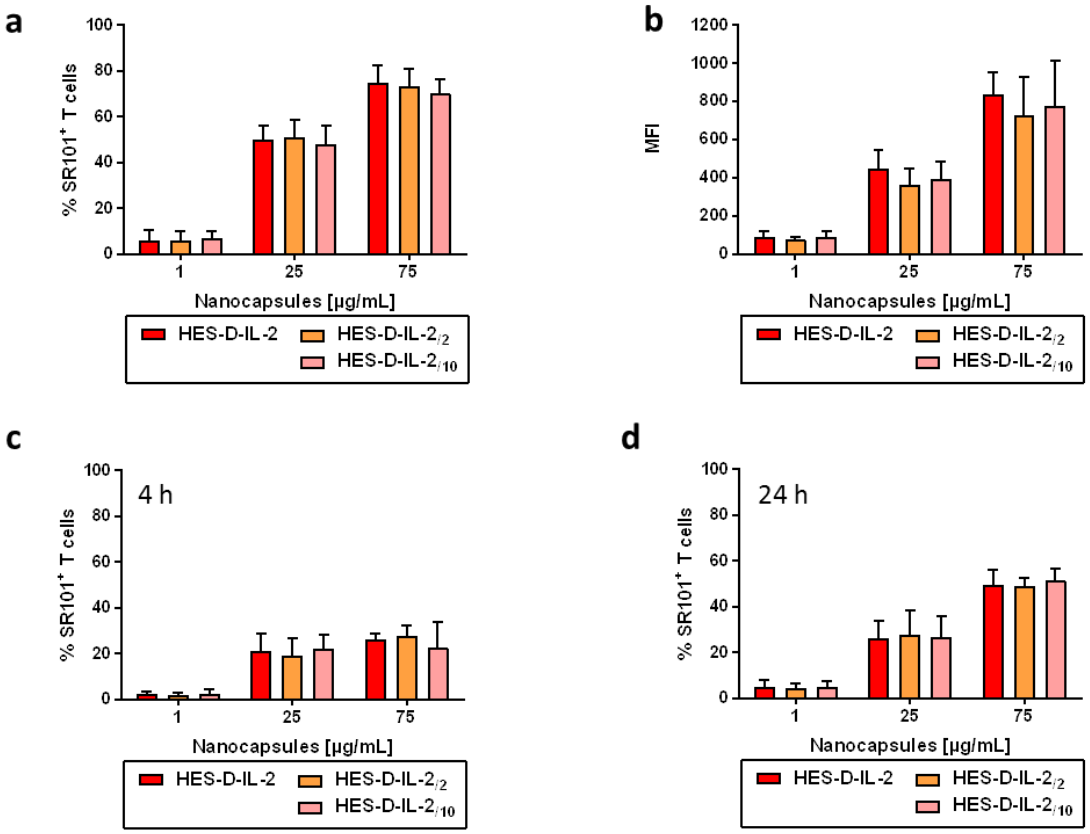

Figure 14: Uptake/binding of HES-D-IL-2, HES-D-IL-2$_{/2}$ and HES-D-IL-2$_{/10}$ by CD4$^+$CD25^{high} Tregs *a)/b)* To assess the uptake/binding by human Tregs, stimulated CD4$^+$CD25^{high} Tregs were incubated with HES-D-IL-2, HES-D-IL-2$_{/2}$ and HES-D-IL-2$_{/10}$ for 72 h and SR101 expression was plotted against CTV expression. Uptake/binding was investigated as percentage of SR101$^+$ cells (a) and as MFI (b). *c)/d)* The percentage of SR101$^+$ Tregs after incubation with HES-D-IL-2, HES-D-IL-2$_{/2}$ and HES-D-IL-2$_{/10}$ was also investigated after 4 h *(c)* and 24 h *(d).*

The figure illustrates summarized data of 4 independent experiments as mean ± SD. Statistics were calculated by two-sided, ungrouped student t tests (*p < 0.05, **p < 0.01, ***p < 0.001).

3.1.2.4. Comparative studies of the HES-D-IL-2 uptake/binding by activated, naïve and Tregs

To compare the uptake/binding of the IL-2 functionalized NC by different human T cell subsets, the results of the aforementioned experiments were summarized in Figure 15. As illustrated, HES-D-IL-2 revealed the highest uptake/binding capacity by CD4$^+$CD25^{high} Tregs, followed by activated CD4$^+$CD25$^+$ T cells. In contrast, naïve CD4$^+$CD25$^-$ T cells exhibited a low amount of incorporated/bound NC. Those results were obtained by all tested NC concentrations and can be expressed by the percentage of NC-positive cells and by MFI. In addition, those results are independent of the amount of IL-2 that is coupled on the NC surface as similar outcomes were observed for HES-D-IL-2$_{/2}$ and HES-D-IL-2$_{/10}$.

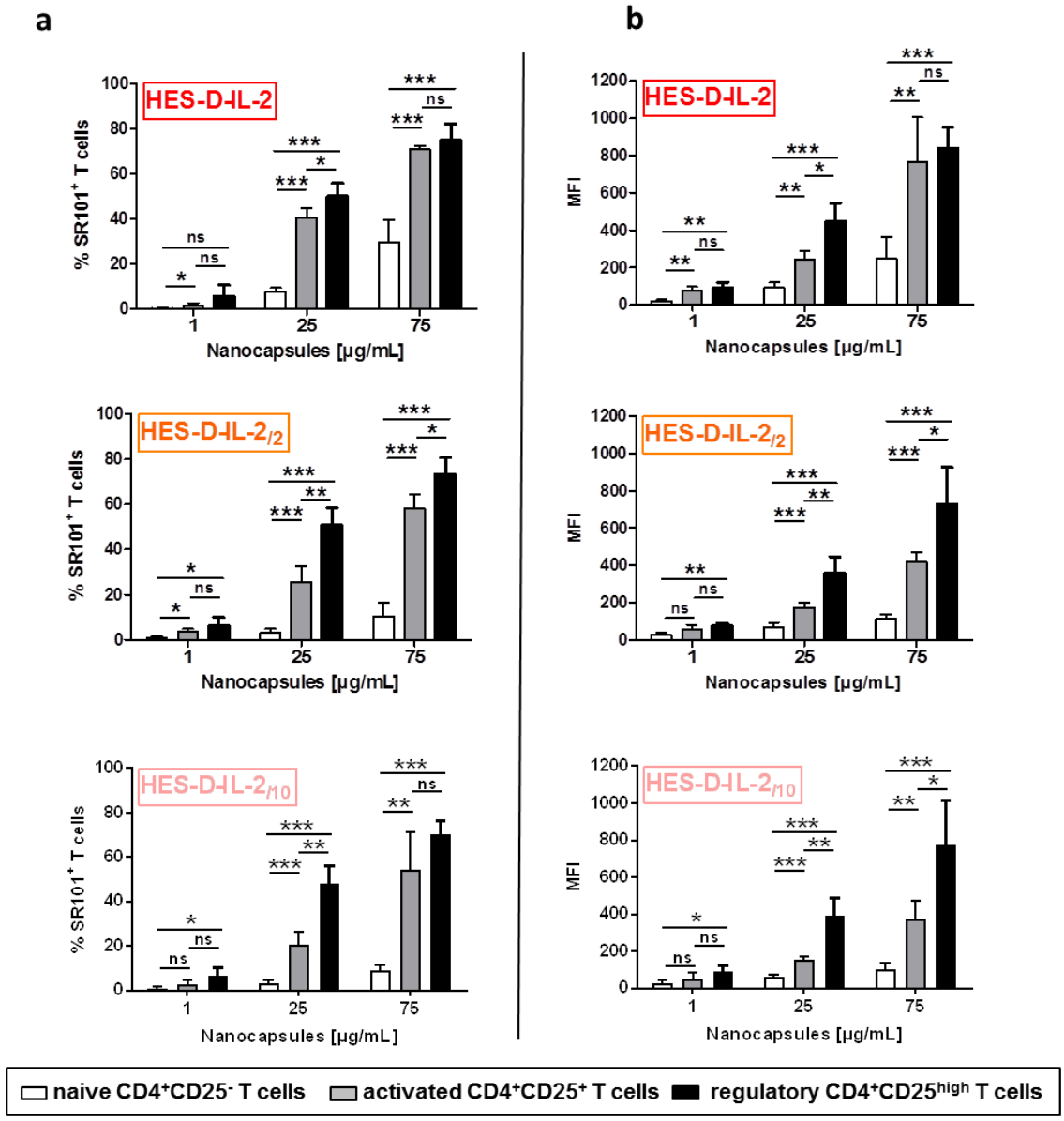

Figure 15: Comparison of the HES-D-IL-2 uptake/binding by human naïve and activated T cells and Tregs.
To compare the uptake/binding of HES-D-IL-2, HES-D-IL-$2_{/2}$ and HES-D-IL-$2_{/10}$ by $CD4^+CD25^-$ naïve T cells, $CD4^+CD25^+$ activated T cells and $CD4^+CD25^{high}$ Tregs, the different T cell populations were incubated with the IL-2 functionalized NC for 72 h and SR10 expression was plotted against CTV expression.
a) The figure illustrates the percentage of $SR101^+$ T cells after 72 h.
b) The figures display the MFI of SR101 expression of T cells after 72 h.
The figure illustrates the mean ± SD percentage of $SR101^+$ cells of 4 independent experiments. The statistics in these experiments were calculated by two-sided, ungrouped student t tests (ns = not significant, *p < 0.05, **p < 0.01, ***p < 0.001).

3.1.3. Specificity of the HES-D-IL-2 uptake

3.1.3.1. CD25 staining

The specificity of the uptake by the IL-2 functionalized NC was first tested by staining of the IL-2 receptor α-chain CD25 which is upregulated upon T cell stimulation, resembling the high

affinity IL-2 receptor together with CD122 and CD132. Activated $CD4^+CD25^+$ T cells were generated, checked for purity and subsequently incubated with 25 µg/ml HES-D-IL-2 for 72 h. After harvesting and Fixable Viability Dye staining, they were additionally stained with anti-CD25 mAb and analyzed by flow cytometry. $CD25^-$, $CD25^{intermediate(int)}$ and $CD25^{high}$ cells were gated as depicted in Figure 16a and uptake/binding by the different subsets was assessed and summarized in Figure 16b. $CD25^-$ cells exhibited only a negligible percentage of $SR101^+$ T cells. In contrast, $CD25^+$ T cells and most pronounced $CD25^{high}$ T cells revealed strong uptake/binding of HES-D-IL-2.

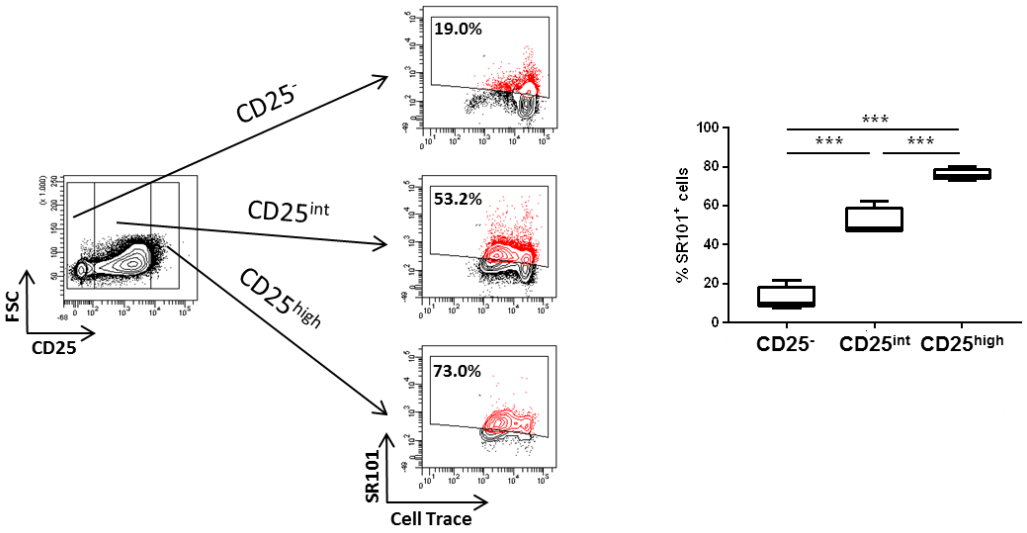

Figure 16: CD25 staining
The CD25-dependence of the HES-D-IL-2 uptake by activated $CD4^+$ T cells was evaluated by staining of the IL-2 receptor α-chain CD25 after 72 h culture of activated T cells with HES-D-IL-2 at a concentration of 25 µg/ml.
a) For flow cytometry analysis, T cells were gated on $CD25^-$, $CD25^{int}$ and $CD25^{high}$ cells and uptake was depicted as percentage of $SR101^+$ T cells plotted against CTV expression. The figure displays a representative result of 4 independent experiments
b) The figure shows uptake/binding results of 5 independent experiments from *a)* which are summarized as mean ± SD. Statistics were calculated by two-sided, ungrouped student t tests (*$p < 0.05$, **$p < 0.01$, ***$p < 0.001$)

3.1.3.2. Blockade of the high affinity IL-2 receptor by the anti-CD25 monoclonal antibody Simulect (basiliximab)

Furthermore, the effect of high affinity IL-2 receptor blockade on the HES-D-IL-2-induced uptake/binding and proliferation was assessed by using the anti-CD25 mAb Simulect (basiliximab). Activated $CD4^+CD25^+$ T cells were generated equally to the former described experiments. Basiliximab was added during incubation of the activated T cells with the NC, to investigate its effect on uptake/binding of HES-D-IL-2. As shown in Figure 17a-c, the number and percentage of HES-D-IL-2-positive T cells was significantly reduced after 72 h when cells were additionally incubated with basiliximab. Presence of basiliximab in experiments with HES-D NC had no effect on the uptake/binding by activated T cell as demonstrated in Figure 17d.

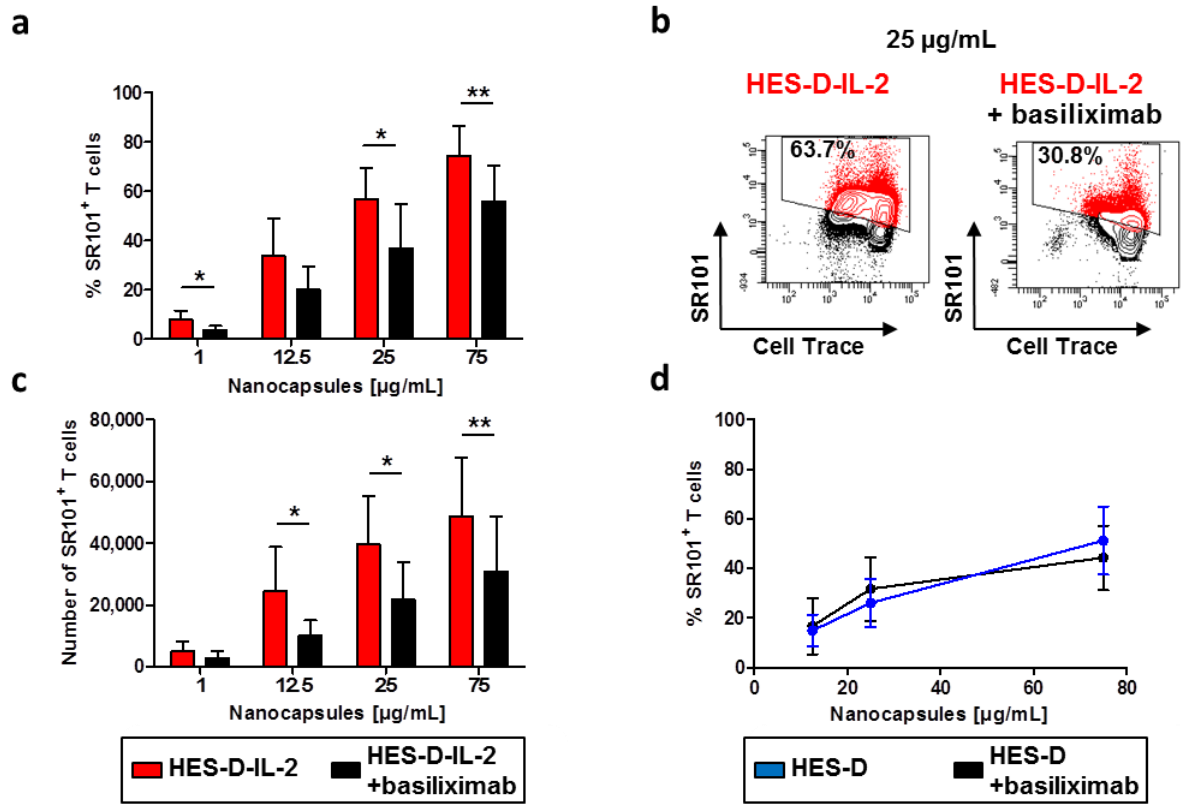

Figure 17: Uptake/binding of HES-D-IL-2 after CD25 blockade
The effect of CD25 inhibition on the uptake of HES-D-IL-2 was investigated by blockade of the high affinity IL-2 receptor-mediated uptake/binding using the anti-CD25 mAb basiliximab during culture of activated $CD4^+$ T cells with HES-D-IL-2 for 72 h.
a) $SR101^+$ T cells were plotted against CTV expression and the percentage of $SR101^+$ T cells was detected. One representative result of 5 independent experiments at a NC concentration of 25 µg/ml is shown.
b) The figure illustrated the uptake/binding results of 5 independent experiments from a) which are summarized as mean ± SD.
c) The number of $SR101^+$ T cells was detected by flow cytometry after incubation of activated $CD4^+CD25^+$ T cells with HES-D-IL-in the presesence or absence of basiliximab. The figure depicts the uptake/binding results of 5 independent experiments which are pooled as mean ± SD.
d) The effect of CD25 blockade by basiliximab on the uptake of HES-D by $CD4^+CD25^+$ activated T cells was evaluated by incubation of stimulated T cells with HES-D in the presence or absence of basiliximab.
The statistics for *b)*, *c)*, and *d)* were calculated by GraphPad Prism using two-sided, ungrouped student t tests (*$p < 0.05$, **$p < 0.01$, ***$p < 0.001$).

Furthermore, the capacity of HES-D-IL-2 to induce a T cell proliferation in combination with high affinity IL-2 receptor blockade by basiliximab was assessed. As shown in the Figures 18a and 18b, the proliferation of activated $CD4^+$ T cells was significantly reduced after blockade of CD25. In line with that, [^{3}H] thymidine cooperation assays revealed a reduced proliferation of activated $CD4^+$ T cells, when basiliximab was present during culture demonstrating (Figure 18c) indicating a CD25-dependet induction of T cell proliferation by HES-D-IL-2.

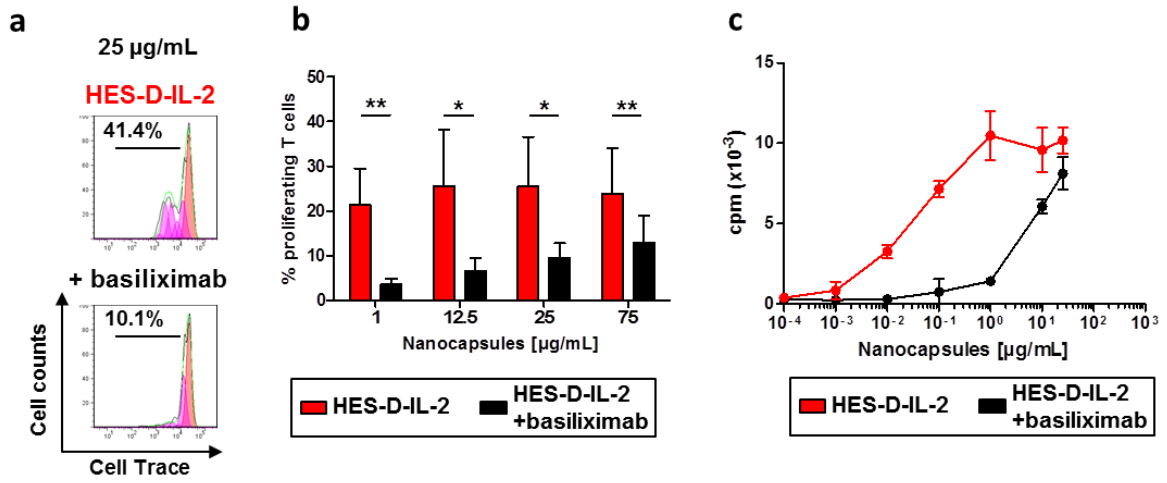

Figure 18: Induction of T cell proliferation by HES-D-IL-2 in the presence of CD25 blockade
To evaluate the induction of proliferation of the NC, by human, activated $CD4^+CD25^+$ T cells were incubated with HES-D-IL-2 with or without basiliximab for 72 h. Proliferation was assessed based on CTV dilution of the proliferating T cells.
a) One representative result of 5 independent experiments is depicted.
b) The figure illustrates pooled proliferation data from of 5 independent experiments from a) as mean ± SD. The statistics were calculated by two-sided, ungrouped student t tests (*p < 0.05, **p < 0.01, ***p < 0.001).
c) The effect of CD25 blockade on the HES-D-IL-2-induced proliferation was also assessed by ^{3}[H] thymidine incorporation for 16 h after 72 h of cell culture. The figure displays one representative result of 3 independent experiments that were set up as triplicates.

3.1.3.3. Competitive studies of HES-D-IL-2 uptake/binding by naïve and activated $CD4^+$ T cells

Competitive studies were performed by incubation of equal numbers of generated CTV^+ $CD25^-$ naïve and $CFDA^+$ $CD25^+$ activated $CD4^+$ T cells with the IL-2 functionalized NC for 72 h in the same wells. CTV and CFDA are both dyes that get diluted during T cell proliferation. As depicted in Figure 19a, $CFDA^+$ and CTV^+ T cells were analyzed separately by gating on the distinct T cell population by flow cytometry. Uptake was then displayed as percentage of $SR101^+$ T cells (Figure 19a). HES-D-IL-2 were strongly incorporated by activated T cells whereas much lower amounts of $SR101^+$ naïve T cells were detected after incubation with all of the tested concentrations (Figure 19b). Furthermore, those results were confirmed by incubation of HES-D-IL-$2_{/2}$ and HES-D-IL-$2_{/10}$ under same conditions. Similar to HES-D-IL-2, activated $CD4^+CD25^+$ T cells exhibited a much higher incorporation of HES-D-IL-$2_{/2}$ and HES-D-IL-$2_{/10}$ than $CD4^+CD25^-$ naïve T cells (Figure 19c). The experiments of Figure 16-18 indicate a specific high affinity IL-2 receptor-dependent uptake of HES-D-IL-2.

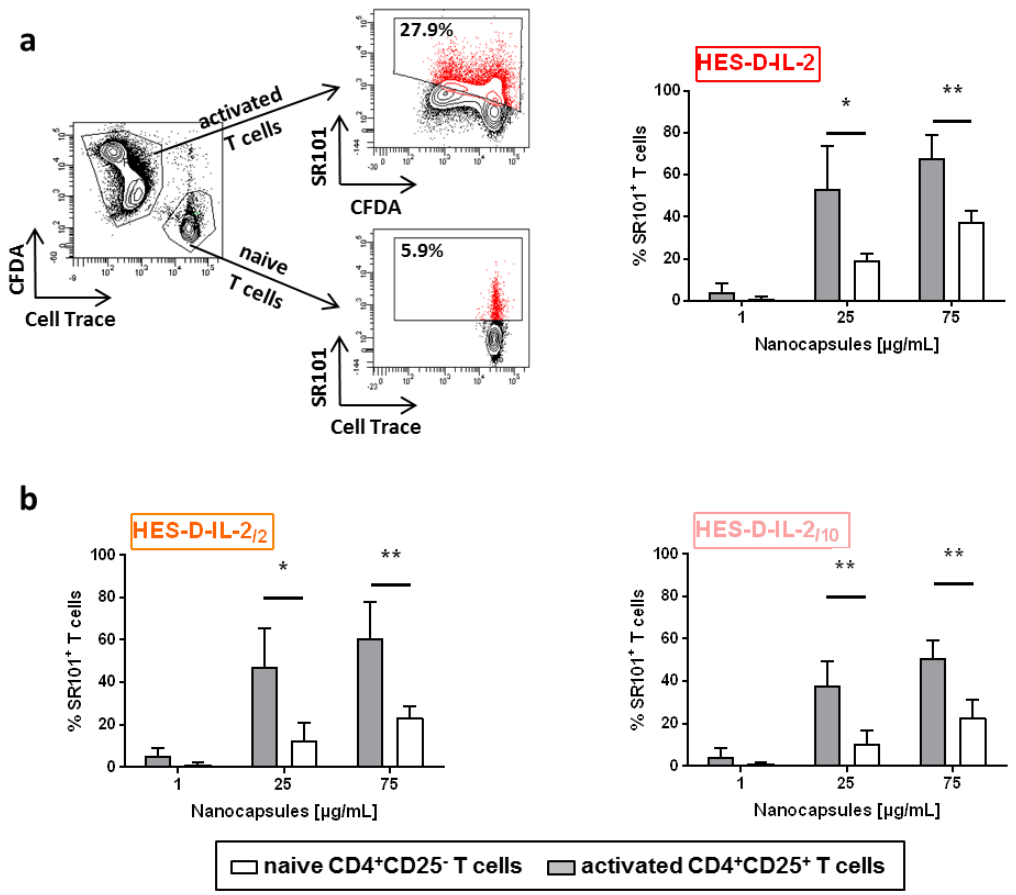

Figure 19: Competitive binding/uptake of HES-D-IL-2 by naïve and activated CD4$^+$ T cells.
The competitive uptake/binding by CTV-positive, naïve CD4$^+$CD25$^-$ T cells and CFDA-positive, activated CD4$^+$CD25$^+$ T cells was assessed by the incubation of HES-D-IL-2 with equal numbers of naïve and activated T cells for 72 h.
a) For flow cytometry analysis, T cells were gated on CFDA$^+$ or CTV$^+$ T cells and uptake/binding was examined by plotting SR101 expression against CTV expression and CFDA$^+$ T cells, respectively. A representative result of 4 independent experiments is depicted.
b) The figure shows the percentages of the uptake/binding of 4 independent experiments from a) which are summarized as mean ± SD.
c) Competition assays were also performed with HES-D-IL-2$_{/2}$ and HES-D-IL-2$_{/10}$. The percentages of the uptake/binding of 4 independent experiments are summarized as mean ± SD.
The statistics in *b)* and *c)* were calculated by GraphPad Prism using two-sided, ungrouped student t tests (*p < 0.05, **p < 0.01, ***p < 0.001).

3.1.4. Different amounts of IL-2 on the NC surface to target different T cell populations

As already illustrated in Figure 15, IL-2 functionalized NC are preferentially taken up by CD4$^+$CD25^{high} Tregs compared to activated CD4$^+$CD25$^+$ and naïve CD4$^+$CD25$^-$ T cells. Furthermore, in contrast to naïve and activated T cells in which uptake/binding clearly depended on the amount of IL-2 on the NC surface, incorporation of HES-D-IL-2 by Tregs was IL-2 concentration-independent. Therefore, it was next tested, whether coupling of different amounts of IL-2 on the NC surface allows preferential targeting of various T cells populations. Those data indicated that IL-2 reduction on the NC surface (most significant at a NC concentration of 25 µg/ml) led to preferential targeting of Tregs compared to naïve T cells but also in comparison to activated T cells as displayed in Figure 20. With reduced amounts

of IL-2, the differences between Tregs and activated T cells, respectively, became more significant which is expressed in a reduction of the p-values which indicated the power of the statistical significance.

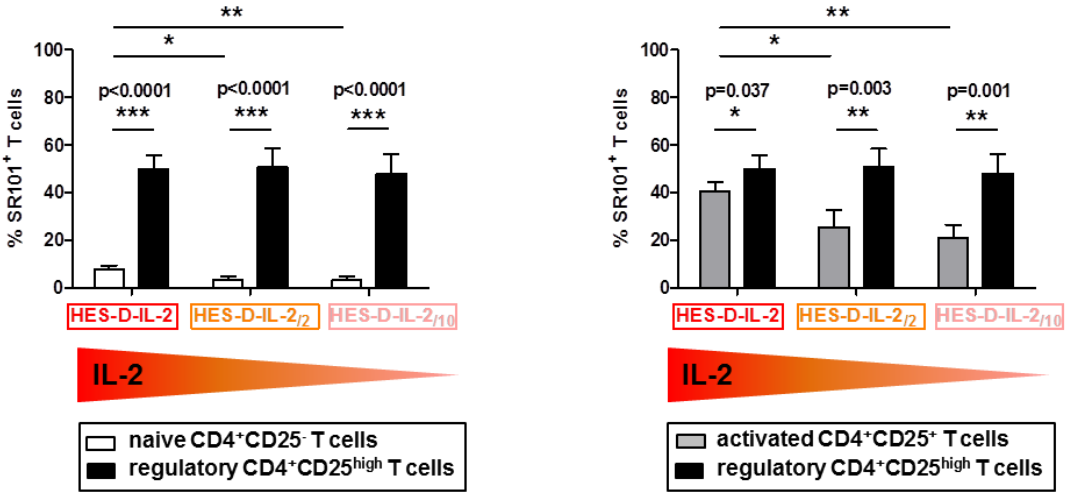

Figure 20: Targeting of different T cell populations by HES-D-IL-2, HES-D-IL-2$_{/2}$ and HES-D-IL-2$_{/10}$. The figures display the differences in uptake/binding of HES-D-IL-2, HES-D-IL-2$_{/2}$ and HES-D-IL-2$_{/10}$ between naïve T cells versus Tregs (left) and activated T cells versus T respectively according to the amount of IL-2 which is present on the NC surface. Therefore, the corresponding T cells were incubated with the IL-2 functionalized NC for 72 h at 25 µg/ml and the percentage of SR101$^+$ T cells was monitored. The figure displays pooled data of 5 independent experiments as mean ± SD and statistics were calculated by two-sided, ungrouped student t tests (*p < 0.05, **p < 0.01, ***p < 0.001).

3.1.5. *In vivo* application of HES-D-IL-2

The targeting properties of the IL-2 functionalized NC of murine and human T cells *in vivo* were investigated by different murine or human T cell-PBMC-reconstituted mouse models.

3.1.5.1. Targeting of murine CD25$^+$ T cell *in vivo*

For targeting of murine CD25$^+$ T cells *in vivo*, HES-D and HES-D-IL-2 were intravenously injected into adult wild-type C57BL/6J mice. After 24 h lymph nodes were harvested and analyzed. For the examination of the uptake by CD4$^+$CD25$^+$ and CD8$^+$CD25$^+$ T cells, cells were pre-gated on Thy1.1$^+$ and subsequently the perentage of CD4$^+$CD25$^+$ and CD8$^+$CD25$^+$ T cells, respectively, was assessed. As shown in Figure 21a approximately 75% of the murine lymph node cells were Thy1.1$^+$. The Thy1.1$^+$ compartment consisted of 55.7% CD4$^+$ and 32.1% CD8$^+$ of which 9.7% and 1.3% were CD25$^+$. Figure 21b illustrates pooled data of the uptake by CD4$^+$CD25$^+$ T cells and CD8$^+$CD25$^+$ T cells. HES-D-IL-2 revealed a significantly enhanced uptake compared to HES-D NC by CD4$^+$CD25$^+$ and CD8$^+$CD25$^+$ T cells. In contrast, CD11c$^+$ dendritic cells, CD11b$^+$ myeloid cells, B220$^+$ B cells and F4/80$^+$ macrophages exhibited no enhanced uptake of HES-D-IL-2 in lymph node cells as highlighted in Figure 21c.

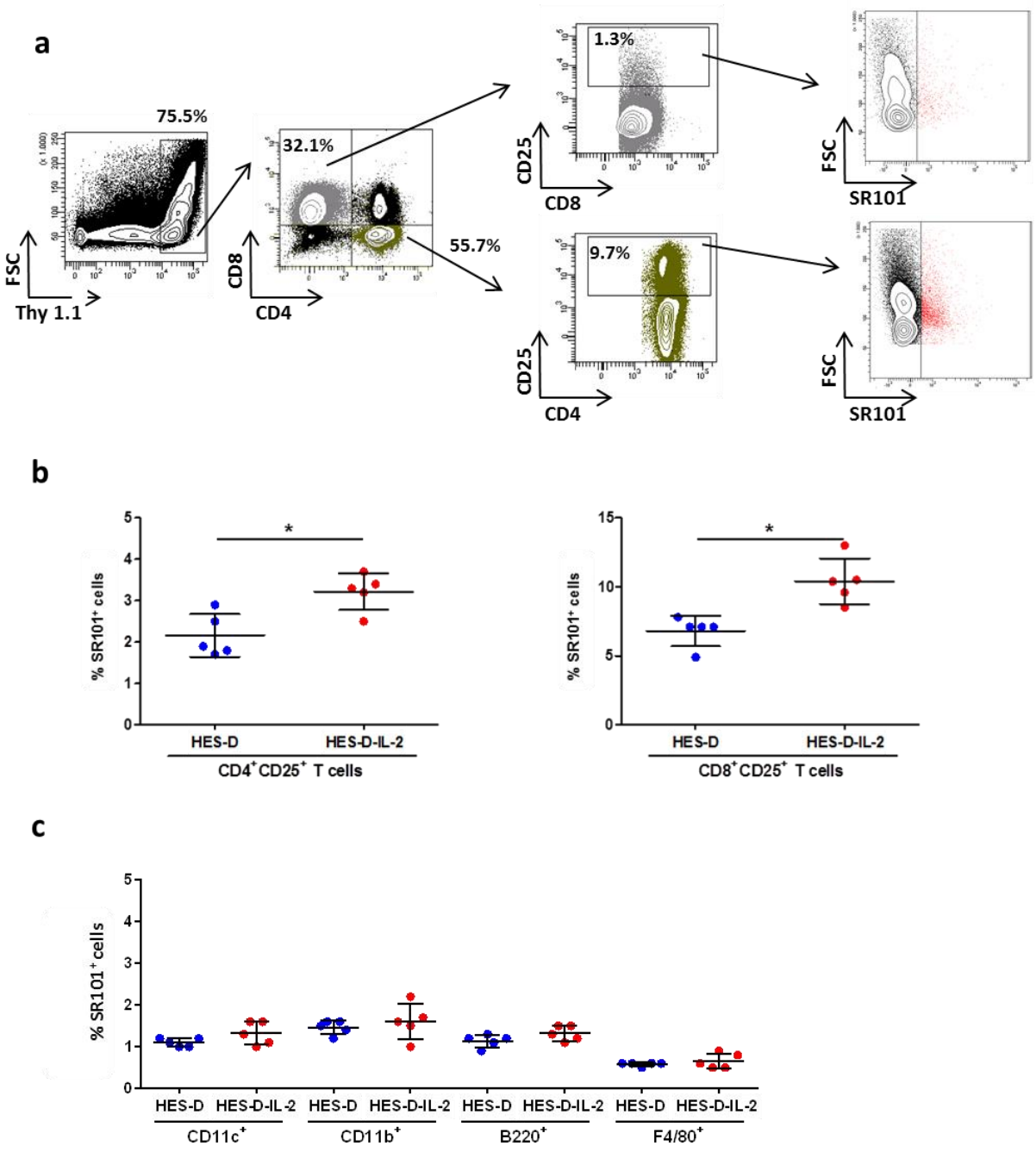

Figure 21: Targeting of murine T cells in vivo.
For the evaluation of murine T cell targeting *in vivo*, wild-type C57BL/6 mice were intravenously injected with SR101$^+$ HES-D-IL-2 and HES-D. After 24 h, lymph nodes were harvested and analyzed.
a) For analysis, lymph node cells were pre-gated on Thy1.1$^+$ cells. These were then divided into CD4$^+$CD25$^+$ and CD8$^+$CD25$^+$ T cells. Afterwards, the percentage of SR101 labeled T cells of each subpopulation was determined. The figure shows a representative result of 10 independently treated mice.
b) The percentages of SR101$^+$ CD4$^+$CD25$^+$ and CD8$^+$CD25$^+$ T cells illustrating the uptake/binding as mean ± SD of 5 different mice are displayed.
c) The percentage of SR101$^+$ immune cells was also assessed after gating on CD11c$^+$ dendritic cellls, CD11b$^+$myeloid cells, B220$^+$ B cells and F4/80$^+$ macrophages. The figure illustrates data as mean ± SD of 5 independently treated mice.
The statistics in these experiments (b) and c)) were calculated by using two-sided, ungrouped student's t tests (*$p < 0.05$, **$p < 0.01$, ***$p < 0.001$).

3.1.5.2. RAG2$^{-/-}$γc$^{-/-}$ mice reconstituted with human T cells for local targeting of human CD25^{+} T cells *in vivo*

The local targeting of human T cells was examined by i.p. injection of human CD4^{+} T cells into RAG2$^{-/-}$γc$^{-/-}$ mice (which are depleted of T cells, B cells and NK cells thus allowing engraftment of transplanted human immune cells). Immediately afterwards, HES-D-IL-2 and HES-D were additionally injected i.p.. After 4 h, human T cells were obtained by an peritoneal lavage and analyzed by flow cytometry. Figure 22a illustrates the gating strategy: first cells were gated on human CD45^{+} immune cells and subsequently on human CD45^{+}CD3^{+} T cells. Then the uptake by CD4^{+}CD25^{+} (11% of CD4^{+} T cells) and CD4^{+}CD25^{-} (89% of CD4^{+} T cells) cells was evaluated. CD4^{+}CD25^{+} T cells revealed a significantly enhanced uptake of HES-D-IL-2 compared to HES-D (Figure 22b left). Furthermore, this uptake/binding was CD25-dependent as CD25^{+} T cells exhibited a significantly augmented percentage of NC-positive cells in comparison to CD25^{-} (Figure 22b right).

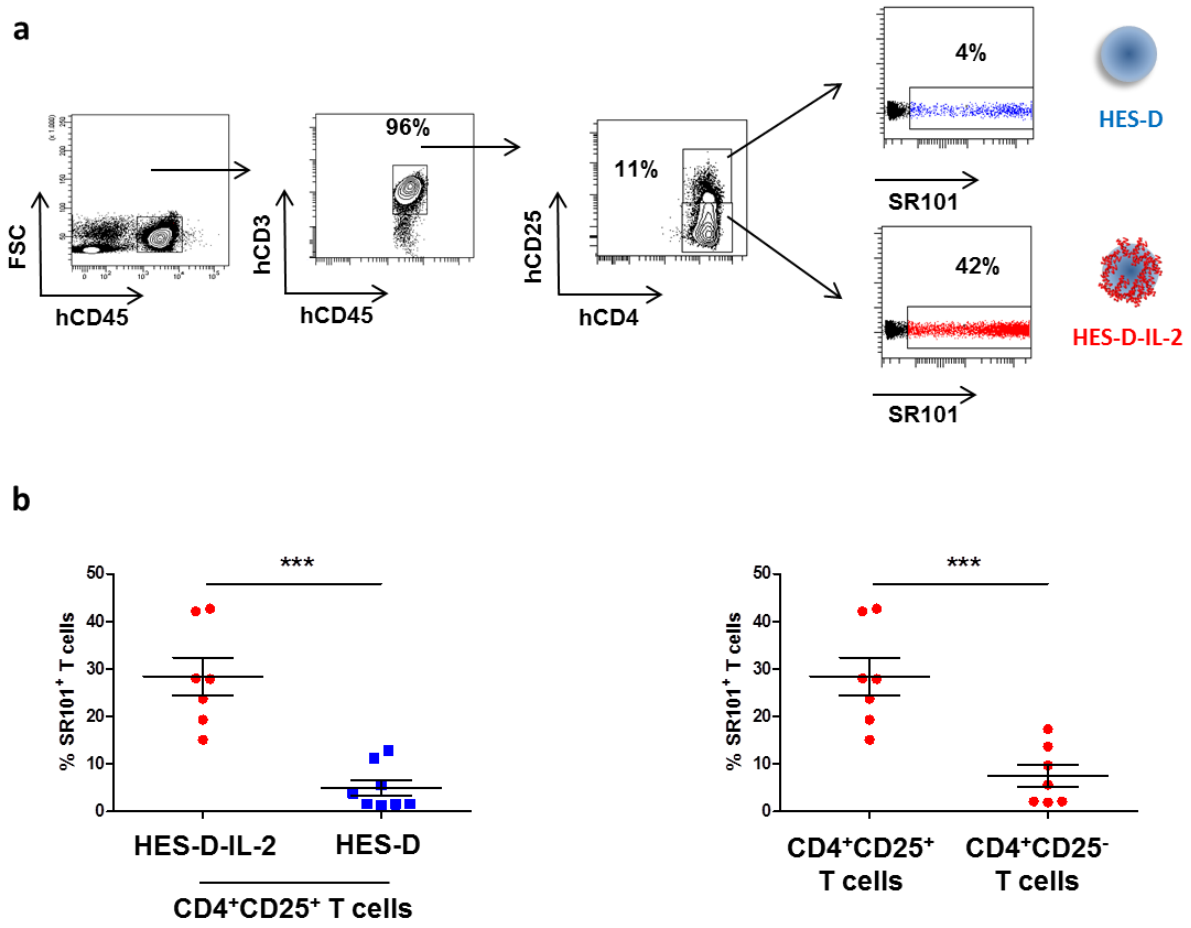

Figure 22: Local targeting of human T cells in vivo.
For the investigation of local targeting of human CD4^{+} T cell *in vivo*, immunodeficient RAG2$^{-/-}$γc$^{-/-}$ mice were i.p. reconstituted with human CD4^{+} T cells. After subsequent injection of HES-D-IL-2 and HES-D, peritoneal cells were obtained by an intraperitoneal lavage.
a) Cells were first gated on human CD45^{+} immune cells. Then, human CD45-/CD3-positive T cells were identified. After gating on human T cells expressing human CD4 and CD25 molecules, the percentage of SR101^{+} cells was assessed. The figure shows a representative result of 2 independent experiments (n=15 mice).

b) The percentages of $SR101^+$ $CD4^+CD25^+$ as mean ± SD of 7 different mice per group after pre-gating, as illustrated in a), are displayed in the left plot. In the right figure, injected human T cells were gated on $CD4^+CD25^-$ and $CD4^+CD25^+$ T cells and the percentage of $SR101^+$ T cells was assessed. Statistics were calculated by two-sided, ungrouped student t tests (*p < 0.05, **p < 0.01, ***p < 0.001).

3.1.5.3. Xenogeneic GvHD model for systemic targeting of human $CD25^+$ T cell *in vivo*

The systemic targeting of human $CD25^+$ T cells *in vivo* by HES-D-IL-2 was investigated using immunodeficient $RAG2^{-/-}\gamma c^{-/-}$ mice which were reconstituted with a human PBMCs. After engraftment of the spleen by human PBMCs without any visible GvHD symptoms 4 weeks after PBMC injection, NC were i.v. injected and spleen cells were analyzed after 24h.Isolated and stained immune cells of one representative animal is depicted in Figure 23a. First, for analysis of the $CD4^+$ and $CD8^+$ T cells, cells were gated on human $CD45^+/CD3^+$ cells which represented 80% of the spleen cell compartment. Thereafter, those cells were further gated on human $CD4^+$ (72%) and $CD8^+$ (10.5%) cells. Among these subsets, $CD25^+$ cells were selected and investigated for SR101 expression to quantify HES-D-IL-2 or HES-D uptake/binding, respectively. Pooled data are summarized in Figure 23b highlighting a significantly increased uptake/binding of HES-D-IL-2 as compared to HES-D. Furthermore, this uptake was CD25-dependent for $CD4^+$ and $CD8^+$ T cells as $CD25^+$ exhibited a significantly enhanced HES-D-IL-2 incorporation which is depicted in Figure 23c.

The *in vivo* experiments demonstrate a successful *in vivo* targeting of murine and human T cells in different organs with different application routes.

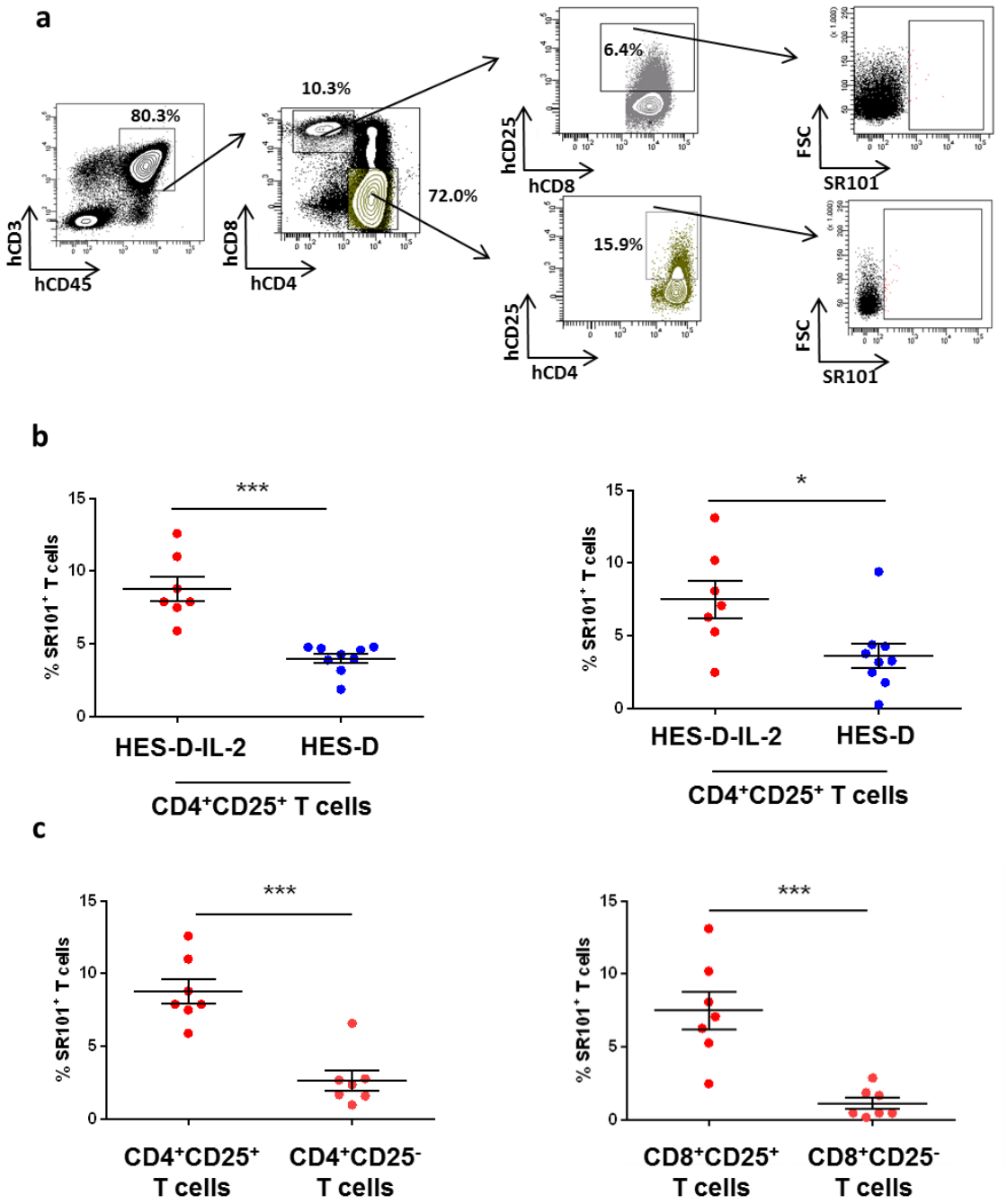

Figure 23: Systemic targeting of human T cells in vivo.
For the investigation of systemic targeting of human $CD4^+$ and $CD8^+$ T cells *in vivo*, immunodeficient $RAG2^{-/-}\gamma c^{-/-}$ mice were engrafted with human PBMCs by i.p. injection. After 4 weeks, HES-D-IL-2 and HES-D were i.v. injected and spleen cells were analyzed 24 h later.
a) Cells were first gated on human CD45 and human CD3 cells. Then, $CD4^+$ T cells and $CD8^+$ T cells were identified and gated on $SR101^+$ $CD4^+CD25^+$ and $CD8^+CD25^+$ T cells. The figure displays a representative result of 3 independent experiments (n=16).
b) The percentages of $SR101^+$ $CD4^+CD25^+$ (left) and $SR101^+$ $CD4^+CD25^+$ (right) as mean ± SD of 7 different mice per group after gating, as shown in a), are illustrated.
c) $CD4^+$ (left) and $CD8^+$ (right) were gate on $CD25^+$ and $CD25^-$ T cells and the percentage of $SR101^+$ T cells was analyzed. The figure illustrates pooled data as mean ± SD of 3 independent experiment (n=16).
The statistics in b) and c) were calculated by GraphPad Prism using two-sided, ungrouped student t tests (*$p < 0.05$, **$p < 0.01$, ***$p < 0.001$).

Furthermore, as shown in Figure 24, murine APCs obtained from the spleen were also analyzed based on their uptake/binding of HES-D and HES-D-IL-2. Therefore, cells were pre-gated on the expression of murine $CD45^+$ immune cells and murine $CD11c^+$ dendritic cells, murine $F4/80^+$ macrophages and murine $CD11b^+$ myeloid cells, respectively. The figure highlights the significantly enhanced uptake of HES-D in relation to HES-D-IL-2 by $F4/80^+$ and $CD11b^+$ cells. In contrast, just slight differences were observed for $CD11c^+$ cells.

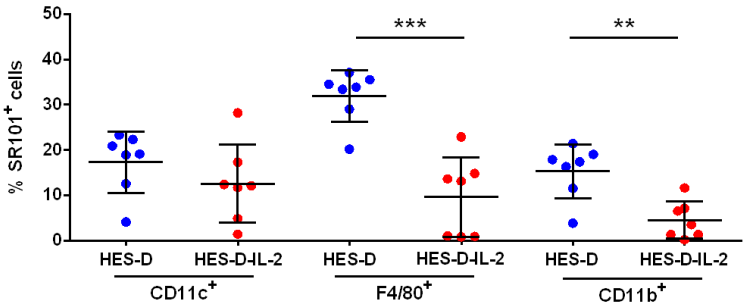

Figure 24: Targeting of murine APCs in the spleen.
For the evaluation of the targeting of murine APCs in the spleen, cells were pre-gated on murine CD45 expression and then CD11c-, F4/80- or CD11b-expressing immune cells were identified. The percentage of $SR101^+$ immune cell populations was validated by flow cytometry. The figure illustrates pooled data as mean ± SD of 3 independent experiments (n = 16) and statistics were calculated by two-sided, ungrouped student t tests (*p < 0.05, **p < 0.01, ***p < 0.001).

3.2. Ovalbumin protein nanocapsules for drug delivery

Because the HES NC did not exhibit any intracellular release (data not shown), ovalbumin protein NC were used as drug delivery system in this study. More precisely, the STAT3 inhibitor S3I-201 was encapsulated into ovalbumin NC to inhibit STAT3 phosphorylation. Similar to the IL-2 functionalized NC in cellular experiments, toxicity of the NC was excluded by Fixable Viability Dye staining.

3.2.1. Quality control of ovalbumin protein nanocapsules

The consistent quality of the ovalbumin protein NC after preparation was ascertained by different physicochemical and biological assays.

The diameter (D_Z) of the ovalbumin protein NC was around 180 nm in water with a narrow size distribution as assessed by dynamic light scattering. After purification of the NC, the zeta potential which was identified by a zeta nanosizer ranged from -10 to -20 mV. The generation and physico-chemical characterization was performed by [redacted] at the Max Planck Institute for Polymer Research in Mainz. Next, it was checked whether the NC are taken up by cells and show intracellular release properties. Therefore, ovalbumin protein NC that contained the cell tracker CMFDA, which can only be detected when it is cleaved by cytosolic esterases, were incubated with HeLa cells. To exclude free CMFDA dye in the NC

supernatant, the supernatant was additionally tested as control. Figure 25 illustrates the results of the cell tracker release in HeLa cells by flow cytometry and CLSM. The ovalbumin protein NC exhibited a detectable CMFDA signal both in flow cytometry (Figure 25a) and by CLSM analysis (Figure 25b). In contrast, no signal was detected when HeLa cells were incubated with the supernatant of the NC (Figure 25).

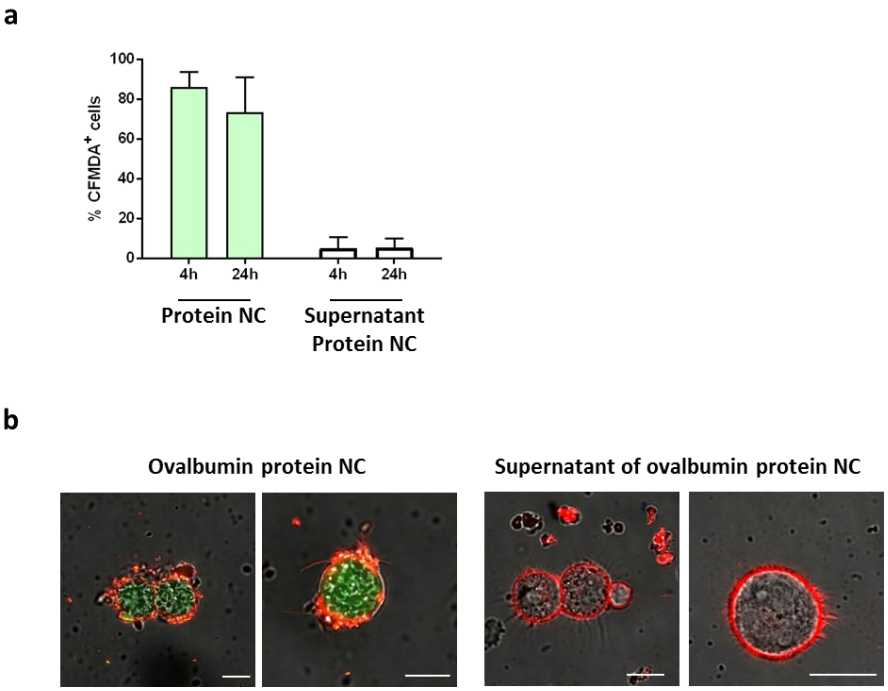

Figure 25: Release properties of ovalbumin protein NC.
The release properties of the ovalbumin protein NC were investigated by encapsulation of the cell tracker CMFDA followed by incubation with HeLa cells.
a) The figure illustrates the CMFDA signal of the ovalbumin protein NC and the supernatant after 4 and 24 h incubation, measured by flow cytometry. Summarized data of 3 independent experiments are depicted as mean ± SD.
b) The CMFDA release was investigated by CLSM. On the left, the ovalbumin protein NC with encapsulated CMFDA are depicted whereas the supernatant of the ovalbumin protein NC is displayed on the right. Cell membrane was stained with CellMask Orange (which is depicted in red), and the cell tracker is depicted in green. Scale bar represents 10 µm.

3.2.2. Inhibition of STAT3 phosphorylation by encapsulated S3I-201

To specifically inhibit the phosphorylation of STAT3, the STAT3 inhibitor S3I-201 was encapsulated into the ovalbumin protein NC. First, the efficacy of soluble S3I-201 was investigated on HeLa cells. Therefore, HeLa cells were incubated with the inhibitor at a concentration of 200 µM for 4h. Within the last 15 min of culture, STAT3 phosphorylation was induced by adding IL-6. Subsequently, STAT3 phosphorylation was assessed by intracellular staining and flow cytometry. After IL-6 stimulation, the amount of phosphorylated STAT3 was significantly elevated in comparison to unstimulated HeLa cells. Furthermore, after pre-incubation with S3I-201, STAT3 phosphorylation was markedly reduced. In contrast, the

amount of total STAT3 protein was identical irrespective of the treatment. Both the percentage and the MFI of phosphorylated STAT3 and STAT3 are summarized in Figure 26.

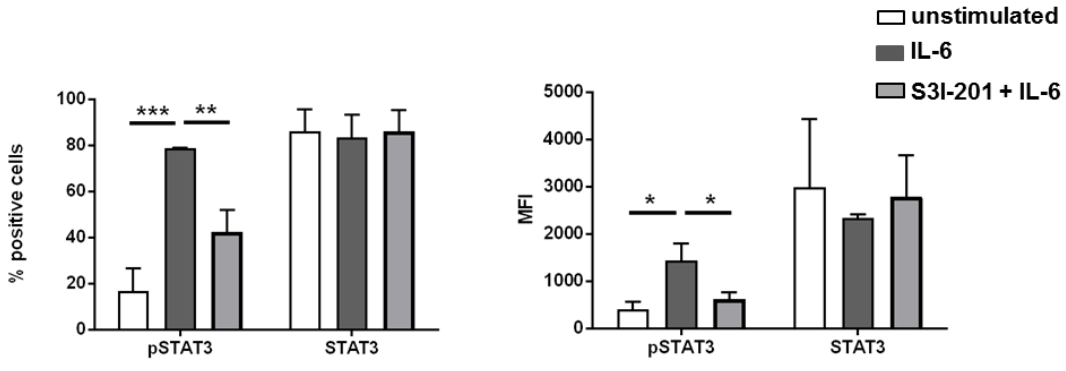

Figure 26: Inhibition of pSTAT3 by soluble S3I-201.
After incubation with S3I-201 and IL-6, pSTAT3 and STAT3 were intracellularly stained in HeLa cells and the expression was evaluated by flow cytometry. The figure illustrates the percentage (left) and MFI (right) of pSTAT3 and STAT3, respectively. Pooled data as mean ± SD of 3 independent experiments are displayed and statistics were calculated by two-sided, ungrouped student t tests (*p < 0.05, **p < 0.01, ***p < 0.001).

Next, S3I-201 was encapsulated into the ovalbumin protein NC. Subsequently, HeLa cells were incubated with the S3I-201-encapsulated ovalbumin protein NC for 4h and within the last 15 min of culture STAT3 phosphorylation was induced by adding IL-6. Ovalbumin protein NC without S3I-201 served as control. Figure 27 displays no significant differences between IL-6 alone and IL-6 with the empty ovalbumin protein NC in percentages of pSTAT3-positive cells and the MFI. However, for ovalbumin protein NC with encapsulated S3I-201, the percentage of pSTAT3-positive cells was significantly reduced, yet STAT3 expression remained unchanged in all settings. In contrast, no significant differences in the MFI were observed.

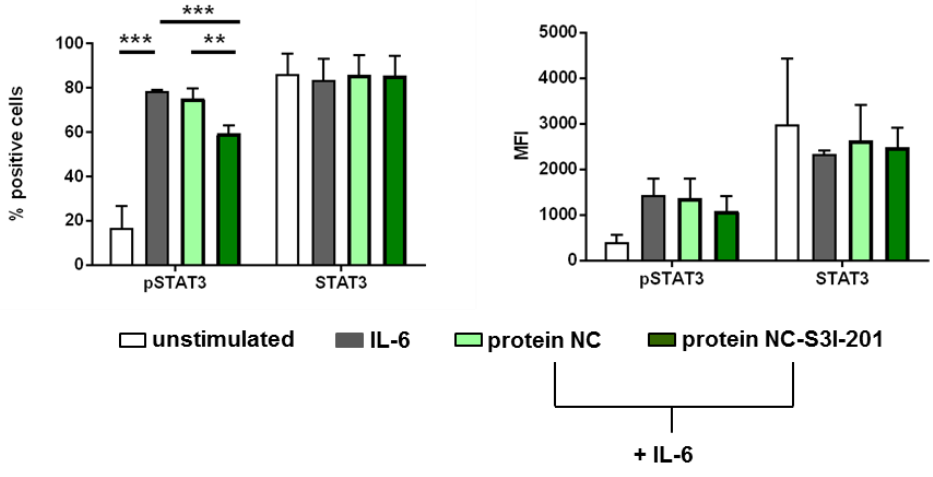

Figure 27: Inhibition of pSTAT3 by encapsulated S3I-201.
The percentage and the MFI of pSTAT3 and STAT3 were evaluated by flow cytometry after incubation of HeLa cells with either empty ovalbumin protein NC, ovalbumin protein NC with encapsulated S3I-

201 plus IL-6 or IL-6 alone. The figure illustrates the percentage (left) and MFI (right) of pSTAT3 and STAT3, respectively. Pooled data as mean ± SD of 3 independent experiments are displayed and statistics were calculated by two-sided, ungrouped student t tests (*$p < 0.05$, **$p < 0.01$, ***$p < 0.001$).

IV Discussion

Cancer immunotherapy is a fast growing field with distinct advantages over conventional therapies because of the opportunity to achieve systemic, long-lasting, antigen-specific tumor protection. Tumor-antigen specific T cells are capable of reaching tissues that are inaccessible to the surgeon, attacking distant microscopically small metastasis and killing slowly dividing tumor cells. In addition, due to immunological memory, tumor immunotherapy can induce lifelong protection against the distinct tumor type. A promising approach in cancer immunotherapy is the inhibition of tumor-associated tolerance mechanisms, that are induced by the tumor, reinforced by immune cells in the tumor microenvironment and can result in augmented tumor growth. However, strong activation of the immune system by immunotherapeutic approaches, which is needed for effective cancer treatment, likely results in serious side effects. Most dominant is the induction of autoimmunity. Hence, cell-type specific drug delivery, that additionally enables the protection of the therapeutic agent, has emerged as a promising approach in cancer immunotherapy.

The motivation of the first part of the present study was to cell-type specifically target T cells with focus on $CD25^{high}$ Tregs by using human IL-2 functionalized HES NC. Tregs are important immune cells for the maintenance of immune hemostasis, yet greatly contributing to tumor-associated immunosuppression in the context of cancer biology [46,161].
The NC, which were used for this project, consisted of hydroxyethyl starch which is a biocompatible, non-toxic, branched polymer and which is used in the clinic as volume expander [162], emphasizing its safety for NC design and the *in vivo* application [163]. Furthermore, studies did not reveal an unspecific uptake of unfunctionalized HES NC [88] which is important for cell type-specific targeting in general. It is in particular important for T cell targeting as T cells represent a low endocytic activity and a small cytoplasm [86].
Cellular uptake and *in vivo* fate of the NC depends on a variety of different factors including, morphology, shape, hydrophobicity and protein adsorption[164-166]. However, size and charge are also critical physico-chemical characteristics that strongly influence NC fate [167]. The NC that were used for T cell targeting revealed a size of ~ 215 nm in diameter. Small nanoparticles of < 10 nm in size are immediately eliminated by renal clearance after injection [168], whereas particles larger than 250 nm are eliminated by the reticulo-endothelial system of the spleen or liver [169]. Thus particles of 100-200 nm in size similar are favourable for efficient circulation times and cellular uptake [165]. The HES-D-IL-2 NC which were used in this study are slightly larger in size (215 nm) but are still too small for being preferentially engulfed by

the reticulo-endothelial system and thus reveal good properties for a long circulation time *in vivo*.

The ζ-potential can be used to as an indicator for the stability of the colloid dispersion: the larger the deviation from zero, the greater the stability [170]. However, colloid stability and ζ-potential depend on and increase with the cytotoxic surfactant SDS that is used for transfer of the NC into an aqueous solution after synthesis [170]. In addition, a ζ-potential closer to neutrality or slightly negative was revealed to be most suitable for low unspecific uptake and a long circulation time [165,171]. The ζ-potential of the capsules used for T cell targeting, ranged from -22 to -7 mV meaning that they are theoretically stable but non toxic and reveal low unspecific uptake.

To cell-type specifically address T cells, in particular Tregs, the 15 kDa cytokine IL-2 was used as targeting ligand. IL-2 preferably interacts with the high affinity IL-2 receptor which consists of CD25 (IL-2 receptor α chain), CD122 (IL-2 receptor ß chain) as well as CD132 (IL-2 receptor γ chain) and is constitutively expressed on Tregs and transiently upregulated on activated T cells [104]. The cytokine was covalently linked to the NC surface by copper-free click reaction. For this purpose, IL-2 was azide-functionalized, and simultaneously, the capsules were equipped with the ring-strained alkyne group of the cyclooctine DBCO by NHS ester reaction chemistry to execute the click reaction between the two chemically reactive groups [129]. The successful azid-functionalization of the IL-2 was revealed as 85% of all IL-2 molecules exhibited at least one azide group. To prevent steric hindering, enable optimal protein mobility and ideally maintain biological activity after coupling, four PEG groups were introduced between the azide and the IL-2 and five between the DBCO and the capsules. The PEG chains may additionally increase circulation time and decrease unspecific uptake by inducing a stealth effect which was already shown for other drug delivery systems [87]. Copper-free click reactions are very mild and biocompatible as the toxic catalyst copper is not required, which is needed when the reaction is initiated at terminal alkyne groups. In addition, the reaction is highly specific as no reactive alkyne and terminal azide groups exist in nature [129]. Thus, this method can even be used for tumor targeting *in situ* by targeting previously conjugated tumor cells [172]. Accordingly, no loss of biological activity was found by comparison of IL-2 coupled to HES-D-IL-2 with the same amount of soluble IL-2. Furthermore, T cell proliferation was induced by IL-2 coupled to HES-D-IL-2 as HES-D did not induce any proliferation of the IL-2 dependent cell line CTLL-2. Confirming the efficacy and stability of the copper-free click reaction only a negligible amount of soluble IL-2 was detected in the NC supernatant as determined by ELISA and CTLL-2 proliferation. However, it needs to be considered that although ELISA and CTLL-2 proliferation are excellent tools to investigate the amount of IL-2 in samples, bioactive IL-2 molecules may not be accessible for detection because the three-dimensional structure of the NC may hinder IL-

2 receptor/antibody binding of all IL-2 molecules. Still, the physicochemical and biological assays represented important quality controls for the further use of IL-2 functionalized NC in cellular uptake and functional experiments.

The human cytokine IL-2 was used for T cell targeting because after binding of IL-2 to the IL-2 receptor the ligand/receptor complex will be internalized, enabling intracellular accumulation of the NC-delivered drug [106,107]. Apart from cytokines, several other targeting ligands, e.g. antibodies, aptamers or carbohydrates are also used for cell type-specific targeting. However, antibodies bear a high risk of potential immunogenicity, which is mainly induced by their binding of complement factors to their Fc parts. Furthermore, undirected, heterogenous antibody orientation on the NC may result in shielding of the antigen-specific variable region. Aptamers are sensitive towards nuclease-based degradation *in vivo* [93,173]. The main obstacle for targeting by carbohydrates is to achieve a sufficient binding strength [93]. Above all, the main advantages of IL-2 as a natural ligand for targeting of IL-2 receptor-bearing T cells, are its internalization after receptor interaction and the high binding strength. As a high binding is needed for receptor mediated internalization it needs to be carefully checked, whether other IL-2 receptor targeting moieties indeed get internalized. [174]. A study of Weissman et al. for example revealed that an antibody binding the IL-2 receptor at high and low receptor binding sites, respectively, was not internalized after binding [174].
In our study, T cell targeting was investigated by the isolation of different T cell subsets with different IL-2 receptor expression, in particular naïve human $CD4^+CD25^-$ T cells, activated $CD4^+CD25^+$ and $CD4^+CD25^{high}$ Tregs. CD132, the IL-2 receptor γ-chain is expressed on all T cell subsets [104,175], whereas CD122 (IL-2 receptor ß chain) and especially CD25 (IL-2 receptor α chain) expression is induced upon stimulation [104,108]. In the present study, activated human T cells were stimulated with anti-CD3 mAb and anti-CD28 mAb for polyclonal activation to induce expression of the high affinity IL-2 receptor [142]. All T cell subsets were analyzed to verify the expression of CD25. As compared to the IL-2 receptor ß chain and the IL-2 receptor γ-chain of the high affinity IL-2 receptor, the IL-2 receptor α chain is highly induced by T cell activation and constantly expressed on Tregs[104]. As expected and in line with the literature, CD25 expression was absent on naïve T cells, whereas it was induced on activated T cells after stimulation and highly expressed on Tregs [104,108,143,144]. To be precise, naïve T cells which are defined as T cells that have not encountered their cognate antigen yet, are only found in the umbilical cord blood. Still the high expression of CD45RA, in contrast to low percentage $CD25^+$ and $CD45RO^+$ T cells indicates a low activation status of the isolated naïve $CD4^+$ T cells [143,176,177]. Furthermore, the high expression of CD25 together with Foxp3, which is the master transcription factor for Treg

development and function implies effective Treg isolation even though Foxp3 is no definite marker for Tregs in humans [46].

First, the uptake/binding of HES-D-IL-2 in comparison to HES-D was investigated by use of activated $CD4^+CD25^+$ T cells. Experiments with HES-D-IL-2 revealed a significantly enhanced uptake/binding by activated $CD4^+$ T cells compared to HES-D, yet also HES-D induced high upake/binding up to 40% dependent on the NC dose. Even though, naked, unfunctionalized HES NC were shown to be biologically inert, revealing no relevant unspecific uptake [88], surface modification by DBCO may influence their biological behavior. Although the natural reaction partner of DBCO does not exist in nature and the reaction was shown to be highly specific [129], the cyclooctyne bears a ring-strained alkyne group which might lead to membrane attachment. Furthermore, HES-D revealed a reduced ζ-potential more distant to zero and a slightly increased size compared to HES-D-IL-2 which also influences the NC-cell interaction. In theory an optimal negative control would be a mutated or truncated IL-2 molecule that exhibits similar characteristics and folding properties as wild-type IL-2 except of the IL-2 receptor binding site. In addition, uptake by HES-D-IL-2 and HES-D is relatively difficult to compare due to proliferation induction by HES-D-IL-2 but not by HES-D. The NC to cell ratio for HES-D is much higher compared to HES-D-IL-2 as the enhanced T cell proliferation may lead to a reduced percentage of $SR101^+$ cells. A possible solution is a normalization of the data to the number of cells after maximal induction of T cell proliferation through IL-2 similar to the experiments with different numbers of IL-2 molecules on the NC surface.

CLSM microscopy confirmed the internalization of HES-D-IL-2 by activated $CD4^+$ T cells as $SR101^+$ NC were located inside the cytoplasm rather than being attached to the membrane. Other opportunities to investigate the differences between uptake and binding are acidic washing steps, which remove membrane-associated NC [178], fluorescence quenching cytofluorometric assays [179] and the coupling of fluorochromes that depend on binding by intracellular proteins or nucleic acids [180,181].

In addition, activated $CD4^+$ T cell proliferation was induced by HES-D-IL-2, whereas HES-D revealed no proliferation induction in agreement with the CTLL-2 proliferation results. These data confirmed the uptake of HES-D-IL-2 as IL-2/IL-2 receptor internalization is indispensable for proliferation induction by IL-2 [118]. In accordance with these results, IL-2 functionalized liposomes were also located inside the T cells after IL-2 receptor engagement [182,183]. Molecules, proteins and also nanoparticles are transported into the cell by endocytosis. Endocytosis can be classified into different endocytic mechanisms including phagocytosis, clathrin-mediated endocytosis, calveolin-mediated endocytosis and macropinocytosis [184]. The IL-2/IL-2 receptor complex is internalized by a clathrin-independent

yet dynamin-dependent mechanism by receptor-mediated endocytosis [185]. After ligand binding, IL-2/IL-2 receptor internalization is regulated by signaling through PI3K-phosphorylated phosphatidylinositol 3 phosphat (PI3P) which activates RhoA and subsequently Rac1 [186]. As consequence p21-activated kinase 1 (Pak1) phosphorylates cortactin which in interaction with Wiskott-Aldrich syndrome protein (N-WASP) regulates IL-2 receptor entry by generation and assembly of F-actin [187-189]. 5-10 min after internalization IL-2 is directed towards lysosomal multivesicular bodies [106]. In contrast to CD25, which is recycled to the membrane surface, CD122 and CD132 also end up in the lysosome [107]. For drug delivery, release into the cytoplasm is favourable compared to lysosomal degradation. Yet it still needs to be assessed whether HES-D-IL-2 are really taken up similar to soluble IL-2 and whether intracellular fate remains identical. Even though observations revealed that particles around 200 nm in size are also internalized by clathrin-independent mechanisms, internalization of IL-2 was rather found to result in vesicles of around 100 nm [189,190]. However, HES-D-IL-2 may also use that way of internalization, e.g. by triggering IL-2 receptor clustering. Endocytotic mechanisms and intracellular fate of HES-D-IL-2 may be assessed by inhibition of distinct endocytotic pathways, co-staining of cellular compartments or live cell imaging [190-192]. Still, although NC are transferred into the endosome, endosomal escape can be achieved by endosomolytic structures like INF-7 or listeriolysin to facilitate entry into the cytoplasm [193,194].

In the experiments with activated $CD4^+CD25^+$ T cells, the uptake/binding of HES-D-IL-2 was already relatively high and according to the literature $CD4^+CD25^{high}$ Tregs exhibit an enhanced IL-2 sensitivity compared to activated $CD4^+CD25^+$ T cells due to constitutive high affinity IL-2 receptor expression [104,108,195]. Therefore, the amount of IL-2 on the NC surface was reduced twofold and tenfold to more preferentially address Tregs. Subsequently, uptake/binding was assessed again by comparing $CD4^+CD25^-$ naïve T cells, $CD4^+CD25^+$ activated T cells and $CD4^+CD25^{high}$ Tregs. Calculation of the number of IL-2 molecules on the NC by determination of free DBCO groups using 9-(azidomethyl)anthracene [140] confirmed the reduced coupling of IL-2 on the surface of HES-D-IL-$2_{/2}$ and HES-D-IL-$2_{/10}$, respectively. In addition, ELISA and proliferation of CTLL-2 cells confirmed the chemically determined differences in the amount of IL-2. In line with that, the uptake/binding of HES-D-IL-2 by activated $CD4^+CD25^+$ T cells and their induction of T cell proliferation also depended on the number of IL-2 molecules on the NC. Uptake/binding was evaluated as normalized percentage of NC-positive cells to 50 U/ml IL-2. This calculation was performed to evaluated whether reduced amounts of IL-2 on the NC surface may induce and inhibited proliferation of activated $CD4^+CD25^+$, resulting in different NC to T cell ratios. In general, naïve $CD4^+CD25^-$ T cells exhibited a reduced uptake of the IL-2 functionalized NC compared to activated

$CD4^+CD25^+$ T cells due to absence of the high affinity IL-2 receptor whose expression is induced upon T cell stimulation[196-198]. In addition, uptake of IL-2 functionalized NC by naïve T cells as well as activated T cells depended on the amount of IL-2 that was present on the NC. In contrast, $CD4^+CD25^{high}$ Tregs revealed the most prominent uptake/binding of the IL-2 functionalized NC compared to naïve and Tregs due to constitutive expression of the high affinity IL-2 receptor [195]. Apparently, the uptake by Tregs was independent on the IL-2 amount on the NC surface. Therefore, a reduction of NC-coupled IL-2 favors Tregs targeting in contrast to naïve and effector T cells at least in the tested concentrations. Multiple studies have already demonstrated that Tregs are more sensitive to IL-2 than effector T cells [199-202]. In particular, Yu et al. revealed a 10-fold reduced activation threshold of Tregs towards IL-2 compared to effector T cells, measured by activation of STAT5 which is phosphorylated downstream of IL-2 signaling [203]. Furthermore, the IL-2 threshold for the expression of target genes downstream of STAT5 was 100-fold reduced compared to effector T cells [203]. Hereby it is also important to consider the differences of IL-2 receptor signaling between effector T cells and Tregs. In response to IL-2 stimulation during activation, activated $CD4^+$ T cells receive signals that are transduced via STAT5, PI3K/PKB and MAPK. In contrast, Tregs express high levels of PTEN which dampens PI3K/PKB signaling by dephosphorylation of PI3P to PI2P [204,205]. Therefore, IL-2 receptor signal transduction in Tregs may exhibit a greater dependency on STAT5 [110]. Furthermore, Tregs not only exhibit a higher IL-2 sensitivity, yet they also depend on low levels of IL-2 for development, homeostasis and survival [206,207]. That dependency was impressively demonstrated by IL-2 or IL-2 receptor-deficient mice that develop autoimmune symptoms which can be reversed by adoptive transfer of functional Tregs [208,209]. However, during the initiation, memory generation and secondary expansion of adaptive immunity local high IL-2 doses are needed especially for sufficient cytotoxic $CD8^+$ T cell responses which upregulate the expression of the high affinity IL-2 receptor upon activation [108]. Those observations confirmed the role of IL-2 as a T cell growth factor which was thought to be the sole function of IL-2 in at its discovery 1976 [102]. The current point of view is that low but constant IL-2 concentration during steady state results in maintenance of Tregs, whereas high local IL-2 secretion leads to the initiation of adaptive immune responses [108,210]. The dual role of IL-2 was exploited in current IL-2-related immunotherapy. Low-dose injection of IL-2 preferably leads to the expansion of Tregs which may be suitable for the treatment of autoimmune diseases like systemic lupus erythematosus (SLE) [211], type 1 diabetes [203] as well as graft versus host disease [212]. In contrast, high-dose IL-2 injection may be used to initiate adaptive immune responses resulting in efficient anti-tumor immunity as observed in metastatic melanoma and metastatic renal cell carcinoma [213]. In addition, patients suffering from viral infection also benefit from high dose IL-2 therapy [214]. The enhanced IL-2 receptor sensitivity may also explain the observation that Tregs do not

depend on the amount of IL-2 on the NC surface in the used concentrations. Even the tenfold reduced amount was sufficient to target Tregs sufficiently, leading to a more specific targeting of Tregs compared to both other T cell subsets. Yet, it needs to be investigated whether HES-D-IL-2 binding on Tregs also leads to internalization of the NC, especially as IL-2 receptor internalization depends on PI3K activated PIP3 which is reduced in Tregs due to high PTEN activity [186,215,216]. In addition, a higher Treg specificity may also be induced by of coupling IL-2/mAb complexes. For instance, the antibody JES6-1, which mimics linkage to CD122 and therefore preferably addresses high affinity IL-2 receptor expressing Tregs, may be used for a more specific Treg targeting when complexed with IL-2 [114].

The specificity of the observed uptake/binding of HES-D-IL-2 by high affinity IL-2 receptor expressing T cells was investigated by a) anti-CD25 mAb staining on activated $CD4^+CD25^-$ T cells after uptake b) inhibition of the high affinity IL-2 receptor-mediated uptake/binding and induction of proliferation by HES-D-IL-2 on activated T cells via blockade by the anti-CD25 mAb basiliximab[149] c) comparison of the uptake by naïve $CD4^+CD25^-$ T cell in competition experiments with activated $CD4^+CD25^+$ T cells. All experiments indicated that uptake/binding and proliferation is dependent on CD25 expression, as the IL-2 receptor α-chain is highly regulated by T cell activation.
In comparison to HES-D, which problems as a control capsule have already been discussed, CD25 staining is probably the better control to test whether the uptake/binding of HES-D-IL-2 is indeed dependent on IL-2 bound to the NC surface. As only negligible numbers of NC-positive cells were found in the $CD25^-$ cell compartment and as the uptake/binding by $CD25^{high}$ T cells was even higher compared to $CD25^{int}$ T cells, the dependency of HES-D-IL-2 uptake/binding on the high affinity IL-2 receptor was already indicated. Those results were confirmed by inhibition of the high affinity IL-2 receptor-mediated uptake/binding by anti-CD25 mAb-blockade which affected the internalization of HES-D-IL-2 but not of HES-D. Furthermore, competitive studies of naïve $CD4^+CD25^-$ and activated $CD4^+CD25^+$ T cells supported those observations and additionally gave a first hint that HES-D-IL-2 also specifically target IL-2 receptor-positive T cells in the presence of other cell types which is an important feature for *in vivo* applications. Specificity of the observed uptake/binding may additionally be investigated in replacement experiments by adding increasing amounts of soluble IL-2 (which is the natural ligand of the IL-2 receptor) to the uptake/binding experiments. Those experiments may also reveal a higher avidity of the NC coupled IL-2 because of a high spartial densitiy on the NC surface which may lead to IL-2 receptor clustering.

For application as an anti-cancer immunotherapeutic, the capability of HES-D-IL-2 on $CD4^+CD25^+$ and $CD8^+CD25^+$ T cell targeting should also be evaluated *in vivo*. Targeting of $CD25^+$ T cells in a living organism displays various additional obstacles compared to the isolated *in vitro* situation [217]. First, when getting in contact with blood, serum proteins may adsorb on the NC surface, forming a protein corona, which greatly influences the cellular uptake and biodistribution of the NC [85,218]. In addition, if proteins adsorb on the NC surface they could theoretically hide the targeting ligand IL-2 resulting in unspecific drug delivery [218]. During *in vivo* application, it also needs to be considered, that the nanoparticles need to reach their destination, either the targeted organ, the targeted cell type or both. As already mentioned, biodistribution and cellular uptake depend on multiple factors including size, charge, and shape of the NC [164-166]. Another limitation of the use of nanodimensional drug delivery systems, especially for targeting of low-endocytotic cells like T cells, is the competition of the NC uptake with phagocytic immune cells like macrophages or DCs [217]. Inducing a stealth effect of the NC by shielding with HES or PEG reduces unspecific uptake by phagocytic cells but due to their natural tasks uptake by phagocytic cells will probably never be prevented completely [87,88]. HES-D-IL-2 used in our study consisted of HES and also included 9 different PEG groups which should prevent rapid clearance from the liver.

The *in vivo* properties of HES-D-IL-2 on the uptake/binding by murine T cells after i.v. injection into wild-type C57BL6 mice was assessed after 24 h in the lymph nodes as sites of adaptive immune response [27]. The uptake of HES-D-IL-2 in comparison to HES-D was significantly enhanced for $CD4^+CD25^+$ and $CD8^+CD25^+$ T cells, demonstrating an efficient $CD25^+$ T cell targeting. Cells were gated on Thy1.1 expression which is used as a T cell marker thereby excluding other $CD4^+CD25^+$ and $CD8^+CD25^+$ expressing immune cells respectively [219]. Those results demonstrated effective IL-2 receptor-dependent targeting properties of HES-D-IL-2 after i.v. injection. Additionally, several phagocytic and antigen presenting lymph node resident cells, in particular $CD11c^+$ dendritic cells, $CD11b^+$ myeloid cells, $B220^+$ B cells, and $F4/80^+$ macrophages revealed no significantly enhanced uptake of HES-D-IL-2 in comparison to HES-D. DCs are highly enriched in the CD11c cell compartment whereas CD11b is mainly expressed on myeloid cells and B cells [220,221]. B220 is a marker that is expressed on all murine B cells [222] but not exclusively similar to F4/80 which was used as a marker for macrophages [223].

However, experimental mouse models have some clear limitations when compared to application in humans which are due to differences between the murine and human immune system [224]. For instance, human IL-2 which was used as the targeting vector in this study has a lower binding affinity towards the murine IL-2 receptor compared to murine IL-2 and vice versa [225].

For targeting of human $CD25^+$ T cells *in vivo*, we used human T cell- or PBMC-reconstituted $RAG2^{-/-}\gamma c^{-/-}$ mice. $RAG2^{-/-}\gamma c^{-/-}$ mice are depleted of T and B cells because of a homozygous knock out of the *rag2* gene resulting in inability to initiate V-(D-)J- recombination and receptor arrangement [156,226]. Furthermore, the knock out of the common γ-chain which is part of the IL-2 receptor, additionally leads to depletion of most NK cells and enhances engraftment by human cells [227]. Yet a great limitation of human cell-reconstituted immunodeficient mice is the development of a severe GvHD [159,228,229]. This GvHD is dependent on the age of the mice that were reconstituted, the duration of engraftment and the number of human immune cells that were injected [177,230].

In a first approach, i.p. injected human $CD4^+CD25^+$ T cells were addressed after directly followed i.p. application of the NC. T cells were analyzed 4 h after injection. HES-IL-2 revealed an enhanced uptake/binding compared to HES-D in $CD4^+CD25^+$ T cells and this uptake was CD25-dependant. Even though this is a very artificial *in vivo* system, because T cells and NC are injected at the same location, so no transfer to the target cells is required, these experiments demonstrated an efficient local HES-D-IL-2 targeting of human $CD4^+CD25^+$ T cells in an *in vivo* environment.

To investigate the targeting of human $CD25^+$ T cells *in vivo* in a more physiological setting, human PBMCs were i.p. injected into $RAG2^{-/-}\gamma c^{-/-}$ mice. After engraftment for 4 weeks, NC were intravenously injected and spleen cells were analyzed for human T cell targeting. The transfer of human PBMCs into immunodeficient mice results in infiltration of human T cells into various organs leading to the GvHD induction. For instance, the spleen is a target organ for human activated T cell infiltration resulting in splenomegaly [177]. Yet, the conditions that were used in this experimental setup did not induce any GvHD symptoms that were measured by a clinical score which was developed by Cooke et al. [160]. However, analysis of the spleens exhibited a pronounced human T cell infiltration with a higher activation status of ~16% $CD4^+CD25^+$ T cells and ~ 7% $CD8^+CD25^+$ T cells which are usually ~ 10% and ~ 5% respectively [231]. Splenic targeting of human $CD4^+CD25^+$ and $CD8^+CD25^+$ T cells by HES-D-IL-2 was indeed successful. Compared to HES-D, HES-D-IL-2 revealed a significantly enhanced uptake that was CD25-dependent. Furthermore, murine phagocytic $CD11c^+$, $CD11b^+$ and $F4/80^+$ immune cells from the spleen exhibited an enhanced uptake of HES-D as compared to HES-D-IL-2 which supports the assumption that the different physico-chemical properties of HES-D may result in an enhanced unspecific uptake.

In contrast to address APCs which is a frequently used approach in nanoparticle-based cancer immunotherapy, targeting T cells remains difficult due to low endocytic activity [117]. However, various different approaches have been evaluated to specifically deliver immunotherapeutic agents to T cells [17]. For instance, nanoparticle-based targeting of effector

T cells was evaluated by coupling of anti-CD3 mAb fragments to the surface of nanoparticles which leads to internalization and expansion of antigen experienced T cells *in vivo* [232,233]. Anti-CD3 mAbs were also used in a study by Smith et al. which directed desoxy-ribonucleic acid (DNA)-bearing nanoparticles to T cells to introduce leukemia-targeting CAR genes [234]. In another antibody-based approach Lee et al. successfully delivered small interfering ribonucleic acid (siRNA) to T cells by using CD7-specific single-chain antibodies [235]. Recent nanoparticle-based T cell targeting studies also focus on the expansion of antigen-experienced T cells *in vivo* either by co-targeting of tumor cells and T cells to induce efficient anti-tumor immune responses [236] or by coating of disease relevant proteins bearing MHC class II molecules to expand Tregs [237]. However, also Tregs in the tumor microenvironment were successfully targeted by nanoparticles which were functionalized with antibodies against the glucocorticoid-induced TNFR-related receptor (GITR), that reveals higher expression on intratumoral Tregs compared to Tregs in the periphery [238].

Moreover, nanoparticle-based functionalization, complexation and encapsulation of IL-2 has been validated for various immunotherapeutic settings. Most studies used IL-2 as an immune stimulating agent to induce anti-tumor immunity. When injected alone, the short half-life of recombinant IL-2 requires multiple injections of high doses that lead to serious side effects [239]. Nanoparticle-coupled IL-2 for cancer immunotherapy is either applied directly *in vivo* [239,240] or for antigen-specific T cell expansion *ex vivo* [241]. Immunostimulatory capacity of nanoparticle-bound IL-2 was also demonstrated for viral infections [242]. Furthermore, IL-2 conjugated nanoparticles were described for co-delivering agents together with other biomolecules or inhibitors to either activate effector T cells or Tregs [240,243]. So far, only two studies focused on IL-2 functionalized liposomes as an intracellular targeting vector for IL-2 receptor-positive T cells [182,183]. Konigsberg et al. used IL-2 functionalized nanoparticles for targeting activated T cells to cell-specifically deliver methotrexate [182]. In contrast, Zheng et al. used IL-2 functionalized nanoparticles to cell-specifically address and stimulate adoptively transferred $CD25^+$ T cells resulting in repeated functional targeting of T cells *in vivo* [183]. In this context it also needs to be mentioned that IL-2 binding by Tregs has also been exploited by fusion of diphtheria toxin to IL-2 (denileukin diftitox, ONTAK) to deplete Tregs for induction of efficient anti-tumor immune responses [244,245].

In this study, targeting of Tregs should be combined with inhibition of Treg function by STAT3 blockade. For Treg-specific inhibition of STAT3 a drug delivery system is required as systemic application would not reach the target cells in sufficient concentration without inducing serious side effects. Systemic STAT3 inhibition results in severe adverse effects like for example neurotoxcicity [121] and inhibition of STAT3 function is life-threatening at least during development. which is best highlighted by the embryonic lethality of STAT3 knockout

mice [246]. Furthermore, STAT3 inibitors in general need to be present at relatively high concentrations to induce effective pSTAT3 inhibition [247]. In undiseased body cells, STAT3 is present in an inactive form under steady state conditions. Activation is triggered by phosphorylation of the critical tyrosine residue Tyr705, yet STAT3 can also be activated by phosphorylation of a serine Ser727. Activation of STAT3 in tumors and tumor-surrounding immnune cells, respectively, is a critical step in cancer progression leading to sustained cancer cell growth, inhibition of apoptosis, induction of angiogenesis, metastasis and tumor escape. Even though, several tyrosine kinases like EGFR or src have been described as activators of STAT3, its phosphorylation is mainly triggered by Janus activated protein kinases (JAKs) with JAK1 as key factor [75]. In various cancer cells, STAT3 is constitutively present in its active, phosphorylated form and it is also induced in tumor surrounding immune cells for instance by tumor-secreted IL-10, which leads to immunosuppression and tumor immune escape [64,71]. Phosphorylation induces STAT3 dimerization due to reciprocal interaction of phosphotyrosine SH2 domain interactions, which subsequently results in translocation to the nucleus and induction of STAT3 target gene transcription [248].

For cell-type specific delivery of immunomodulatory drugs, the targeting vector needs to fulfill different requirements: First, the immunomodulatory substance needs to be packed up, to be protected from the environment and to still be biologically functional. Furthermore, the drug needs to be released once taken up by the target cell. The HES NC that were used for Treg targeting showed limited release capacities and were thus replaced by ovalbumin protein NC for an optimal delivery of STAT3 inhibitors like S3I-201. S3I-201 (also known as NSC 7485) binds to the SH2 domain of STAT3, thereby abrogating STAT3 phosphorylation, dimerization and DNA binding [131,247].

As the ovalbumin protein NC revealed a size of 180 nm and a zeta potential of -20 to -10 mV, they displayed the ideal physico-chemical properties for a long circulation time and a low unspecific uptake *in vivo* [165]. Furthermore, intracellular release was demonstrated by the CMFDA Dye Cell Tracker Green and this was not due to free CMFDA dye in the NC supernatant as demonstrated by flow cytometry experiments. CMFDA requires cleavage by intracellular enzymes to activate its fluorescence by an esterase-catalyzed hydrolysis reaction [150]. The supernatant of the ovalbumin protein NC is an important control as free CMFDA also diffuses through the cellular membrane [249]. Intracellular release is probably triggered by intracellular proteinases and was already demonstrated in former studies [100].

When free S3I-201 is applied to HeLa cells, they revealed a significant knockdown of phosphorylated STAT3 at a concentration of 200 µM, which is similar to other studies [250-252]. In this experiments, HeLa cells were stimulated with IL-6 to induce STAT3 phosphorylation [151]. IL-6 induces STAT3 phosphorylation after binding to the IL-6 receptor, that consists of the type 1 cytokine α-receptor subunit CD126 and gp130 (CD130) [253]. After IL-6 binding gp130

activates Jak1, Jak2 and Tyk, which in turn results in STAT3 recruitment and phosphorylation [151]. Encapsulated S3I-201 revealed a significant inhibition of STAT3 phosphorylation in IL-6-stimulated HeLa cells, demonstrating an efficient encapsulation and an intracellular drug release. Unfortunately, the reduced STAT3 phosphorylation could not be compared to the same amount of soluble S3I-201 as the exact amount of encapsulated inhibitor could not be determined for this study. In addition, *in vivo* application of ovalbumin-consisting NC is quite challenging as free ovalbumin is used for induction of various allergies in murine models of allergic diseases [254,255]. However, those experiments clearly revealed that encapsulated S3I-201 still exerts its biological function of phosphorylated STAT3 inhibition.

As already mentioned, inhibition of STAT3-mediated processes does also affect tumor-surrounding immune cells [256]. For instance, conditional STAT3 inhibition in hematopoietic cells results in efficient anti-tumor immunity which is expressed by enhanced function of DCs, T cells, natural killer cells and neutrophils [257]. This is probably due to tumor-mediated secretion of immunomodulatory cytokines, like most prominently IL-10, leading to phosphorylation of STAT3, and thereby takes part in tumor immune escape mechanisms, [64,256]. Investigation on IL-10 and STAT3-mediated tolerance-inducing processes has mainly focused on DCs, macrophages and other myeloid cells, in which inhibition of STAT3 activation leads to reduced maturation and immunogenicity [70,71,256]. However, activation of STAT3 in Tregs probably leads to the expression of Foxp3, resulting in enhanced Treg function and a more pronounced suppressive phenotype [67,68]. In addition, STAT3 inhibition also induces enhanced effector T cell function [66]. Those processes are at least in part IL-10 dependent and thus Treg-specific inhibition of STAT3 may lead to enhanced anti-tumor immune responses [67-69,258,259].

In the context of cancer immunotherapy, different nanoparticle-based approaches focused on targeting of immune cells in combination with tumor targeting for STAT3 inhibition, leading to efficient anti-tumor responses [92,260-262]. In addition, S3I-201 was also efficiently encapsulated into micellar nano-carriers, however, a fast release profile of the inhibitor under physiological conditions prevented the investigation of their therapeutic efficacy [252].

Conclusion and outlook

The aim of the present study was first, to develop a cell type-specifc targeting of Tregs by IL-2 functionalized NC and second, to establish a drug delivery system for inhibition STAT3-mediated tolerance mechanisms.

The experiments revealed that coupling of IL-2 to the surface of HES NC enables an efficient *in vitro* and *in vivo* targeting of CD25-expressing human and murine T cells. The uptake/binding by human Tregs was enhanced compared to human T cell subsets with a

lower expression of the high affinity IL-2 receptor. Furthermore, the uptake/binding was CD25-dependent and binding of IL-2 to the receptor resulted in internalization of the NC. By reducing the amount of IL-2 on the NC surface Tregs were even more preferentially targeted when compared to naïve or activated T cells. In addition, HES-D-IL-2 also enabled CD25-specific targeting of murine and human T cells *in vivo*.

For a combination of Treg targeting with STAT3 inhibition, the inhibitor S3I-201, which specifically inhibits STAT3 phosphorylation was encapsulated into ovalbumin protein NC which showed intracellular release properties after uptake. In proof-of-concept experiments, those capsules induced a significantly reduced STAT3 phosphorylation *in vitro* in IL-6 stimulated HeLa cells.

In future studies, specific Treg targeting needs to be further improved and evaluated. The cellular uptake of NC by activated T cells was revealed by CLSM, however for Treg targeting it needs to be investigated whether HES-D-IL-2 are also incorporated. For drug delivery the intracellular location of the drug release may also be important, so it is essential to perform experiments to investigate the intracellular fate of the NC. Furthermore, specificity of Treg targeting in comparison to other T cell subsets was enhanced by reducing the number of IL-2 molecules on the NC surface up to a tenfold reduced amount. Here, a further dilution of IL-2 coupled to the NC may lead to a more preferential Treg targeting. However, an even better cell-type specific targeting may be achieved by functionalization of HES NC with a complex of IL-2 with the aforementioned antibody JES6-1, which mimics linkage to CD122 and may therefore induce preferential targeting of high-affinity IL-2 receptor-expressing Tregs [114]. Yet, the therapeutic *in vivo* application of the IL-2 functionalized NC bears a noteworthy obstacle. Instead of solely serving as a targeting ligand, IL-2 may additionally activate Tregs thereby enhancing their immunosuppressive capacities [245].

In a next step, a combination of Treg targeting with the drug release properties NC for to cell-type specific inhibition of IL-10- and STAT3-mediated tolerance mechanisms in Tregs (Figure 28a). STAT3 is important for Treg function, which was also revealed for tumor-infiltrating Tregs and may be IL-10 dependent [67-69,258,259]. In addition, STAT3 inhibition also induced enhanced cytotoxic $CD8^+$ T cell function, so residual additional targeting of activated cytotoxic $CD8^+$ T cells is propably negligible [66]. Therefore, IL-2 functionalized mediated drug delivery of the STAT3 inhibitor S3I-201 may lead to efficient disruption of IL-10- and STAT3-mediated tolerance in Tregs and cytotxic $CD8^+$ T cells, thereby enhancing anti-tumor immunity. This concept is depicted in Figure 28b. The efficacy of such therapy may ideally be evaluated in tumor models of human immune cell engrafted mice to prevent interference of differences in the IL-2 receptor binding affinity between mice and human.

Treg- and cytotoxic T cell-specific inhibition of IL-10- and STAT3-mediated tolerance mechanisms may thus lead to efficient anti-tumor immune responses counteracting tumor

immune evasion which is one of the hallmarks of cancer suggested by Hanahan and Weinberg [5].

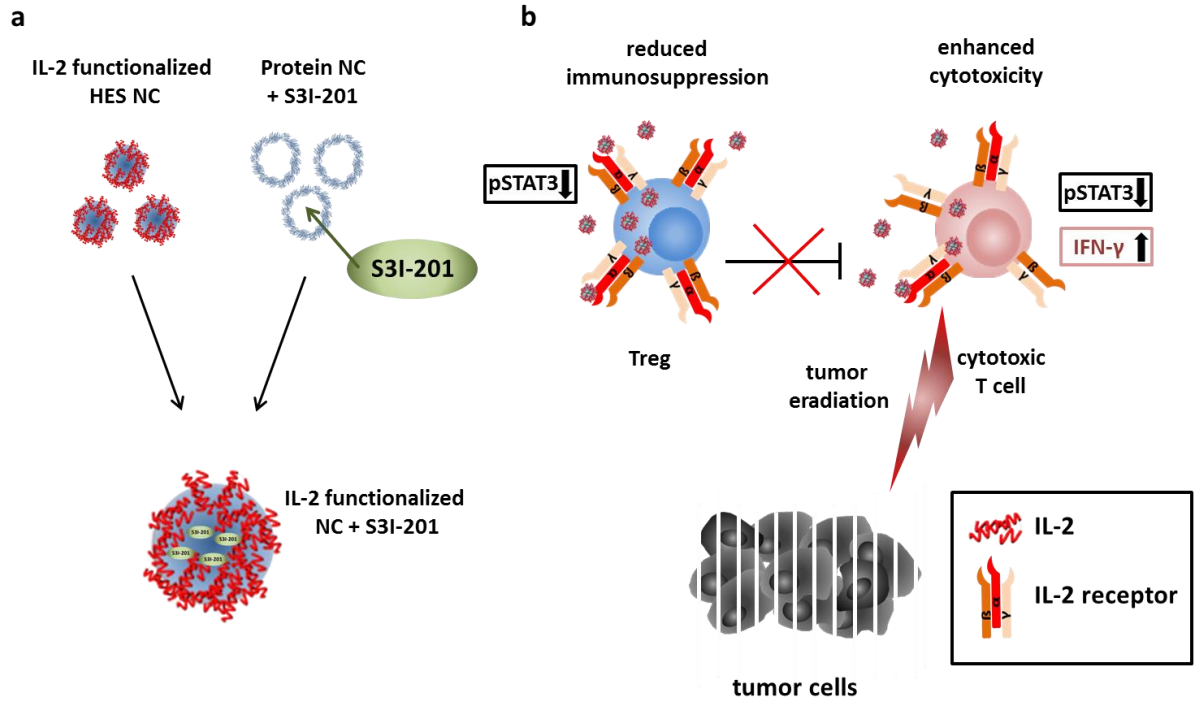

Figure 27: Nanocapsule based vaccination for inhibition of tumor escape mechanisms.
The inhibition of IL-10 and STAT3-mediated, tumor associated tolerance mechanisms in Tregs and cytotxic T cells by usage of IL-2 functionalized NC for the induction of efficient anti-tumor immune responses is illustrated.
a) The NC are designed combine the T cell-specific targeting of the IL-2 functionalized HES NC with the release properties of the ovalbumin protein NC to achieve Treg and/or cytotoxic T cell specific drug release.
b) The figure highlights the simplified mechanisms of action of the S3I-201-encapsulated IL-2 functionalized NC on Treg and cytotoxic T cells.

Part of this work has been published in ACS Nano 10 (10): 9216–26. DOI: 10.1021/acsnano.5b07973.

References

1 Siegel, R. L., Miller, K. D. & Jemal, A. Cancer Statistics, 2017. *CA Cancer J. Clin.* **67**, 7-30, doi:10.3322/caac.21387 (2017).

2 Alizadeh, A. A. *et al.* Toward understanding and exploiting tumor heterogeneity. *Nat. Med.* **21**, 846-853, doi:10.1038/nm.3915 (2015).

3 McGranahan, N. & Swanton, C. Clonal Heterogeneity and Tumor Evolution: Past, Present, and the Future. *Cell* **168**, 613-628, doi:10.1016/j.cell.2017.01.018 (2017).

4 Hanahan, D. & Weinberg, R. A. The hallmarks of cancer. *Cell* **100**, 57-70 (2000).

5 Hanahan, D. & Weinberg, R. A. Hallmarks of cancer: the next generation. *Cell* **144**, 646-674, doi:10.1016/j.cell.2011.02.013 (2011).

6 Fridman, W. H., Pages, F., Sautes-Fridman, C. & Galon, J. The immune contexture in human tumours: impact on clinical outcome. *Nat. Rev. Cancer* **12**, 298-306, doi:10.1038/nrc3245 (2012).

7 Dunn, G. P., Old, L. J. & Schreiber, R. D. The three Es of cancer immunoediting. *Annu. Rev. Immunol.* **22**, 329-360, doi:10.1146/annurev.immunol.22.012703.104803 (2004).

8 Schreiber, R. D., Old, L. J. & Smyth, M. J. Cancer immunoediting: integrating immunity's roles in cancer suppression and promotion. *Science* **331**, 1565-1570, doi:10.1126/science.1203486 (2011).

9 Braumuller, H. *et al.* T-helper-1-cell cytokines drive cancer into senescence. *Nature* **494**, 361-365, doi:10.1038/nature11824 (2013).

10 Coley, W. B. The treatment of malignant tumors by repeated inoculations of erysipelas. With a report of ten original cases. 1893. *Clin. Orthop. Relat. Res.*, 3-11 (1991).

11 Dougan, M. & Dranoff, G. Immune therapy for cancer. *Annu. Rev. Immunol.* **27**, 83-117, doi:10.1146/annurev.immunol.021908.132544 (2009).

12 Farkona, S., Diamandis, E. P. & Blasutig, I. M. Cancer immunotherapy: the beginning of the end of cancer? *BMC medicine* **14**, 73, doi:10.1186/s12916-016-0623-5 (2016).

13 Spitzer, M. H. *et al.* Systemic Immunity Is Required for Effective Cancer Immunotherapy. *Cell* **168**, 487-502 e415, doi:10.1016/j.cell.2016.12.022 (2017).

14 The double edge of cancer immunotherapy. *Nat. Med.* **23**, 137, doi:10.1038/nm.4286 (2017).

15 Irvine, D. J., Hanson, M. C., Rakhra, K. & Tokatlian, T. Synthetic Nanoparticles for Vaccines and Immunotherapy. *Rev. Chem.* **115**, 11109-11146, doi:10.1021/acs.chemrev.5b00109 (2015).

16 Shao, K. *et al.* Nanoparticle-Based Immunotherapy for Cancer. *ACS nano* **9**, 16-30, doi:10.1021/nn5062029 (2015).

17 Milling, L., Zhang, Y. & Irvine, D. J. Delivering safer immunotherapies for cancer. *Adv. Drug Deliv. Sys.*, doi:10.1016/j.addr.2017.05.011 (2017).

18 Eberl, G. Immunity by equilibrium. *Nat. Rev. Immunol.* **16**, 524-532, doi:10.1038/nri.2016.75 (2016).

19 Hoebe, K., Janssen, E. & Beutler, B. The interface between innate and adaptive immunity. *Nat. Immunol.* **5**, 971-974, doi:10.1038/ni1004-971 (2004).

20 Janeway, C. A., Jr. & Medzhitov, R. Innate immune recognition. *Annu. Rev. Immunol.* **20**, 197-216, doi:10.1146/annurev.immunol.20.083001.084359 (2002).

21 Brubaker, S. W., Bonham, K. S., Zanoni, I. & Kagan, J. C. Innate immune pattern recognition: a cell biological perspective. *Annu. Rev. Immunol.* **33**, 257-290, doi:10.1146/annurev-immunol-032414-112240 (2015).

22 Bedoui, S., Gebhardt, T., Gasteiger, G. & Kastenmuller, W. Parallels and differences between innate and adaptive lymphocytes. *Nat. Immunol.* **17**, 490-494, doi:10.1038/ni.3432 (2016).

23 Steinman, R. M. & Cohn, Z. A. Identification of a novel cell type in peripheral lymphoid organs of mice. I. Morphology, quantitation, tissue distribution. *J. Exp. Med.* **137**, 1142-1162 (1973).

24 Iwasaki, A. & Medzhitov, R. Control of adaptive immunity by the innate immune system. *Nat. Immunol.* **16**, 343-353, doi:10.1038/ni.3123 (2015).

25 Steinman, R. M. Some interfaces of dendritic cell biology. *APMIS* **111**, 675-697 (2003).
26 Trombetta, E. S. & Mellman, I. Cell biology of antigen processing in vitro and in vivo. *Annu. Rev. Immunol.* **23**, 975-1028, doi:10.1146/annurev.immunol.22.012703.104538 (2005).
27 Steinman, R. M. & Banchereau, J. Taking dendritic cells into medicine. *Nature* **449**, 419-426, doi:10.1038/nature06175 (2007).
28 Kono, H. & Rock, K. L. How dying cells alert the immune system to danger. *Nat. Rev. Immunol.* **8**, 279-289, doi:10.1038/nri2215 (2008).
29 Zhu, J., Yamane, H. & Paul, W. E. Differentiation of effector CD4 T cell populations (*). *Annu. Rev. Immunol.* **28**, 445-489, doi:10.1146/annurev-immunol-030409-101212 (2010).
30 Adler, H. S. & Steinbrink, K. Tolerogenic dendritic cells in health and disease: friend and foe! *Europ. J. Dermatol.* **17**, 476-491, doi:10.1684/ejd.2007.0262 (2007).
31 Raker, V. K., Domogalla, M. P. & Steinbrink, K. Tolerogenic Dendritic Cells for Regulatory T Cell Induction in Man. *Front. Immunol.* **6**, 569, doi:10.3389/fimmu.2015.00569 (2015).
32 Van Laethem, F., Tikhonova, A. N. & Singer, A. MHC restriction is imposed on a diverse T cell receptor repertoire by CD4 and CD8 co-receptors during thymic selection. *Trend. Immunol.* **33**, 437-441, doi:10.1016/j.it.2012.05.006 (2012).
33 Adams, E. J. & Luoma, A. M. The adaptable major histocompatibility complex (MHC) fold: structure and function of nonclassical and MHC class I-like molecules. *Annu. Rev. Immunol.* **31**, 529-561, doi:10.1146/annurev-immunol-032712-095912 (2013).
34 Rammensee, H. G., Falk, K. & Rotzschke, O. Peptides naturally presented by MHC class I molecules. *Annu. Rev. Immunol.* **11**, 213-244, doi:10.1146/annurev.iy.11.040193.001241 (1993).
35 Vyas, J. M., Van der Veen, A. G. & Ploegh, H. L. The known unknowns of antigen processing and presentation. *Nat. Rev. Immunol.* **8**, 607-618, doi:10.1038/nri2368 (2008).
36 Roche, P. A. & Furuta, K. The ins and outs of MHC class II-mediated antigen processing and presentation. *Nat. Rev. Immunol.* **15**, 203-216, doi:10.1038/nri3818 (2015).
37 Stavnezer, J., Guikema, J. E. & Schrader, C. E. Mechanism and regulation of class switch recombination. *Annu. Rev. Immunol.* **26**, 261-292, doi:10.1146/annurev.immunol.26.021607.090248 (2008).
38 Born, W. K., Reardon, C. L. & O'Brien, R. L. The function of gammadelta T cells in innate immunity. *Curr. Opin. Immunol.* **18**, 31-38, doi:10.1016/j.coi.2005.11.007 (2006).
39 Luoma, A. M., Castro, C. D. & Adams, E. J. gammadelta T cell surveillance via CD1 molecules. *Trend. Immunol.* **35**, 613-621, doi:10.1016/j.it.2014.09.003 (2014).
40 Kapsenberg, M. L. Dendritic-cell control of pathogen-driven T-cell polarization. *Nat. Rev. Immunol.* **3**, 984-993, doi:10.1038/nri1246 (2003).
41 Bevan, M. J. Helping the CD8(+) T-cell response. *Nat. Rev. Immunol.* **4**, 595-602, doi:10.1038/nri1413 (2004).
42 Zhang, N. & Bevan, M. J. CD8(+) T cells: foot soldiers of the immune system. *Immunity* **35**, 161-168, doi:10.1016/j.immuni.2011.07.010 (2011).
43 Lazarevic, V., Glimcher, L. H. & Lord, G. M. T-bet: a bridge between innate and adaptive immunity. *Nat. Rev. Immunol.* **13**, 777-789, doi:10.1038/nri3536 (2013).
44 Nakayama, T. *et al.* Th2 Cells in Health and Disease. *Annu. Rev. Immunol.* **35**, 53-84, doi:10.1146/annurev-immunol-051116-052350 (2017).
45 Korn, T., Bettelli, E., Oukka, M. & Kuchroo, V. K. IL-17 and Th17 Cells. *Annu. Rev. Immunol.* **27**, 485-517, doi:10.1146/annurev.immunol.021908.132710 (2009).
46 Josefowicz, S. Z., Lu, L. F. & Rudensky, A. Y. Regulatory T cells: mechanisms of differentiation and function. *Annu. Rev. Immunol.* **30**, 531-564, doi:10.1146/annurev.immunol.25.022106.141623 (2012).
47 Kugelberg, E. Immune tolerance: A window of opportunity. *Nat. Rev. Immunol.* **16**, 4, doi:10.1038/nri.2015.6 (2016).
48 Hogquist, K. A., Baldwin, T. A. & Jameson, S. C. Central tolerance: learning self-control in the thymus. *Nat. Rev. Immunol.* **5**, 772-782, doi:10.1038/nri1707 (2005).

49 Klein, L., Kyewski, B., Allen, P. M. & Hogquist, K. A. Positive and negative selection of the T cell repertoire: what thymocytes see (and don't see). *Nat. Rev. Immunol.* **14**, 377-391, doi:10.1038/nri3667 (2014).
50 Starr, T. K., Jameson, S. C. & Hogquist, K. A. Positive and negative selection of T cells. *Annu. Rev. Immunol.* **21**, 139-176, doi:10.1146/annurev.immunol.21.120601.141107 (2003).
51 Mueller, D. L. Mechanisms maintaining peripheral tolerance. *Nat. Immunol.* **11**, 21-27, doi:10.1038/ni.1817 (2010).
52 Schwartz, R. H. T cell anergy. *Annu. Rev. Immunol.* **21**, 305-334, doi:10.1146/annurev.immunol.21.120601.141110 (2003).
53 Li, M. O. & Rudensky, A. Y. T cell receptor signalling in the control of regulatory T cell differentiation and function. *Nat. Rev. Immunol.* **16**, 220-233, doi:10.1038/nri.2016.26 (2016).
54 Mahmud, S. A., Manlove, L. S. & Farrar, M. A. Interleukin-2 and STAT5 in regulatory T cell development and function. *Jak-Stat* **2**, e23154, doi:10.4161/jkst.23154 (2013).
55 Sakaguchi, S., Sakaguchi, N., Asano, M., Itoh, M. & Toda, M. Immunologic self-tolerance maintained by activated T cells expressing IL-2 receptor alpha-chains (CD25). Breakdown of a single mechanism of self-tolerance causes various autoimmune diseases. *J. Immunol.* **155**, 1151-1164 (1995).
56 Vignali, D. A., Collison, L. W. & Workman, C. J. How regulatory T cells work. *Nat. Rev. Immunol.* **8**, 523-532, doi:10.1038/nri2343 (2008).
57 Vignali, D. A. Mechanisms of T(reg) Suppression: Still a Long Way to Go. *Front. Immunol.* **3**, 191, doi:10.3389/fimmu.2012.00191 (2012).
58 von Bubnoff, D. *et al.* Antigen-presenting cells and tolerance induction. *Allergy* **57**, 2-8 (2002).
59 Cohen, P. L. & Eisenberg, R. A. Lpr and gld: single gene models of systemic autoimmunity and lymphoproliferative disease. *Annu. Rev. Immunol.* **9**, 243-269, doi:10.1146/annurev.iy.09.040191.001331 (1991).
60 Balkwill, F. & Mantovani, A. Inflammation and cancer: back to Virchow? *Lancet* **357**, 539-545, doi:10.1016/S0140-6736(00)04046-0 (2001).
61 Rabinovich, G. A., Gabrilovich, D. & Sotomayor, E. M. Immunosuppressive strategies that are mediated by tumor cells. *Annu. Rev. Immunol.* **25**, 267-296, doi:10.1146/annurev.immunol.25.022106.141609 (2007).
62 Zou, W. Immunosuppressive networks in the tumour environment and their therapeutic relevance. *Nat. Rev. Cancer* **5**, 263-274, doi:10.1038/nrc1586 (2005).
63 Itakura, E. *et al.* IL-10 expression by primary tumor cells correlates with melanoma progression from radial to vertical growth phase and development of metastatic competence. *Modern pathology : an official journal of the United States and Canadian Academy of Pathology, Inc* **24**, 801-809, doi:10.1038/modpathol.2011.5 (2011).
64 Moore, K. W., de Waal Malefyt, R., Coffman, R. L. & O'Garra, A. Interleukin-10 and the interleukin-10 receptor. *Annu. Rev. Immunol.* **19**, 683-765, doi:10.1146/annurev.immunol.19.1.683 (2001).
65 Saraiva, M. & O'Garra, A. The regulation of IL-10 production by immune cells. *Nat. Rev. Immunol.* **10**, 170-181, doi:10.1038/nri2711 (2010).
66 Kujawski, M. *et al.* Targeting STAT3 in adoptively transferred T cells promotes their in vivo expansion and antitumor effects. *Cancer Res.* **70**, 9599-9610, doi:10.1158/0008-5472.CAN-10-1293 (2010).
67 Pallandre, J. R. *et al.* Role of STAT3 in CD4+CD25+FOXP3+ regulatory lymphocyte generation: implications in graft-versus-host disease and antitumor immunity. *J. Immunol.* **179**, 7593-7604 (2007).
68 Murai, M. *et al.* Interleukin 10 acts on regulatory T cells to maintain expression of the transcription factor Foxp3 and suppressive function in mice with colitis. *Nat. Immunol.* **10**, 1178-1184, doi:10.1038/ni.1791 (2009).

69 Hsu, P. *et al.* IL-10 Potentiates Differentiation of Human Induced Regulatory T Cells via STAT3 and Foxo1. *J. Immunol.* **195**, 3665-3674, doi:10.4049/jimmunol.1402898 (2015).
70 Yu, H., Pardoll, D. & Jove, R. STATs in cancer inflammation and immunity: a leading role for STAT3. *Nat. Rev. Cancer* **9**, 798-809, doi:10.1038/nrc2734 (2009).
71 Yu, H., Lee, H., Herrmann, A., Buettner, R. & Jove, R. Revisiting STAT3 signalling in cancer: new and unexpected biological functions. *Nat. Rev. Cancer* **14**, 736-746, doi:10.1038/nrc3818 (2014).
72 Lee, S. & Margolin, K. Cytokines in cancer immunotherapy. *Cancers* **3**, 3856-3893, doi:10.3390/cancers3043856 (2011).
73 Higano, C. S. *et al.* Sipuleucel-T. *Nat. Rev. Drug Discov.* **9**, 513-514, doi:10.1038/nrd3220 (2010).
74 Restifo, N. P., Dudley, M. E. & Rosenberg, S. A. Adoptive immunotherapy for cancer: harnessing the T cell response. *Nat. Rev. Immunol.* **12**, 269-281, doi:10.1038/nri3191 (2012).
75 Hinrichs, C. S. & Rosenberg, S. A. Exploiting the curative potential of adoptive T-cell therapy for cancer. *Immunological Rev.* **257**, 56-71, doi:10.1111/imr.12132 (2014).
76 Schuster, S. J. *et al.* Treatment with Chimeric Antigen Receptor Modified T Cells Directed Against CD19 (CTL019) Results in Durable Remissions in Patients with Relapsed or Refractory Diffuse Large B Cell Lymphomas of Germinal Center and Non-Germinal Center Origin, "Double Hit" Diffuse Large B Cell Lymphomas, and Transformed Follicular to Diffuse Large B Cell Lymphomas. *Blood* **128** (2016).
77 Schuster, S. J. *et al.* Global Pivotal Phase 2 Trial of the Cd19-Targeted Therapy Ctl019 in Adult Patients with Relapsed or Refractory Diffuse Large B-Cell Lymphoma - an Interim Analysis. *Haematologica* **102** (2017).
78 Khalil, D. N., Smith, E. L., Brentjens, R. J. & Wolchok, J. D. The future of cancer treatment: immunomodulation, CARs and combination immunotherapy. *Nature reviews. Clinical oncology* **13**, 394, doi:10.1038/nrclinonc.2016.65 (2016).
79 Fesnak, A. D., June, C. H. & Levine, B. L. Engineered T cells: the promise and challenges of cancer immunotherapy. *Nat. Rev. Cancer* **16**, 566-581, doi:10.1038/nrc.2016.97 (2016).
80 Shields, B. D. *et al.* Indicators of responsiveness to immune checkpoint inhibitors. *Scientific reports* **7**, 807, doi:10.1038/s41598-017-01000-2 (2017).
81 Walker, L. S. & Sansom, D. M. The emerging role of CTLA4 as a cell-extrinsic regulator of T cell responses. *Nat. Rev. Immunol.* **11**, 852-863, doi:10.1038/nri3108 (2011).
82 Keir, M. E., Butte, M. J., Freeman, G. J. & Sharpe, A. H. PD-1 and its ligands in tolerance and immunity. *Annu. Rev. Immunol.* **26**, 677-704, doi:10.1146/annurev.immunol.26.021607.090331 (2008).
83 Jia, Y., Omri, A., Krishnan, L. & McCluskie, M. J. Potential applications of nanoparticles in cancer immunotherapy. *Human vaccines & immunotherapeutics* **13**, 63-74, doi:10.1080/21645515.2016.1245251 (2017).
84 Yoo, J. W., Chambers, E. & Mitragotri, S. Factors that control the circulation time of nanoparticles in blood: challenges, solutions and future prospects. *Curr. Pharm. Des.* **16**, 2298-2307 (2010).
85 Schottler, S. *et al.* Protein adsorption is required for stealth effect of poly(ethylene glycol)- and poly(phosphoester)-coated nanocarriers. *Nat. Nanotechnol.* **11**, 372-377, doi:10.1038/nnano.2015.330 (2016).
86 Butcher, N. J., Mortimer, G. M. & Minchin, R. F. Drug delivery: Unravelling the stealth effect. *Nat. Nanotechnol.* **11**, 310-311, doi:10.1038/nnano.2016.6 (2016).
87 Knop, K., Hoogenboom, R., Fischer, D. & Schubert, U. S. Poly(ethylene glycol) in drug delivery: pros and cons as well as potential alternatives. *Angew. Chem. Int. Edt.* **49**, 6288-6308, doi:10.1002/anie.200902672 (2010).
88 Baier, G. *et al.* Suppressing unspecific cell uptake for targeted delivery using hydroxyethyl starch nanocapsules. *Biomacromolecules* **13**, 2704-2715, doi:10.1021/bm300653v (2012).

89 Maeda, H., Wu, J., Sawa, T., Matsumura, Y. & Hori, K. Tumor vascular permeability and the EPR effect in macromolecular therapeutics: a review. *J. Control. Release* **65**, 271-284 (2000).
90 Shi, J., Kantoff, P. W., Wooster, R. & Farokhzad, O. C. Cancer nanomedicine: progress, challenges and opportunities. *Nat. Rev. Cancer* **17**, 20-37, doi:10.1038/nrc.2016.108 (2017).
91 Prabhakar, U. *et al.* Challenges and key considerations of the enhanced permeability and retention effect for nanomedicine drug delivery in oncology. *Cancer Res.* **73**, 2412-2417, doi:10.1158/0008-5472.CAN-12-4561 (2013).
92 Huo, M. *et al.* Tumor-targeted delivery of sunitinib base enhances vaccine therapy for advanced melanoma by remodeling the tumor microenvironment. *J. Control. Release* **245**, 81-94, doi:10.1016/j.jconrel.2016.11.013 (2017).
93 Friedman, A. D., Claypool, S. E. & Liu, R. The smart targeting of nanoparticles. *Curr. Pharm. Des.* **19**, 6315-6329 (2013).
94 Cruz, L. J. *et al.* Targeting nanoparticles to dendritic cells for immunotherapy. *Methods Enzymol.* **509**, 143-163, doi:10.1016/B978-0-12-391858-1.00008-3 (2012).
95 Paulis, L. E., Mandal, S., Kreutz, M. & Figdor, C. G. Dendritic cell-based nanovaccines for cancer immunotherapy. *Curr. Opin. Immunol.* **25**, 389-395, doi:10.1016/j.coi.2013.03.001 (2013).
96 Dhodapkar, M. V. & Steinman, R. M. Antigen-bearing immature dendritic cells induce peptide-specific CD8(+) regulatory T cells in vivo in humans. *Blood* **100**, 174-177 (2002).
97 Hruby, M., Konak, C. & Ulbrich, K. Poly(ethylene oxide)-coated polyamide nanoparticles degradable by glutathione. *Colloid Polym. Sci.* **285**, 569-574, doi:10.1007/s00396-006-1585-5 (2007).
98 Kwon, Y. J., Standley, S. M., Goodwin, A. P., Gillies, E. R. & Frechet, J. M. Directed antigen presentation using polymeric microparticulate carriers degradable at lysosomal pH for controlled immune responses. *Mol. Pharamaceut.* **2**, 83-91, doi:10.1021/mp0498953 (2005).
99 Kwon, Y. J., James, E., Shastri, N. & Frechet, J. M. In vivo targeting of dendritic cells for activation of cellular immunity using vaccine carriers based on pH-responsive microparticles. *Proc. Natl. Acad. Sci. U.S.A.* **102**, 18264-18268, doi:10.1073/pnas.0509541102 (2005).
100 Piradashvili, K. *et al.* Biodegradable protein nanocontainers. *Biomacromolecules* **16**, 815-821, doi:10.1021/bm5016915 (2015).
101 Renner, K. *et al.* Metabolic Hallmarks of Tumor and Immune Cells in the Tumor Microenvironment. *Front. Immunol.* **8**, 248, doi:10.3389/fimmu.2017.00248 (2017).
102 Morgan, D. A., Ruscetti, F. W. & Gallo, R. Selective in vitro growth of T lymphocytes from normal human bone marrows. *Science* **193**, 1007-1008 (1976).
103 Malek, T. R. The biology of interleukin-2. *Annu. Rev. Immunol.* **26**, 453-479, doi:10.1146/annurev.immunol.26.021607.090357 (2008).
104 Boyman, O. & Sprent, J. The role of interleukin-2 during homeostasis and activation of the immune system. *Nat. Rev. Immunol.* **12**, 180-190, doi:10.1038/nri3156 (2012).
105 Wang, X., Rickert, M. & Garcia, K. C. Structure of the quaternary complex of interleukin-2 with its alpha, beta, and gammac receptors. *Science* **310**, 1159-1163, doi:10.1126/science.1117893 (2005).
106 Lowenthal, J. W., MacDonald, H. R. & Iacopetta, B. J. Intracellular pathway of interleukin 2 following receptor-mediated endocytosis. *Europ. J. Immunol.* **16**, 1461-1463, doi:10.1002/eji.1830161125 (1986).
107 Hemar, A. *et al.* Endocytosis of interleukin 2 receptors in human T lymphocytes: distinct intracellular localization and fate of the receptor alpha, beta, and gamma chains. *J. Cell Biol.* **129**, 55-64 (1995).
108 Arenas-Ramirez, N., Woytschak, J. & Boyman, O. Interleukin-2: Biology, Design and Application. *Trend. Immunol.* **36**, 763-777, doi:10.1016/j.it.2015.10.003 (2015).
109 Liao, W., Lin, J. X. & Leonard, W. J. Interleukin-2 at the crossroads of effector responses, tolerance, and immunotherapy. *Immunity* **38**, 13-25, doi:10.1016/j.immuni.2013.01.004 (2013).

110 Klatzmann, D. & Abbas, A. K. The promise of low-dose interleukin-2 therapy for autoimmune and inflammatory diseases. *Nat. Rev. Immunol.* **15**, 283-294, doi:10.1038/nri3823 (2015).
111 Chu, M. B. *et al.* High-Dose Interleukin-2 (HD IL-2) Therapy Should Be Considered for Treatment of Patients with Melanoma Brain Metastases. *Chemother. Res. Pract.* **2013**, 726925, doi:10.1155/2013/726925 (2013).
112 Hanzly, M. *et al.* High-dose interleukin-2 therapy for metastatic renal cell carcinoma: a contemporary experience. *Urology* **83**, 1129-1134, doi:10.1016/j.urology.2014.02.005 (2014).
113 Baluna, R. & Vitetta, E. S. Vascular leak syndrome: a side effect of immunotherapy. *Immunopharmacol.* **37**, 117-132 (1997).
114 Letourneau, S. *et al.* IL-2/anti-IL-2 antibody complexes show strong biological activity by avoiding interaction with IL-2 receptor alpha subunit CD25. *Proc. Natl. Acad. Sci. U.S.A.* **107**, 2171-2176, doi:10.1073/pnas.0909384107 (2010).
115 Kugelberg, E. Tumour immunology: Reducing silence to improve therapy. *Nat. Rev. Immunol.* **15**, 730, doi:10.1038/nri3941 (2015).
116 Schmidt, A., Oberle, N. & Krammer, P. H. Molecular mechanisms of treg-mediated T cell suppression. *Front. Immunol.* **3**, 51, doi:10.3389/fimmu.2012.00051 (2012).
117 Fomina, A. F., Deerinck, T. J., Ellisman, M. H. & Cahalan, M. D. Regulation of membrane trafficking and subcellular organization of endocytic compartments revealed with FM1-43 in resting and activated human T cells. *Exp. Cell Res.* **291**, 150-166 (2003).
118 Duprez, V., Ferrer, M., Cornet, V., Olive, D. & Dautry-Varsat, A. Modulation of interleukin 2 internalization and interleukin 2-dependent cell growth by antireceptor antibodies. *J. Biol. Chem.* **266**, 1497-1501 (1991).
119 Yu, A., Olosz, F., Choi, C. Y. & Malek, T. R. Efficient internalization of IL-2 depends on the distal portion of the cytoplasmic tail of the IL-2R common gamma-chain and a lymphoid cell environment. *J. Immunol.* **165**, 2556-2562 (2000).
120 Facciabene, A., Motz, G. T. & Coukos, G. T-regulatory cells: key players in tumor immune escape and angiogenesis. *Cancer Res.* **72**, 2162-2171, doi:10.1158/0008-5472.CAN-11-3687 (2012).
121 Chiba, T., Mack, L., Delis, N., Brill, B. & Groner, B. Stat3 inhibition in neural lineage cells. *Horm. Mol. Biol. Clin.* **10**, 255-263, doi:10.1515/hmbci-2012-0005 (2012).
122 Landfester, K. Miniemulsions for nanoparticle synthesis. *Top Curr. Chem.* **227**, 75-123, doi:10.1007/b10835 (2003).
123 Slomkowski, S. *et al.* Terminology of polymers and polymerization processes in dispersed systems (IUPAC Recommendations 2011). *Pure Appl. Chem.* **83**, 2229-2259, doi:10.1351/Pac-Rec-10-06-03 (2011).
124 Mason, T. G., Wilking, J. N., Meleson, K., Chang, C. B. & Graves, S. M. Nanoemulsions: formation, structure, and physical properties. *J. Phys. Condens. Mat.* **18**, R635-R666, doi:10.1088/0953-8984/18/41/R01 (2006).
125 Landfester, K. Miniemulsion Polymerization and the Structure of Polymer and Hybrid Nanoparticles. *Angew. Chem. Int. Edt.* **48**, 4488-4507, doi:10.1002/anie.200900723 (2009).
126 Bibette, J., Leal-Calderon, F., Schmitt, V. & Poulin, P. Emulsion science - Basic principles. An overview - Introduction. *Springer Trac. Mod. Ph.***181**, 1-4 (2002).
127 Gupta, A., Eral, H. B., Hatton, T. A. & Doyle, P. S. Nanoemulsions: formation, properties and applications. *Soft Matter* **12**, 2826-2841, doi:10.1039/c5sm02958a (2016).
128 Baier, G., Musyanovych, A., Dass, M., Theisinger, S. & Landfester, K. Cross-Linked Starch Capsules Containing dsDNA Prepared in Inverse Miniemulsion as "Nanoreactors" for Polymerase Chain Reaction. *Biomacromolecules* **11**, 960-968, doi:10.1021/bm901414k (2010).
129 Jewett, J. C. & Bertozzi, C. R. Cu-free click cycloaddition reactions in chemical biology. *Chem. Soc. Rev.* **39**, 1272-1279, doi:10.1039/b901970g (2010).

130 Piradashvili, K. *et al.* Biodegradable Protein Nanocontainers. *Biomacromolecules* **16**, 815-821, doi:10.1021/bm5016915 (2015).
131 Siddiquee, K. *et al.* Selective chemical probe inhibitor of Stat3, identified through structure-based virtual screening, induces antitumor activity. *Proc. Natl. Acad. Sci. U.S.A.* **104**, 7391-7396, doi:10.1073/pnas.0609757104 (2007).
132 Beem, E. & Segal, M. S. Evaluation of stability and sensitivity of cell fluorescent labels when used for cell migration. *J. Fluoresc.* **23**, 975-987, doi:10.1007/s10895-013-1224-8 (2013).
133 Klang, V., Valenta, C. & Matsko, N. B. Electron microscopy of pharmaceutical systems. *Micron* **44**, 45-74, doi:10.1016/j.micron.2012.07.008 (2013).
134 Buseck, P. R. Principles of Transmission Electron-Microscopy. *Rev Mineral* **27**, 1-36 (1992).
135 Cochrane, J. C. An introduction to scanning electron microscopy. *Microsc. Res. Tech.* **33**, 87-87 (1996).
136 Pecora, R. Dynamic light scattering measurement of nanometer particles in liquids. *J Nanopart. Res.* **2**, 123-131, doi:Doi 10.1023/A:1010067107182 (2000).
137 Aragon, S. R. & Pecora, R. Theory of Dynamic Light-Scattering from Polydisperse Systems. *J. Chem. Phys.* **64**, 2395-2404 (1976).
138 Clogston, J. D. & Patri, A. K. Zeta potential measurement. *Meth. Mol. Biol.***697**, 63-70, doi:10.1007/978-1-60327-198-1_6 (2011).
139 Xie, F. *et al.* A fluorogenic 'click' reaction of azidoanthracene derivatives. *Tetrahedron* **64**, 2906-2914, doi:10.1016/j.tet.2008.01.080 (2008).
140 Baier, G., Siebert, J. M., Landfester, K. & Musyanovych, A. Surface Click Reactions on Polymeric Nanocapsules for Versatile Functionalization. *Macromolecules* **45**, 3419-3427, doi:10.1021/ma300312n (2012).
141 Filby, A., Begum, J., Jalal, M. & Day, W. Appraising the suitability of succinimidyl and lipophilic fluorescent dyes to track proliferation in non-quiescent cells by dye dilution. *Methods* **82**, 29-37, doi:10.1016/j.ymeth.2015.02.016 (2015).
142 Trickett, A. & Kwan, Y. L. T cell stimulation and expansion using anti-CD3/CD28 beads.J. Meth. Immunol. **275**, 251-255 (2003).
143 Kryczanowsky, F., Raker, V., Graulich, E., Domogalla, M. P. & Steinbrink, K. IL-10-Modulated Human Dendritic Cells for Clinical Use: Identification of a Stable and Migratory Subset with Improved Tolerogenic Activity. *J. Immunol.* **197**, 3607-3617, doi:10.4049/jimmunol.1501769 (2016).
144 Bacher, N. *et al.* Interferon-alpha suppresses cAMP to disarm human regulatory T cells. *Cancer Res.* **73**, 5647-5656, doi:10.1158/0008-5472.CAN-12-3788 (2013).
145 Masters, J. R. HeLa cells 50 years on: the good, the bad and the ugly. *Nat. Rev. Cancer* **2**, 315-319, doi:10.1038/nrc775 (2002).
146 Gillis, S. & Smith, K. A. Long term culture of tumour-specific cytotoxic T cells. *Nature* **268**, 154-156 (1977).
147 Fukushima, K. & Yamashita, K. Interleukin-2 carbohydrate recognition modulates CTLL-2 cell proliferation. *J. Biol. Chem.* **276**, 7351-7356, doi:10.1074/jbc.M008781200 (2001).
148 Andreani, G. *et al.* Leishmania infantum amastigotes trigger a subpopulation of human B cells with an immunoregulatory phenotype. *PLoS Negl. Trop. Dis.* **9**, e0003543, doi:10.1371/journal.pntd.0003543 (2015).
149 Du, J. *et al.* Structural basis for the blockage of IL-2 signaling by therapeutic antibody basiliximab. *J. Immunol.* **184**, 1361-1368, doi:10.4049/jimmunol.0903178 (2010).
150 Lulevich, V., Shih, Y. P., Lo, S. H. & Liu, G. Y. Cell tracing dyes significantly change single cell mechanics. *J. Phys. Chem.. B* **113**, 6511-6519, doi:10.1021/jp8103358 (2009).
151 Hunter, C. A. & Jones, S. A. IL-6 as a keystone cytokine in health and disease. *Nat. Immunol.* **16**, 448-457, doi:10.1038/ni.3153 (2015).
152 Duque, A. & Rakic, P. Different effects of bromodeoxyuridine and [3H]thymidine incorporation into DNA on cell proliferation, position, and fate. J. Neurosci. **31**, 15205-15217, doi:10.1523/JNEUROSCI.3092-11.2011 (2011).

153 Engvall, E. & Perlmann, P. Enzyme-linked immunosorbent assay (ELISA). Quantitative assay of immunoglobulin G. *Immunochemistry* **8**, 871-874 (1971).
154 Byrne, B., Stack, E., Gilmartin, N. & O'Kennedy, R. Antibody-Based Sensors: Principles, Problems and Potential for Detection of Pathogens and Associated Toxins. *Sensors-Basel* **9**, 4407-4445, doi:10.3390/s90604407 (2009).
155 Adan, A., Alizada, G., Kiraz, Y., Baran, Y. & Nalbant, A. Flow cytometry: basic principles and applications. *Crit. Rev. Biotechnol.* **37**, 163-176, doi:10.3109/07388551.2015.1128876 (2017).
156 Shinkai, Y. *et al.* RAG-2-deficient mice lack mature lymphocytes owing to inability to initiate V(D)J rearrangement. *Cell* **68**, 855-867 (1992).
157 Shultz, L. D., Ishikawa, F. & Greiner, D. L. Humanized mice in translational biomedical research. *Nat. Rev. Immunol.* **7**, 118-130, doi:10.1038/nri2017 (2007).
158 Manz, M. G. Human-hemato-lymphoid-system mice: opportunities and challenges. *Immunity* **26**, 537-541, doi:10.1016/j.immuni.2007.05.001 (2007).
159 Mutis, T. *et al.* Human regulatory T cells control xenogeneic graft-versus-host disease induced by autologous T cells in RAG2-/-gammac-/- immunodeficient mice. *Clin. Cancer Res.* **12**, 5520-5525, doi:10.1158/1078-0432.CCR-06-0035 (2006).
160 Cooke, K. R. *et al.* An experimental model of idiopathic pneumonia syndrome after bone marrow transplantation: I. The roles of minor H antigens and endotoxin. *Blood* **88**, 3230-3239 (1996).
161 Tanaka, A. & Sakaguchi, S. Regulatory T cells in cancer immunotherapy. *Cell Res.* **27**, 109-118, doi:10.1038/cr.2016.151 (2017).
162 Macintyre, E. *et al.* The haemostatic effects of hydroxyethyl starch (HES) used as a volume expander. *Intensive Care Med.* **11**, 300-303 (1985).
163 Glover, P. A., Rudloff, E. & Kirby, R. Hydroxyethyl starch: a review of pharmacokinetics, pharmacodynamics, current products, and potential clinical risks, benefits, and use. *J Vet. Emerg. Crit. Care* **24**, 642-661, doi:10.1111/vec.12208 (2014).
164 Cabral, H. *et al.* Accumulation of sub-100 nm polymeric micelles in poorly permeable tumours depends on size. *Nat. Nanotechnol.* **6**, 815-823, doi:10.1038/nnano.2011.166 (2011).
165 Petros, R. A. & DeSimone, J. M. Strategies in the design of nanoparticles for therapeutic applications. *Nat. Rev. Drug Discov.* **9**, 615-627, doi:10.1038/nrd2591 (2010).
166 Seong, S. Y. & Matzinger, P. Hydrophobicity: an ancient damage-associated molecular pattern that initiates innate immune responses. *Nat. Rev. Immunol.* **4**, 469-478, doi:10.1038/nri1372 (2004).
167 Singh, R. & Lillard, J. W., Jr. Nanoparticle-based targeted drug delivery. *Experimental and molecular pathology* **86**, 215-223, doi:10.1016/j.yexmp.2008.12.004 (2009).
168 Alexis, F., Pridgen, E., Molnar, L. K. & Farokhzad, O. C. Factors affecting the clearance and biodistribution of polymeric nanoparticles. *Mol. Pharamaceut.* **5**, 505-515, doi:10.1021/mp800051m (2008).
169 Wang, J., Byrne, J. D., Napier, M. E. & DeSimone, J. M. More effective nanomedicines through particle design. *Small* **7**, 1919-1931, doi:10.1002/smll.201100442 (2011).
170 Kvitek, L. *et al.* Effect of surfactants and polymers on stability and antibacterial activity of silver nanoparticles (NPs). *J Phys Chem C* **112**, 5825-5834, doi:10.1021/jp711616v (2008).
171 Frohlich, E. The role of surface charge in cellular uptake and cytotoxicity of medical nanoparticles. *Int. J. Nanomed.* **7**, 5577-5591, doi:10.2147/IJN.S36111 (2012).
172 Hapuarachchige, S., Zhu, W., Kato, Y. & Artemov, D. Bioorthogonal, two-component delivery systems based on antibody and drug-loaded nanocarriers for enhanced internalization of nanotherapeutics. *Biomaterials* **35**, 2346-2354, doi:10.1016/j.biomaterials.2013.11.075 (2014).
173 Sun, H. *et al.* Oligonucleotide aptamers: new tools for targeted cancer therapy. *Mol. Ther. Nuc. Acid* **3**, e182, doi:10.1038/mtna.2014.32 (2014).

174 Weissman, A. M. *et al.* Only high-affinity receptors for interleukin 2 mediate internalization of ligand. *Proc. Natl. Acad. Sci. U.S.A.* **83**, 1463-1466 (1986).
175 Alves, N. L., Arosa, F. A. & van Lier, R. A. Common gamma chain cytokines: dissidence in the details. *Immunology letters* **108**, 113-120, doi:10.1016/j.imlet.2006.11.006 (2007).
176 McNeill, L. *et al.* CD45 isoforms in T cell signalling and development. *Immunology letters* **92**, 125-134, doi:10.1016/j.imlet.2003.10.018 (2004).
177 Trinschek, B., Luessi, F., Gross, C. C., Wiendl, H. & Jonuleit, H. Interferon-Beta Therapy of Multiple Sclerosis Patients Improves the Responsiveness of T Cells for Immune Suppression by Regulatory T Cells. *Int. J. Mol. Sci.* **16**, 16330-16346, doi:10.3390/ijms160716330 (2015).
178 Lee, R. J. & Low, P. S. Delivery of liposomes into cultured KB cells via folate receptor-mediated endocytosis. *J. Biol. Chem.* **269**, 3198-3204 (1994).
179 Sahlin, S., Hed, J. & Rundquist, I. Differentiation between attached and ingested immune complexes by a fluorescence quenching cytofluorometric assay.J. Meth. Immunol. **60**, 115-124 (1983).
180 Neumeyer, A., Bukowski, M., Veith, M., Lehr, C. M. & Daum, N. Propidium iodide labeling of nanoparticles as a novel tool for the quantification of cellular binding and uptake. *Nanomedicine : nanotechnology, biology, and medicine* **7**, 410-419, doi:10.1016/j.nano.2010.12.007 (2011).
181 Gottstein, C., Wu, G., Wong, B. J. & Zasadzinski, J. A. Precise quantification of nanoparticle internalization. *ACS nano* **7**, 4933-4945, doi:10.1021/nn400243d (2013).
182 Konigsberg, P. J., Godtel, R., Kissel, T. & Richer, L. L. The development of IL-2 conjugated liposomes for therapeutic purposes. *Biochimica et biophysica acta* **1370**, 243-251 (1998).
183 Zheng, Y. *et al.* In vivo targeting of adoptively transferred T-cells with antibody- and cytokine-conjugated liposomes. *J. Control. Release* **172**, 426-435, doi:10.1016/j.jconrel.2013.05.037 (2013).
184 Conner, S. D. & Schmid, S. L. Regulated portals of entry into the cell. *Nature* **422**, 37-44, doi:10.1038/nature01451 (2003).
185 Lamaze, C. *et al.* Interleukin 2 receptors and detergent-resistant membrane domains define a clathrin-independent endocytic pathway. *Molecular cell* **7**, 661-671 (2001).
186 Basquin, C. *et al.* The signalling factor PI3K is a specific regulator of the clathrin-independent dynamin-dependent endocytosis of IL-2 receptors. *Journal of cell science* **126**, 1099-1108, doi:10.1242/jcs.110932 (2013).
187 Grassart, A., Dujeancourt, A., Lazarow, P. B., Dautry-Varsat, A. & Sauvonnet, N. Clathrin-independent endocytosis used by the IL-2 receptor is regulated by Rac1, Pak1 and Pak2. *EMBO reports* **9**, 356-362, doi:10.1038/embor.2008.28 (2008).
188 Grassart, A. *et al.* Pak1 phosphorylation enhances cortactin-N-WASP interaction in clathrin-caveolin-independent endocytosis. *Traffic* **11**, 1079-1091, doi:10.1111/j.1600-0854.2010.01075.x (2010).
189 Mayor, S., Parton, R. G. & Donaldson, J. G. Clathrin-independent pathways of endocytosis. *Cold Spring Harbor perspectives in biology* **6**, doi:10.1101/cshperspect.a016758 (2014).
190 Rejman, J., Oberle, V., Zuhorn, I. S. & Hoekstra, D. Size-dependent internalization of particles via the pathways of clathrin- and caveolae-mediated endocytosis. *The Biochemical journal* **377**, 159-169, doi:10.1042/BJ20031253 (2004).
191 Dutta, D. & Donaldson, J. G. Search for inhibitors of endocytosis: Intended specificity and unintended consequences. *Cellular logistics* **2**, 203-208, doi:10.4161/cl.23967 (2012).
192 Rigal, A., Doyle, S. M. & Robert, S. Live cell imaging of FM4-64, a tool for tracing the endocytic pathways in Arabidopsis root cells. *Meth. Mol. Biol.* **1242**, 93-103, doi:10.1007/978-1-4939-1902-4_9 (2015).
193 Walls, Z. F., Gong, H. & Wilson, R. J. Liposomal Coencapsulation of Doxorubicin with Listeriolysin O Increases Potency via Subcellular Targeting. *Mol. Pharamaceut.* **13**, 1185-1190, doi:10.1021/acs.molpharmaceut.5b00674 (2016).

194 Kim, Y. J. *et al.* Protamine sulfate precipitation method depletes abundant plant seed-storage proteins: A case study on legume plants. *Proteomics* **15**, 1760-1764, doi:10.1002/pmic.201400488 (2015).
195 Setoguchi, R., Hori, S., Takahashi, T. & Sakaguchi, S. Homeostatic maintenance of natural Foxp3(+) CD25(+) CD4(+) regulatory T cells by interleukin (IL)-2 and induction of autoimmune disease by IL-2 neutralization. *J. Exp. Med.* **201**, 723-735, doi:10.1084/jem.20041982 (2005).
196 Boyman, O., Kovar, M., Rubinstein, M. P., Surh, C. D. & Sprent, J. Selective stimulation of T cell subsets with antibody-cytokine immune complexes. *Science* **311**, 1924-1927, doi:10.1126/science.1122927 (2006).
197 Obar, J. J. *et al.* CD4+ T cell regulation of CD25 expression controls development of short-lived effector CD8+ T cells in primary and secondary responses. *Proc. Natl. Acad. Sci. U.S.A.* **107**, 193-198, doi:10.1073/pnas.0909945107 (2010).
198 Pepper, M., Pagan, A. J., Igyarto, B. Z., Taylor, J. J. & Jenkins, M. K. Opposing signals from the Bcl6 transcription factor and the interleukin-2 receptor generate T helper 1 central and effector memory cells. *Immunity* **35**, 583-595, doi:10.1016/j.immuni.2011.09.009 (2011).
199 Yu, A., Zhu, L., Altman, N. H. & Malek, T. R. A low interleukin-2 receptor signaling threshold supports the development and homeostasis of T regulatory cells. *Immunity* **30**, 204-217, doi:10.1016/j.immuni.2008.11.014 (2009).
200 Hartemann, A. *et al.* Low-dose interleukin 2 in patients with type 1 diabetes: a phase 1/2 randomised, double-blind, placebo-controlled trial. *The lancet. Diabetes & endocrinology* **1**, 295-305, doi:10.1016/S2213-8587(13)70113-X (2013).
201 Koreth, J. *et al.* Interleukin-2 and regulatory T cells in graft-versus-host disease. *N. Engl. J. Med.* **365**, 2055-2066, doi:10.1056/NEJMoa1108188 (2011).
202 Asano, T. *et al.* PD-1 modulates regulatory T-cell homeostasis during low-dose interleukin-2 therapy. *Blood* **129**, 2186-2197, doi:10.1182/blood-2016-09-741629 (2017).
203 Yu, A. *et al.* Selective IL-2 responsiveness of regulatory T cells through multiple intrinsic mechanisms supports the use of low-dose IL-2 therapy in type 1 diabetes. *Diabetes* **64**, 2172-2183, doi:10.2337/db14-1322 (2015).
204 Bensinger, S. J. *et al.* Distinct IL-2 receptor signaling pattern in CD4+CD25+ regulatory T cells. *J. Immunol* **172**, 5287-5296 (2004).
205 Song, M. S., Salmena, L. & Pandolfi, P. P. The functions and regulation of the PTEN tumour suppressor. *Nat. Rev. Mol. Cell Biol.* **13**, 283-296, doi:10.1038/nrm3330 (2012).
206 Malek, T. R. & Castro, I. Interleukin-2 Receptor Signaling: At the Interface between Tolerance and Immunity. *Immunity* **33**, 153-165, doi:10.1016/j.immuni.2010.08.004 (2010).
207 Fontenot, J. D., Rasmussen, J. P., Gavin, M. A. & Rudensky, A. Y. A function for interleukin 2 in Foxp3-expressing regulatory T cells. *Nat. Immunol.* **6**, 1142-1151, doi:10.1038/ni1263 (2005).
208 Sadlack, B. *et al.* Ulcerative colitis-like disease in mice with a disrupted interleukin-2 gene. *Cell* **75**, 253-261 (1993).
209 Malek, T. R., Yu, A., Vincek, V., Scibelli, P. & Kong, L. CD4 regulatory T cells prevent lethal autoimmunity in IL-2Rbeta-deficient mice. Implications for the nonredundant function of IL-2. *Immunity* **17**, 167-178 (2002).
210 Boyman, O., Cho, J. H. & Sprent, J. The role of interleukin-2 in memory CD8 cell differentiation. *Adv. Exp. Med. Biol.* **684**, 28-41 (2010).
211 von Spee-Mayer, C. *et al.* Low-dose interleukin-2 selectively corrects regulatory T cell defects in patients with systemic lupus erythematosus. *Ann. Rheum. Dis.* **75**, 1407-1415, doi:10.1136/annrheumdis-2015-207776 (2016).
212 Matsuoka, K. *et al.* Low-dose interleukin-2 therapy restores regulatory T cell homeostasis in patients with chronic graft-versus-host disease. *Science Translat. Med.* **5**, 179ra143, doi:10.1126/scitranslmed.3005265 (2013).
213 Rosenberg, S. A. IL-2: the first effective immunotherapy for human cancer. *J. Immunol.* **192**, 5451-5458, doi:10.4049/jimmunol.1490019 (2014).

214 Group, I.-E. S. *et al.* Interleukin-2 therapy in patients with HIV infection. *N. Engl. J. Med.* **361**, 1548-1559, doi:10.1056/NEJMoa0903175 (2009).
215 Busse, D. *et al.* Competing feedback loops shape IL-2 signaling between helper and regulatory T lymphocytes in cellular microenvironments. *Proc. Natl. Acad. Sci. U.S.A.* **107**, 3058-3063, doi:10.1073/pnas.0812851107 (2010).
216 Cheng, G., Yu, A. & Malek, T. R. T-cell tolerance and the multi-functional role of IL-2R signaling in T-regulatory cells. *Immunological Rev.* **241**, 63-76, doi:10.1111/j.1600-065X.2011.01004.x (2011).
217 Blanco, E., Shen, H. & Ferrari, M. Principles of nanoparticle design for overcoming biological barriers to drug delivery. *Nature biotechnology* **33**, 941-951, doi:10.1038/nbt.3330 (2015).
218 Nguyen, V. H. & Lee, B. J. Protein corona: a new approach for nanomedicine design. *Int. J. Nanomed.* **12**, 3137-3151, doi:10.2147/IJN.S129300 (2017).
219 Haeryfar, S. M. & Hoskin, D. W. Thy-1: more than a mouse pan-T cell marker. *J. Immunol.* **173**, 3581-3588 (2004).
220 Hey, Y. Y., Tan, J. K. & O'Neill, H. C. Redefining Myeloid Cell Subsets in Murine Spleen. *Front. Immunol.* **6**, 652, doi:10.3389/fimmu.2015.00652 (2015).
221 Ghosn, E. E., Yang, Y., Tung, J., Herzenberg, L. A. & Herzenberg, L. A. CD11b expression distinguishes sequential stages of peritoneal B-1 development. *Proc. Natl. Acad. Sci. U.S.A.* **105**, 5195-5200, doi:10.1073/pnas.0712350105 (2008).
222 Kaminski, D. A., Wei, C., Qian, Y., Rosenberg, A. F. & Sanz, I. Advances in human B cell phenotypic profiling. *Front. Immunol.* **3**, 302, doi:10.3389/fimmu.2012.00302 (2012).
223 Murray, P. J. & Wynn, T. A. Protective and pathogenic functions of macrophage subsets. *Nat. Rev. Immunol.* **11**, 723-737, doi:10.1038/nri3073 (2011).
224 Mestas, J. & Hughes, C. C. Of mice and not men: differences between mouse and human immunology. J. Immunol. **172**, 2731-2738 (2004).
225 Collins, M. K. Species specificity of interleukin 2 binding to individual receptor components. *Europ. J. Immunol.* **19**, 1517-1520, doi:10.1002/eji.1830190828 (1989).
226 Schultz, S. G. From a pump handle to oral rehydration therapy: a model of translational research. *Adv. Physiol. Ed.* **31**, 288-293, doi:10.1152/advan.00068.2007 (2007).
227 Brehm, M. A., Shultz, L. D. & Greiner, D. L. Humanized mouse models to study human diseases. *Curr. Opin. Endocrinol. Diabetes Obes.* **17**, 120-125, doi:10.1097/MED.0b013e328337282f (2010).
228 Schroeder, M. A. & DiPersio, J. F. Mouse models of graft-versus-host disease: advances and limitations. *Disease models & mechanisms* **4**, 318-333, doi:10.1242/dmm.006668 (2011).
229 Becker, C. *et al.* Protection from graft-versus-host disease by HIV-1 envelope protein gp120-mediated activation of human CD4+CD25+ regulatory T cells. *Blood* **114**, 1263-1269, doi:10.1182/blood-2009-02-206730 (2009).
230 Hahn, S. A., Bellinghausen, I., Trinschek, B. & Becker, C. Translating Treg Therapy in Humanized Mice. *Front. Immunol.* **6**, 623, doi:10.3389/fimmu.2015.00623 (2015).
231 Cosmi, L. *et al.* Human CD8+CD25+ thymocytes share phenotypic and functional features with CD4+CD25+ regulatory thymocytes. *Blood* **102**, 4107-4114, doi:10.1182/blood-2003-04-1320 (2003).
232 Dinauer, N. *et al.* Selective targeting of antibody-conjugated nanoparticles to leukemic cells and primary T-lymphocytes. *Biomaterials* **26**, 5898-5906, doi:10.1016/j.biomaterials.2005.02.038 (2005).
233 Lo, Y. C., Edidin, M. A. & Powell, J. D. Selective activation of antigen-experienced T cells by anti-CD3 constrained on nanoparticles. *J. Immunol.* **191**, 5107-5114, doi:10.4049/jimmunol.1301433 (2013).
234 Smith, T. T. *et al.* In situ programming of leukaemia-specific T cells using synthetic DNA nanocarriers. *Nat. Nanotechnol.* **12**, 813-820, doi:10.1038/nnano.2017.57 (2017).
235 Lee, J. *et al.* T cell-specific siRNA delivery using antibody-conjugated chitosan nanoparticles. *Bioconjugate Chem.* **23**, 1174-1180, doi:10.1021/bc2006219 (2012).

236 Schutz, C. *et al.* Antigen-specific T cell Redirectors: a nanoparticle based approach for redirecting T cells. *Oncotarget* **7**, 68503-68512, doi:10.18632/oncotarget.11785 (2016).
237 Clemente-Casares, X. *et al.* Expanding antigen-specific regulatory networks to treat autoimmunity. *Nature* **530**, 434-440, doi:10.1038/nature16962 (2016).
238 Sacchetti, C. *et al.* In vivo targeting of intratumor regulatory T cells using PEG-modified single-walled carbon nanotubes. *Bioconjugate Chem.* **24**, 852-858, doi:10.1021/bc400070q (2013).
239 Yao, H. *et al.* Effective melanoma immunotherapy with interleukin-2 delivered by a novel polymeric nanoparticle. *Mol. Cancer Ther.* **10**, 1082-1092, doi:10.1158/1535-7163.MCT-10-0717 (2011).
240 Park, J. *et al.* Combination delivery of TGF-beta inhibitor and IL-2 by nanoscale liposomal polymeric gels enhances tumour immunotherapy. *Nat. Mat.* **11**, 895-905, doi:10.1038/nmat3355 (2012).
241 Fadel, T. R. *et al.* A carbon nanotube-polymer composite for T-cell therapy. *Nat. Nanotechnol.* **9**, 639-647, doi:10.1038/nnano.2014.154 (2014).
242 Liu, M. *et al.* IL-2-engineered nano-APC effectively activates viral antigen-mediated T cell responses from chronic hepatitis B virus-infected patients. *J. Immunol.* **188**, 1534-1543, doi:10.4049/jimmunol.1102709 (2012).
243 McHugh, M. D. *et al.* Paracrine co-delivery of TGF-beta and IL-2 using CD4-targeted nanoparticles for induction and maintenance of regulatory T cells. *Biomaterials* **59**, 172-181, doi:10.1016/j.biomaterials.2015.04.003 (2015).
244 Turturro, F. Denileukin diftitox: a biotherapeutic paradigm shift in the treatment of lymphoid-derived disorders. *Exp. Rev. Anticancer Ther.* **7**, 11-17, doi:10.1586/14737140.7.1.11 (2007).
245 Colombo, M. P. & Piconese, S. Regulatory-T-cell inhibition versus depletion: the right choice in cancer immunotherapy. *Nat. Rev. Cancer* **7**, 880-887, doi:10.1038/nrc2250 (2007).
246 Takeda, K. *et al.* Targeted disruption of the mouse Stat3 gene leads to early embryonic lethality. *Proc. Natl. Acad. Sci. U.S.A.* **94**, 3801-3804 (1997).
247 Yue, P. & Turkson, J. Targeting STAT3 in cancer: how successful are we? *Expert opinion on investigational drugs* **18**, 45-56, doi:10.1517/13543780802565791 (2009).
248 Yoshimura, A., Naka, T. & Kubo, M. SOCS proteins, cytokine signalling and immune regulation. *Nat. Rev. Immunol.* **7**, 454-465, doi:10.1038/nri2093 (2007).
249 Lantz, R. C., Lemus, R., Lange, R. W. & Karol, M. H. Rapid reduction of intracellular glutathione in human bronchial epithelial cells exposed to occupational levels of toluene diisocyanate. *Toxicol. Sci.* **60**, 348-355, doi:DOI 10.1093/toxsci/60.2.348 (2001).
250 Gurbuz, V. *et al.* Effects of AG490 and S3I-201 on regulation of the JAK/STAT3 signaling pathway in relation to angiogenesis in TRAIL-resistant prostate cancer cells in vitro. *Oncology Letters* **7**, 755-763, doi:10.3892/ol.2014.1795 (2014).
251 Bu, L. L. *et al.* STAT3 blockade enhances the efficacy of conventional chemotherapeutic agents by eradicating head neck stemloid cancer cell. *Oncotarget* **6**, 41944-41958, doi:10.18632/oncotarget.5986 (2015).
252 Soleimani, A. H. *et al.* Micellar nano-carriers for the delivery of STAT3 dimerization inhibitors to melanoma. *Drug Deliv. Translat. Res.* **7**, 571-581, doi:10.1007/s13346-017-0369-4 (2017).
253 Hibi, M. *et al.* Molecular cloning and expression of an IL-6 signal transducer, gp130. *Cell* **63**, 1149-1157 (1990).
254 Zosky, G. R. *et al.* Ovalbumin-sensitized mice are good models for airway hyperresponsiveness but not acute physiological responses to allergen inhalation. *Clin. Exp. Allergol.* **38**, 829-838, doi:10.1111/j.1365-2222.2007.02884.x (2008).
255 Bihouee, T. *et al.* Food allergy enhances allergic asthma in mice. *Resp. Res.* **15**, 142, doi:10.1186/s12931-014-0142-x (2014).

256 Yu, H., Kortylewski, M. & Pardoll, D. Crosstalk between cancer and immune cells: role of STAT3 in the tumour microenvironment. *Nat. Rev. Immunol.* **7**, 41-51, doi:10.1038/nri1995 (2007).
257 Kortylewski, M. *et al.* Inhibiting Stat3 signaling in the hematopoietic system elicits multicomponent antitumor immunity. *Nat. Med.* **11**, 1314-1321, doi:10.1038/nm1325 (2005).
258 Chaudhry, A. *et al.* CD4+ regulatory T cells control TH17 responses in a Stat3-dependent manner. *Science* **326**, 986-991, doi:10.1126/science.1172702 (2009).
259 Hossain, D. M. *et al.* FoxP3 acts as a cotranscription factor with STAT3 in tumor-induced regulatory T cells. *Immunity* **39**, 1057-1069, doi:10.1016/j.immuni.2013.11.005 (2013).
260 Molavi, L. *et al.* Development of a Poly(D,L-lactic-co-glycolic acid) Nanoparticle Formulation of STAT3 Inhibitor JSI-124: Implication for Cancer Immunotherapy. *Mol. Pharamaceut.* **7**, 364-374, doi:10.1021/mp900145g (2010).
261 Alshamsan, A. *et al.* STAT3 silencing in dendritic cells by siRNA polyplexes encapsulated in PLGA nanoparticles for the modulation of anticancer immune response. *Mol. Pharamaceut.* **7**, 1643-1654, doi:10.1021/mp100067u (2010).
262 Heo, M. B. & Lim, Y. T. Programmed nanoparticles for combined immunomodulation, antigen presentation and tracking of immunotherapeutic cells. *Biomaterials* **35**, 590-600, doi:10.1016/j.biomaterials.2013.10.009 (2014).

Appendix

List of Figures

List of Tables

Abbreviations

APC	Antigen presenting cell
CAR	Chimeric antigen receptor
CCL	C-C chemokine ligand
CCR	C-C chemokine receptor type
CD	Cluster of differentiation
CFDA	(5-(and -6))-carboxyfluorescein diacetate
CLSM	Confocal laser scanning microscopy
CMFDA	5-chloromethylfluorescein diacetate
CTLA-4	Cytotoxic T lymphocyte-associated protein 4
CTV	Cell Trace Violet
DAMP	Danger-associated molecular pattern
DC	Dendritic cell
DLS	Dynamic light scattering
DMEM	Dulbecco’s modified eagle medium
DNA	Desoxy ribonucleic acid
DPBS	Dulbecco’s phosphate buffered saline
EGFR	Epidermal growth factor receptor
ELISA	Enzyme-linked immune-sorbent assay
EPR	Enhanced permeability and retention effect
FACS	Fluorescence activated cell sorting
FCS	Fetal calf serum
FDA	Federal drug administration
FSC	Forward scattered
GITR	Glucocorticoid-induced TNFR family-related protein
GM-CSF	Granulocyte macrophage colony stimulating factor
HES	Hydroxethyl starch
irAE	immune-related adverse effect
IFN	Interferon
IL	Interleukin
MALDI	Matrix-assisted laser desorption and ionization
MDSC	Monocyte-derived suppressor cells
MHC	Major histocompatibility complex
NC	Nanocapsules
NK cell	Natural killer cell
NLR	NOD-like receptor

nTreg	thymus-derived regulatory T cells
PAMP	Pathogen-associated molecular pattern
PBMC	Peripheral blood mononuclear cell
PBS	Phosphate buffered saline
PD-1	Programmed cell death 1
PEG	Poly-ethylene-glycol
PFA	Paraformaldehyde
PI3K	Phosphoinositide 3- kinase
PKB	Proteine kinase B
PRR	Patter recognition receptor
pTreg	peripheral regulatory T cells
RLR	RIG-I like receptor
rSD	Relative size distribution
SDS	Sodium dodecylsulfat
SEM	Scanning electron microscopy
siRNA	small interfering ribonucleic acid
SSC	Sideward scattered
STAT	Signal transducer and activator of transcription
TCR	T cell receptor
TEM	Transmission electron microscopy
TDI	Toluol-2,4-diisocyanat
TGF	Transforming growth factor
TIL	Tumor-infiltrating lymphocyte
TLR	Toll like receptor
TOF	Time of flight
Treg	regulatory T cells
V-(D-)J- recombination	Variable- (diverse-) joining-recombination

Statutory declaration

“I hereby declare that I wrote the dissertation submitted without any unauthorized external assistance and used only sources acknowledged in the work. All textual passages which are appropriated verbatim or paraphrased from published and unpublished texts as well as all information obtained from oral sources are duly indicated and listed in accordance with bibliographical rules. In carrying out this research, I complied with the rules of standard scientific practice as formulated in the statutes of Johannes Gutenberg-University Mainz to insure standard scientific practice.”

Mainz, November 2017 Matthias Domogalla

Acknowledgement

An dieser Stelle möchte ich mich bei allen bedanken, die mich auf dem Wege zu dieser Dissertation begleitet und unterstützt haben. Ohne ihre Hilfe würde die Arbeit nicht in dieser Form vorliegen.

Ein besonderes Dankeschön gilt meiner Doktormutter [redacted], die mich über die Zeit meiner Dissertation mit wertvollen Ideen unterstützt und mir dennoch ausreichend Raum für eigene Einfälle gegeben hat. Außerdem waren unsere zahlreichen, intensiven Diskussionen inspirierend meine eigenen wissenschaftlichen Ansichten weiter zu entwickeln. Ebenfalls möchte ich mich herzlich bei meiner Betreuerin [redacted] bedanken, die in vielen Meetings kostbare Anregungen für diese wissenschaftliche Arbeit gegeben und mich jederzeit mit viel Interesse unterstützt hat. Vor allem die chemischen Aspekte hat sie mir mit Geduld und Hilfsbereitschaft erklärt und verständlich gemacht.

An dieser Stelle möchte ich mich auch beim [redacted] und dem [redacted] für die finanzielle Unterstützung dieser Promotion bedanken. Insbesondere der interdisziplinäre, interkulturelle Austausch im Zuge der „Lecture cycles“, die Möglichkeit meine Arbeit bei internationalen Konferenzen vorzustellen und die angebotenen Soft Skill Seminare haben meinen wissenschaftlichen Werdegang nachhaltig geprägt.

Mein Dank gilt außerdem meinem Mentor [redacted], der bei Fragen immer ein offenes Ohr für mich hatte und mir mit Rat zur Seite stand. Auch G[redacted] und [redacted] gebührt mein Dankeschön; vor allem für die Synthese und Charakterisierung der Kapseln und für die wertvollen Diskussionen beziehungsweise die angenehmen Kooperationen. Ergänzend vielen Dank an [redacted], [redacted] und [redacted] für die tatkräftige Unterstützung bei den *in vivo* Versuchen.

An meine Arbeitsgruppe, die immer für ein angenehmes, motivierendes Arbeitsklima gesorgt hat. Besonder hervorzuheben ist hierbei [redacted], die mich mit ihrer Faszination für die interdisziplinäre Forschung angespornt und bei Fragen sowohl zu wissenschaftlichen Gebieten als auch auf persönlicher Ebene unterstützt hat. [redacted] danke ich zunächst für die Hilfe bei zahlreichen *in vitro* Versuchen, aber vor allem auch dafür, dass sie immer ein offenes Ohr für mich hatte. Mein Dank gilt außerdem [redacted] und [redacted] für die Hilfe bei den *in vivo* Versuchen, sowie [redacted] für ihre Unterstützung und Anregungen bei wissenschaftlichen und persönlichen Fragen.

Nicht zuletzt möchte ich mich bei meiner Familie bedanken, die immer an mich geglaubt hat. Trotz eigener Verpflichtungen war sie sowohl während des Studiums als auch der Promotion immer für mich da.